Disruption of Microhomology-mediated End-joining in Ewing Sarcoma

Shuhei Asada[1#, *], Guangli Zhu[1,2#], Jithma Prasad Abeykoon[1,3], Yutaro Tanaka[4,5], Huy Nguyen[1,6], Yuna Hirohashi[1], Divya R. Iyer[1], Nicholas William Ashton[1], Sirisha Mukkavalli[1], Martha Velazquez[1], Lige Jiang[1], Miles Del Busso[3], Judith Jebastin Thangaiah[7], Steven I. Robinson[8], Kalindi Parmar[1,6], Eliezer M. Van Allen[5,9,10,11], Riaz Gillani[4,5,9,12,] Geoffrey I. Shapiro[10], Alan D. D'Andrea[1, 6, 13*]

1. Division of Radiation and Genome Stability, Department of Radiation Oncology, Dana-Farber Cancer Institute, Harvard Medical School, Boston, MA, USA.
2. Department of Radiation Oncology, First Affiliated Hospital of Sun Yat-sen University, Guangzhou, China
3. Division of Hematology, Department of Internal Medicine, Mayo Clinic, MN, USA
4. Department of Pediatric Oncology, Dana-Farber Cancer Institute, Boston, MA, USA.
5. Cancer Program, Broad Institute of MIT and Harvard, Cambridge, MA, USA.
6. Center for DNA Damage and Repair, Dana-Farber Cancer Institute, Harvard Medical School, Boston, MA, USA.
7. Department of Pathology, Mayo Clinic, MN, USA
8. Department of Oncology, Mayo Clinic, MN, USA
9. Harvard Medical School, Boston, MA, USA.
10. Department of Medical Oncology, Dana-Farber Cancer Institute, Harvard Medical School, Boston, MA, USA.
11. Center for Cancer Genomics, Dana-Farber Cancer Institute, Boston, MA, USA.
12. Boston Children's Hospital, Boston, MA, USA.
13. Lead contact
# These authors contributed equally to this work.

*Corresponding authors: Shuhei Asada (shuhei_asada@dfci.harvard.edu) and Alan D. D'Andrea (alan_dandrea@dfci.harvard.edu)

Keywords: Ewing's Sarcoma, DNA double-strand breaks, Alternative end-joining, TMEJ, the Fanconi Anemia pathway, DNA-PKc, CDK12

SUMMARY

Ewing sarcoma (EwS) is a group of bone and soft tissue cancers in children and young adults. Since EwS cells have pronounced sensitivity to radiation and chemotherapy-induced DNA damage, the role of the oncoprotein, EWS-FLI1, in DNA repair is likely. Here, we demonstrate that EWS-FLI1 causes a defect in microhomology-mediated end-joining (MMEJ) repair. EWSR1 is a splicing factor that promotes the faithful splicing of the *POLQ* pre-mRNA, required for the expression of POLΘ, a critical protein in the MMEJ pathway. Expression of EWS-FLI1, or loss of EWSR1, causes exon 25 skipping of the *POLQ* transcript, decreased POLΘ expression, impaired MMEJ, and cellular sensitivity to inhibitors of the Fanconi Anemia (FA), NHEJ, or HR pathways, through the mechanism of synthetic lethality. Knockdown of EWS-FLI1 expression restores POLΘ mitotic foci and increases MMEJ activity. Inhibitors of the FA, NHEJ, or HR therefore may provide a targeted therapy for patients with EwS.

Highlights:

-Ewing sarcoma tumors have a deficiency in POLθ expression and a corresponding loss of MMEJ activity

-EWSR1 is a splicing factor that interacts with other splicing factors such as FUBP1 and KHSRP/FUBP2 to accurately splice the *POLQ* mRNA.

-The EWS-FLI1 fusion oncoprotein, or loss of EWSR1, causes a splicing defect, leading to exon25 skipping of the *POLQ* pre-mRNA and loss of POLθ expression

-The MMEJ deficiency of EwS cells results in cellular sensitivity to inhibitors of Fanconi Anemia, Homologous Recombination or Non-Homologous End-Joining

-Exon 25 skipping of *POLQ* mRNA is a predictive biomarker for HR inhibitors in human cancers

66 **INTRODUCTION**

67

68 Ewing sarcoma (EwS) is a group of bone and soft tissue cancers in children and young
69 adults[1,2]. EwS tumor cells have a chromosome 11;22 translocation, resulting in expression of
70 the EWS-FLI1 fusion oncoprotein. Their elevated sensitivity to ionizing radiation and DNA-
71 damaging chemotherapy, as well as their relatively low level of somatic mutations, suggest that
72 EwS cells have an underlying defect in an error-prone DNA repair (DDR) pathway. Despite this
73 high drug sensitivity, novel treatments for EwS are required, especially for patients with relapsed
74 and/or refractory disease, who have a low 5-year overall survival rate of only 10%.

75 Recent studies have identified some abnormalities in DDR in Ewing sarcoma cells.
76 Expression of EWS-FLI1 fusion protein promotes R-loop formation and impaired BRCA1
77 recruitment to chromatin, suggesting a defect in the homologous-recombination repair pathway
78 (HRD) [3]. Despite this preclinical observation, PARP inhibition, an approved treatment for HR-
79 deficient tumors, was ineffective in the treatment of EwS patients[4]. Other cellular defects
80 resulting from EWS-FLI1 expression may indirectly affect DDR, such as defects in BAF
81 complex-mediated transcription [5,6], condensate generation [7-9], and mRNA splicing [10]. However,
82 the mechanism by which EWS-FLI1 specifically influences DDR pathways is unknown, and
83 other more profound DNA repair defects, beyond the HRD phenotype, may exist.

84 DNA double-strand breaks (DSBs) are the most critical forms of DNA damage in cells.
85 There are three main pathways for repairing DSBs - non-homologous end-joining (NHEJ),
86 homologous recombination (HR), and microhomology-mediated end-joining (MMEJ). For a
87 cancer cell to survive and proliferate, DSBs must be repaired, and the cell must rely on at least
88 one of these pathways. DNA polymerase theta (POLΘ), an error-prone polymerase encoded by
89 the *POLQ* gene, is required for the MMEJ pathway. Overexpression of *POLQ* confers

90 chemoresistance, whereas depletion of POLΘ results in cancer predisposition and
91 hypersensitivity to irradiation and chemotherapy [11,12]. *To date, there are no reported human*
92 *cancers with defects in the MMEJ pathway.*
93 Here, we demonstrate that EwS cells have an underlying defect in MMEJ. Expression of
94 EWS-FLI1, or loss of EWSR1, in these cells promotes exon skipping of the *POLQ* pre-mRNA,
95 generating a premature termination codon and a profound reduction of POLΘ protein expression.
96 EWS-FLI1 expressing cells exhibit a phenotype like *POLQ* deficient cells, including
97 hypersensitivity to topoisomerase inhibitors, irradiation, and synthetic lethality with loss of the
98 Fanconi Anemia, NHEJ, or HR pathways. Knockout of the EWS-FLI1 oncoprotein in EwS cells
99 results in reduced exon skipping, re-expression of the POLΘ protein, and a rescue of MMEJ
100 activity. Accordingly, the DDR defect in EwS tumors could be exploited for therapeutic benefit
101 by inhibiting another DSB repair pathway.
102
103
104

105 **RESULTS**

106 ***EWSR1* knock-out cells phenocopy MMEJ-deficient cells.**

107 Previous CRISPR screens and Depmap analyses have demonstrated that genes in the
108 MMEJ pathway are synthetic lethal in cells with an underlying defect in an HR gene [13,14],
109 Interestingly, in these screens, knockout of the *EWSR1* gene was highly similar to knockout of
110 known MMEJ genes, including *POLQ* [15], *XRCC1* [16], *APEX2* [17], and *RHNO1* [18], in the killing of
111 HR-deficient tumor cells (**Fig. S1A)**. To investigate the function of EWSR1 in DNA repair, we
112 initially generated an *EWSR1* knock-out in RPE *TP53-/-* cells (**Fig. 1A**). *EWSR1* knockout resulted
113 in hypersensitivity to ionizing irradiation, topoisomerase inhibitors, and ATR inhibitors, but not to
114 the PARP inhibitor, suggesting a loss of MMEJ activity (**Fig. S1 B-F**). The DDR defect observed
115 in *EWSR1* knockout cells was similar to the defect observed in *POLQ* knockout cells [11].
116 Consistently, *EWSR1* is mapped closely to *POLQ* in the previous repair-seq, indicating a functional
117 relationship between these genes in DNA damage repair [19].

118 Next, the impact of *EWSR1* loss on the activity of DNA double-strand break repair
119 pathways in U2OS cells was evaluated, using established Isce-I-based reporter systems [20,21].
120 *EWSR1* knockout mildly decreased HR activity (**Fig. S1G**); however, the *EWSR1*-deficient cells
121 were not sensitive to the PARP inhibitor, Olaparib. Interestingly, *EWSR1* knockout significantly
122 decreased MMEJ activity (**Fig. 1B**). To further confirm a MMEJ reduction upon *EWSR1* depletion,
123 a novel Cas9-based MMEJ reporter system was generated (**Fig. S1H**). Again, *EWSR1* knockout
124 decreased MMEJ activity in this Cas9-based reporter cells (**Fig. 1C**). Consistent with this result,
125 *EWSR1*-deficient cells were resistant to the *POLQ* inhibitor, Novobiocin [22](**Fig. S1I**).

126 Recent studies suggest that *EWSR1* knockdown is synthetic lethal with BRCA2 loss [13,14].
127 To validate these results, depletion of EWSR1 in BRCA2-proficient and BRCA2-deficient DLD1

128 cells was evaluated. Like *POLQ* loss, EWSR1 loss profoundly decreased colony-forming activity
129 in the *BRCA2*-deficient DLD1 cells (**Fig. 1D**). EWSR1 loss also efficiently decreased clonogenic
130 activity of the *BRCA1*-mutated breast cancer cell lines, MDA-MB-468 and HCC1937 cells (**Fig**
131 **S1. J, K**). To further confirm the synthetic lethality of EWSR1 and BRCA1/2, we generated RPE
132 *TP53-/-* cells stably expressing Cas9 (**Fig. S1L)**. These cells were subsequently lentivirally-
133 transduced with a sgRNA targeting control, *POLQ,* or *EWSR1* (co-expressing GFP) together with
134 another sgRNA targeting control, *BRCA1* or *BRCA2* (co-expressing tRFP657), and changes in the
135 frequency of GFP/tRFP657 cells were monitored. Again, like *POLQ* loss, *EWSR1* loss resulted in
136 synthetic lethality with *BRCA1/2* loss in this system. Taken together, *EWSR1* functions as a MMEJ
137 gene.
138
139 **EWSR1 promotes MMEJ by maintaining POLΘ expression.**
140 Since EWSR1 loss caused a reduction of MMEJ activity, we examined the impact of
141 EWSR1 loss on protein expression of known MMEJ-related proteins. To monitor the POLΘ
142 protein expression, RPE *TP53-/-* cells expressing 3xFLAG-tagged *POLQ* were generated.
143 Interestingly, *EWSR1* knockout resulted in decreased POLΘ expression (**Fig. 1E, Fig. S2A**).
144 Increased radiosensitivity of the *EWSR1* knockout cells was observed (**Fig. S2B**). To further
145 evaluate the direct and acute effect of EWSR1 loss on POLΘ expression, we tagged endogenous
146 EWSR1 protein with the mutant cytosolic prolyl isomerase $FKBP12^{F36V}$ in endogenously
147 3xFLAG-tagged *POLQ* expressing HEK293T cells [23,24]. In this targeted protein degradation
148 system, the small bifunctional molecule $dTAG^{v1}$ bridges $FKBP12^{F36V}$ with the E3 ubiquitin ligase
149 VHL, resulting in substrate ubiquitination and proteasomal degradation. Treatment of cells
150 harboring the $FKBP12^{F36V}$-tagged EWSR1 with $dTAG^{v1}$ resulted in rapid degradation of EWSR1

151 protein (**Fig. S2C-F**). Interestingly, this acute depletion of EWSR1 rapidly reduced the expression
152 of POLΘ but did not affect the expression of other known MMEJ-related proteins, including
153 APEX2, HMCES, FEN1, LIG3, PARP1, and XRCC1 nor HR-related proteins such as BRCA1
154 and BRCA2 (**Fig 1F, Fig. S2G).** Since EWSR1, as well as FUS and TAF15, belongs to the FET
155 family of proteins [25], we speculated that POLΘ loss and MMEJ deficiency might be a common
156 phenotype of the loss of FET family genes. However, FUS or TAF15 loss did not affect the protein
157 level of POLΘ or MMEJ activity (**Fig. S2H, I**). Consistently, *EWSR1* knockout reduced the POLΘ
158 foci assembly upon irradiation-induced DNA damage (**Fig. 1G**).

159 The functional significance of the loss of POLΘ on MMEJ activity in *EWSR1*-depleted
160 cells was next examined. Transduction with the WT *POLQ* cDNA rescued MMEJ activity in
161 *EWSR1* knockout cells (**Fig 1H**). Moreover, *POLQ* cDNA transduction corrected the
162 hypersensitivity to the topoisomerase inhibitors, indicating that loss of POLΘ protein is
163 responsible for these phenotypes in *EWSR1* knockout cells (**Fig 1I, Fig S2J**). Like POLΘ loss,
164 EWSR1 loss increased unrepaired DNA damage and micronuclei in BRCA-deficient cells (**Fig**
165 **S2K, L**). Collectively, EWSR1 promotes MMEJ via the maintenance of POLΘ protein
166 expression.

167

168 **EWSR1 directly binds to the *POLQ* transcript and prevents *POLQ* exon skipping.**

169

170 To investigate the cause of the reduced POLΘ protein expression following loss of
171 EWSR1, we evaluated the stability of POLΘ protein in the presence or absence of EWSR1. U2OS
172 MMEJ-reporter cells were transduced with the *POLQ* cDNA, followed by *EWSR1* knockout by
173 the CRISPR-Cas9 system. However, the protein level of POLΘ expressed by *POLQ* cDNA did
174 not change after *EWSR1* depletion (**Fig. S3A**). Furthermore, a proteasome inhibitor MG132, or the

175 autophagy inhibitor chloroquine, did not rescue endogenous POLΘ expression in *EWSR1*-depleted
176 cell (**Fig. S3B**), suggesting a pre-translational mechanism.

177 To assess the overall influence of EWSR1 loss on transcript levels, including the POLQ
178 transcripts, we next performed an RNA-seq analysis on RPE1 *TP53-/-* cells and RPE1 *TP53-/-*
179 *EWSR1* knockout cells. Alternative splicing events were analyzed by the MISO framework [26] as
180 well as the rMATs framework[27]. Based on this analysis, various alternative splicing events,
181 including exon skipping events, were observed in *EWSR1* knock-out cells (**Fig. S3C-G)**. Among
182 DNA repair genes with exon skipping events, we identified several exon skipping events of the
183 *POLQ* transcript, including exon 7, exon 21 and exon 25, as top hits (**Fig. 2A**). Among these exon
184 skipping events within the *POLQ* transcript, the skipping of exon 25 was the most prominent (**Fig.**
185 **2B)**. Of note, *POLQ* exon 25 is located between long introns, intron 24 and intron 25. Furthermore,
186 we re-analyzed previously published RNA-seq datasets using si-control and si-EWSR1 cells, and
187 again the *POLQ* exon 25 skipping is one of the most significant events (**Fig. S3H, I**). We validated
188 the results in multiple *EWSR1* knockout clones by RT-PCR (**Fig. S3J**).

189 To evaluate the impact of exon-skipping events on POLΘ protein expression, we
190 transduced sgRNAs targeting individual exons. Targeting *POLQ* exon 7, exon 21, or exon 25 by
191 CRISPR-Cas9-mediated gene knockout induced profound protein loss of POLΘ as well as a
192 reduction of MMEJ activity (**Fig.2C, D**). Moreover, a cycloheximide chase assay revealed that a
193 shorter isoform of the POLΘ protein, expressed from a *POLQ* cDNA lacking exon 25, is more
194 unstable than the full-length POLΘ protein (**Fig. 2E**). Exon 25 skipping causes premature
195 termination of POLΘ protein synthesis, preventing the complete expression of the "Fingers" and
196 "Palm" of the encoded polymerase. Structural modeling by AlphaFold 3 demonstrated that this
197 truncation disrupts the structural integrity of this domain, likely explaining the instability

198 compared to the full-length protein (**Fig. S3K**). The *POLQ* cDNA lacking exon 25 or exon7 failed
199 to rescue the MMEJ-deficiencies in *POLQ* knockout cells (**Fig. 2F**).

200 To further investigate the biological significance of *POLQ* exon 25 skipping in the MMEJ
201 activity, we designed antisense oligonucleotides (ASOs) that target exon 25 and induce exon 25
202 skipping (**Fig. S4A**). *POLQ* exon 25 skipping decreased POLΘ protein expression and MMEJ
203 activity (**Fig. S4B, C**). Moreover, a mNeongreen-based minigene reporter, as previously described
204 [28], was generated in which the mNeongreen is split into two exons with synthetic genes derived
205 from the partial intron 24/25 and exon 25 of *POLQ* inserted in between (**Fig. S4D**). The minigene
206 reporter recapitulated the *POLQ* exon 25 skipping driven by depletion of EWSR1, indicating a
207 direct involvement of EWSR1 in the reduction of *POLQ* exon 25 skipping by binding the *POLQ*
208 pre-mRNA near the exon 25 (**Fig. 2G, Fig. S4E**). Using an RNA immunoprecipitation protocol [29],
209 we determined whether EWSR1 interacts with the *POLQ* pre-mRNA, using HEK293T cells
210 harboring the FKBP12^{F36V}-tagged EWSR1 (**Fig. S4F**). Indeed, EWSR1 efficiently co-
211 immunoprecipitated with the *POLQ* pre-mRNA near exon 7 and exon 25, as compared to the
212 *GAPDH* control (**Fig. S4G, H**). Taken together, EWSR1 binds directly to *POLQ* pre-mRNA and
213 prevents exon skipping of the *POLQ* transcript, leading to maintenance of POLΘ protein levels
214 and MMEJ activity.

215 Given that one allele of *EWSR1* is lost in EwS cells, we speculated that these phenomena
216 would also be observed in EwS cells, including patient samples. A higher level of exon 7 and
217 exon 25 skipping and decreased expression of POLΘ protein were evident in EwS cell lines,
218 compared to the osteosarcoma cell line U2OS (**Fig. 2H, I**). Importantly, patient-derived EwS
219 tumor samples exhibited a higher frequency of *POLQ* exon 25 skipping than primary tumors from
220 other pediatric solid tumors, including Neuroblastoma, Osteosarcoma, and Wilms tumor (**Fig. 2J**).

221 Moreover, *POLQ* mRNA levels in Ewing sarcoma were comparable to or lower than other
222 pediatric solid tumors (**Fig. 2K**).

223 We also evaluated single nucleotide variants (SNVs), the mutational signature, and small
224 deletions in patient-derived EwS tumors. Consistent with previous studies [30], the EwS tumors have
225 a low SNV frequency compared to Neuroblastoma, consistent with a MMEJ deficiency in the
226 tumors (**Fig. 2L**). Although the level of HRD hallmarks, ID-6 and signature 3, were overall low,
227 which is consistent with a previous study [31], Ewing sarcoma tumors showed an even lower level
228 of signature 3 or ID-6, compared to Neuroblastomas, again confirming that EwS is an HR-
229 proficient tumor **(Fig. S5A-F**). In contrast, the indels observed in the EwS samples, compared
230 with neuroblastoma samples, have a lower frequency of deletions with >3bp micro-homologies
231 and templated insertions, consistent with a low level of *POLQ*-mediated MMEJ in EwS [32] **(Fig.
232 2M, Fig. S5G-I**). To validate our findings in the primary patient samples, we measured the degree
233 of microhomology at breakpoints of the *EWSR1* fusion in EwS tumor samples from two different
234 EwS patient cohorts. Interestingly, the degree of microhomology at canonical translocation
235 breakpoints was very low in the EwS genomes, consistent with a cellular defect in the MMEJ
236 pathway and a compensatory increase in NHEJ (**Fig. S5J, K**). Collectively, EwS tumor cells have
237 a bona fide defect in MMEJ, which is probably due to increased *POLQ* exon 25 skipping.

238

239 **The Prion-like domain of EWSR1 is required for the faithful splicing of the *POLQ***
240 **transcript.**

241 To identify the functional domain of EWSR1 required for accurate *POLQ* splicing, we next
242 generated EWSR1 mutants lacking individual domains (**Fig. 3A**). Deletion of the prion-like
243 domain (M1) or the C-terminus RRG2 domain (M6) resulted in failure to rescue the *POLQ* exon

244 skipping and POLΘ protein expression level (**Fig. 3B, C, Fig. S6A**). Consistent with these results,
245 MMEJ activity was not restored in *EWSR1*-depleted cells by these two mutant forms of EWSR1
246 (**Fig. S6B**). In addition, these mutant proteins were unable to rescue the cellular hypersensitivity
247 to topoisomerase inhibitors or an ATR inhibitor. The mutants also failed to rescue the synthetic
248 lethality resulting from BRCA2 loss in *EWSR1*-deficient cells (**Fig. S6C-G**).

249 A nuclear localization signal (NLS) is located at the RRG2 domain, and its loss is likely to
250 destabilize the EWSR1 protein. The NLS mutant protein failed to rescue *POLQ* exon skipping and
251 failed to restore POLΘ protein expression. To further evaluate the prion-like domain, the domain
252 was subdivided into five parts, and mutant proteins lacking the individual regions were generated
253 (**Fig. S6H**). Interestingly, all mutant forms were able to rescue the POLΘ protein level, albeit with
254 some minor differences, suggesting that the domains have functional redundancies (**Fig. S6I**).
255 Since the prion-like domain of EWSR1 is critical for the formation of condensates of EWSR1 [33],
256 we infer that the formation of EWSR1 condensates may play a role in maintaining the faithful
257 splicing of POLΘ. To test this hypothesis, we generated multiple mutant forms of EWSR1 in which
258 tyrosine residues of the prion-like domain were substituted with serine residues, as previously
259 described[33]. Strikingly, an EWSR1-7YS mutant, in which tyrosine residues were substituted by
260 serine residues, failed to rescue the *POLQ* exon skipping and POLΘ protein expression level in
261 *EWSR1*-depleted cells (**Fig. 3D, E, Fig. S6J, K**). Furthermore, an EWSR1-37YS mutant, in which
262 all thirty-seven tyrosine residues in the prion-like domain were replaced with serine residues, and
263 known to be defective in condensate formation, abolished the ability of EWSR1 to prevent exon
264 skipping of the *POLQ* transcript, further suggesting that condensate formation is critical for
265 faithful splicing. Consistent with these findings, the EWSR1-7YS and EWSR1-37YS mutants
266 failed to rescue MMEJ activity in EWSR1-depleted cells (**Fig. 3F**). Taken together, the prion-like

267 domain of EWSR1 is required for the faithful splicing of the *POLQ* transcript and for the
268 expression of the POLΘ protein, suggesting that condensate formation of EWSR1 is also required
269 for these activities as previously described [5,33].
270
271
272 **The prion-like domain of EWSR1 is critical for interaction with spliceosomes including**
273 **FUBP1 and KHSRP.**
274 The condensate-defective EWSR1 mutant may have lost the ability to bind the *POLQ*-pre
275 mRNA. However, RNA-immunoprecipitation revealed that the EWSR1-7YS and EWSR1-37YS
276 mutants can still bind to the *POLQ* pre-mRNA (**Fig. S4 F-I**). Alternatively, the condensate-
277 defective EWSR1 mutant may be competent for *POLQ* mRNA binding but defective in its
278 interaction with RNA-binding proteins in spliceosomes. To test this hypothesis, we performed an
279 IP/mass spectrometry analysis using HEK293T cells with a biallelic FKBP12-V36F knock-in at
280 the N-terminus of *EWSR1* (**Fig. 3G**). The cDNAs encoding the control V5-tagged *EWSR1*-WT,
281 or the *EWSR1* 37YS mutant, were transduced into the cells and, following dTAG^{v1} treatment,
282 cellular proteins were immunoprecipitated with the anti-V5 antibody. A previous study
283 demonstrated that the prion-like domain of EWS-FLI1 interacts with BAF complex subunit
284 components in condensates [5]. Accordingly, wildtype EWSR1, but not the EWSR1 37YS mutant
285 protein, preferentially bound to BAF subunits, including ARID1A, SMARCA2, SMARCA4, and
286 SMARCC1 (**Fig. 3G, I, Fig. S7A**). In addition to these BAF subunits, additional RNA binding
287 proteins were identified as binding partners of wild-type EWSR1. Intriguingly, the interactors
288 contain prion-like domains, further indicating a functional interaction of EWSR1 with these
289 proteins in spliceosomes (**Fig. 3H**).

290 Since exon skipping in *EWSR1* KO cells is typically observed for exons that are flanked
291 by longer introns (**Fig. S7B**), we focused on FUBP1, among the prion-like domain-dependent
292 EWSR1 binding partners. FUBP1 is a spliceosome known to mediate the splicing of long introns
293 [34] (**Fig. 3H, I**). In addition, KHSRP/FUBP2, known to have a similar function in splicing, was
294 further evaluated. Depletion of FUBP1 or KHSRP alone cause only a minor reduction in POLΘ
295 protein expression or MMEJ activity. However, dual depletion of FUBP1 and KHSRP increased
296 *POLQ* exon25 skipping, reduced the POLΘ protein level, and reduced the cellular MMEJ
297 activity, indicating a functional redundancy between FUBP1 and KHSRP (**Fig. 3 J, K, Fig.**
298 **S7C).** A FUBP1-16YS mutant, with tyrosine residues of its C-terminus region substituted with
299 serine residues, failed to bind to wildtype EWSR1 and failed to rescue the phenotype of
300 FUBP1/KHSRP DKO cells, suggesting that tyrosine residues of EWSR1 and FUBP1 are critical
301 for the protein-protein interaction and for *POLQ* exon25 inclusion (**Fig. 3 L-Q, Fig. S7D)**.
302 Similarly, a KHSRP-17YS mutant failed to rescue the phenotype of FUBP1/KHSRP DKO cells
303 **(Fig. S7E-H)**. Taken together, the protein-protein interaction between EWSR1 and FUBP1 or
304 KHSRP via the prion-like domain is critical for the faithful splicing of the *POLQ* pre-mRNA.
305
306
307 **The EWS-FLI1 oncoprotein inhibits formation of POLQ mitotic foci at DSB loci and**
308 **disrupts MMEJ.**
309 The chromosomal translocation of 11;22 leads not only to the loss of one wildtype EWSR1
310 allele but also to the generation of an oncogenic fusion protein EWS-FLI1 in EwS cells (**Fig. S8A**).
311 Moreover, EWS-FLI1 is known to heterodimerize with EWSR1 and to disrupt its activity [5,35,36].
312 We therefore hypothesized that this oncoprotein may directly or indirectly interfere with MMEJ
313 activity. To test this hypothesis, the EWS-FLI1 oncoprotein was lentivirally expressed in U2OS-

314 based MMEJ reporter cells and evaluated for MMEJ activity. Interestingly, EWS-FLI1 diminished
315 the MMEJ activity in U2OS MMEJ reporter cells (**Fig.4A, Fig. S8B**). Consistent with these
316 results, EwS cell lines exhibited resistance to POLΘ inhibitors, Novobiocin and ART558 [37],
317 compared with osteosarcoma cells U2OS (**Fig. S8C, D)**. The influence of various mutant forms
318 of the EWS-FLI1 fusion oncoprotein on MMEJ activity was tested (**Fig. 4B**). Expression of the
319 SYGQ1-FLI1, SYGQ2-FLI1, ΔSYGQ1, or ΔSYGQ2 mutant by cDNA-mediated transfection
320 decreased the MMEJ activity in the U2OS reporter cells, indicating functional redundancies in the
321 prion-like domain of EWS-FLI1. Interestingly, the EWS-FLI1 37YS mutant, which failed to
322 disrupt MMEJ activity (**Fig. 4B, Fig. S8B**), is defective in condensate formation and in binding to
323 wild-type EWSR1 protein [5,36]. Moreover, expression of EWS-FLI1, but not the EWS-FLI1 37YS
324 mutant, conferred hypersensitivity to topoisomerase inhibitors (**Fig. S8E, F**).
325 To determine the effect of the EWS-FLI1 oncoprotein on MMEJ activity in Ewing sarcoma
326 cells, we transduced an Isce-I-based MMEJ reporter into the A673, RH1, and RD-ES EwS lines.
327 As expected, depletion of EWS-FLI1 from these cells by sgFLI1, as confirmed by western blot,
328 restored MMEJ activity (**Fig. 4C, Fig. S8G**). These EwS lines, with EWS-FLI1 depletion,
329 exhibited resistance to the POLΘ inhibitor, ART558 (**Fig. S8H),** consistent with their restoration
330 of MMEJ following EWS-FLI1 depletion. The minigene reporter assay showed that expression of
331 EWS-FLI1 but not the EWS-FLI1 37YS mutant increased the *POLQ* exon 25 skipping, whereas
332 depletion of EWS-FLI1 in EwS cells ameliorated the *POLQ* exon 25 skipping (**Fig. 4D, E)**.
333 Consistent with a previous study [5], EWS-FLI1 preferentially bound to EWSR1 compared with the
334 EWS-FLI1 37YS mutant, suggesting an inhibitory effect of EWS-FLI1 on EWSR1-mediated
335 splicing (**Fig. 4F**). Given that R-loop accumulation driven by the EWS-FLI1 expression inhibits
336 the recruitment of BRCA1 to the DSB loci, we asked whether R-loop accumulation may be

337 involved in the MMEJ reduction in Ewing sarcoma. Expression of wildtype RNaseH1 or mutant
338 RNaseH1 did not affect EWS-FLI1-mediated MMEJ reduction (**Fig. S8I, J**).
339 Recent studies indicate that DSB repair by POLΘ and MMEJ occurs during mitosis of the
340 cell cycle [38]. POLΘ is phosphorylated by PLK1 and assembles with TOPBP1, along with Rhino
341 and the 9-1-1 complex, into POLΘ foci [18,39]. To assess the influence of EWS-FLI1 expression on
342 the assembly of DSB loci, we engineered endogenously V5-tagged POLΘ expressing MMEJ
343 reporter U2OS cells by CRISPR/Cas9-mediated knock-in. After generation of adenoviral I-SceI-
344 induced DSBs, we performed chromatin-immunoprecipitation (ChIP) with an anti-V5 antibody,
345 followed by qPCR analysis. Overexpression of EWS-FLI1 in these cells disrupted the assembly
346 of POLΘ with sites of DNA double-strand breaks **(Fig. 4G).** Consistent with this result, MMEJ
347 activity and the assembly of POLΘ foci assembly, as measured by immunofluorescence, was
348 decreased by the overexpression of EWS-FLI1 (**Fig. 4H**). Moreover, EWS-FLI1 overexpression
349 in these U2OS cells also increased γH2AX foci, consistent with the loss of MMEJ activity in
350 mitosis. EWS-FLI1 overexpression can therefore reduce POLΘ-mediated DSB repair in mitosis,
351 at a time when POLΘ-mediated MMEJ is highly active [18,39]. EWS-FLI1 was also depleted in
352 endogenously V5-tagged POLΘ expressing A673 cells. As predicted, the loss of EWS-FLI1
353 restored POLΘ foci assembly (**Fig. 4I).** Collectively, the EWS-FLI1 oncoprotein can reduce the
354 level of POLΘ mitotic foci, leading to a functional impairment of MMEJ in EwS cells.
355
356
357 **Inhibition of the FA, NHEJ, or HR pathways efficiently kills the MMEJ-deficient Ewing**
358 **sarcoma cells via synthetic lethality.**
359 Recent studies have shown that targeting the Fanconi Anemia (FA) pathway is synthetic
360 lethal with MMEJ deficiency[40-43]. We therefore hypothesized that MMEJ-defective Ewing

361 sarcoma cells would exhibit high dependence on the FA/BRCA signaling pathway. Indeed,
362 depletion of FANCA, FANCI or FANCL efficiently reduced colony forming activity in the
363 control A673 cells, whereas it showed only a minor impact on the EWS-FLI1-depleted A673
364 cells (**Fig. 5A**). Moreover, depletion of the EWS-FLI1 oncoprotein reduced FANCD2 foci
365 assembly with Mitomycin C (MMC) treatment in Ewing sarcoma cells, A673 and TC32 cells,
366 whereas sgFLI1 did not affect the activation of the pathway in U2OS cells (**Fig. 5B, S5A, B**).
367 Since RBM39 degraders are potent FA pathway inhibitors, by inducing intron retention of the
368 *FANCD2* pre-mRNA[44], we tested the effect of RBM39 degraders, E7820 and Indisulam, on the
369 FA pathway in Ewing sarcoma cells, A673 cells. Consistently, RBM39 degraders decreased
370 FANCA and FANCD2 protein expression in A673 cells (**Fig. 5C**). Intriguingly, RBM39
371 degraders eliminated Ewing sarcoma cells efficiently (**Fig. 5D, E**), which can be rescued by
372 depletion of the EWS-FLI1 oncoprotein in A673 and TC32 cells (**Fig. 5F, G, S5C, D**). These
373 data indicate that targeting the FA/BRCA pathway by the RBM39 degraders is a promising
374 therapeutic strategy for Ewing sarcoma cells.
375 Since inhibiting two of three DSB repair pathways is synthetically lethal in cells [45,46], we
376 asked whether inhibition of NHEJ or HR would also provide a viable therapeutic modality in
377 MMEJ-deficient Ewing sarcoma cells. Previous studies have shown that inhibitors of NHEJ are
378 synthetic lethal with MMEJ loss [45,46]. Consistent with our study, EwS cells are sensitive to DNA-
379 PK inhibitors, known to inhibit NHEJ and enhance the activity of cytotoxic agents in these cells
380 [47]. We confirmed that EwS cell lines are sensitive to the DNA-PKci (**Fig. S5E**) and have an
381 elevated baseline level of activated pDNA-PKc (**Fig. S5F**). EwS cells exhibited high phospho-
382 RPA, a replication stress biomarker, and were hypersensitive to the topoisomerase inhibitors,
383 topotecan, and etoposide (**Fig. S8A, S9G, H**). Since etoposide is used in dose-intensive

384 chemotherapy of Ewing sarcoma, we asked whether inhibition of NHEJ could increase the
385 therapeutic efficacy of etoposide in EWS cells. Strikingly, the DNA-PK inhibitor, Peposertib,
386 enhanced the activity of etoposide in two EWS cell lines (**Fig. S9I, J)**. Moreover, the EwS cell
387 line A673, grown as a xenograft, was also sensitive to peposertib, *in vivo*, and the drug enhanced
388 the activity of etoposide (**Fig. 5H, I, Fig. S9K, L**). Consistent with the enhanced sensitivity to
389 peposertib, immunohistochemistry analysis of the EwS primary patient samples revealed an
390 elevated baseline level of pDNA-PKc compared with Osteosarcoma patient samples (**Fig. 5J**).
391 On the other hand, EWS-FLI1- but not EWS-FLI1-YS mutant-expressing cells are more
392 dependent on BRCA2, confirming that the HR pathway is also a rational target in MMEJ-
393 deficient EwS cells (**Fig. 5A, K**). Previous studies have also suggested that EwS cells are
394 sensitive to HR inhibitors, perhaps through a mechanism of synthetic lethality. CDK12 is a
395 known activator of HR repair, based on its ability to promote the transcription of long HR genes
396 [48]. A targeted inhibitor of CDK12 is known to enhance the killing of EwS cells [49], though the
397 mechanism of this cell killing was unclear. Consistent with this report, EwS cell lines are
398 sensitive to the CDK12 inhibitors THZ531 and MFH290 (**Fig 5 L, M**). Depletion of the EWS-
399 FLI1 oncoprotein in the EwS cells resulted in a restoration of MMEJ activity and acquisition of
400 CDK12i resistance (**Fig 5N, O, Fig. S9M, N**). Taken together, the killing of the EwS cells by an
401 HR inhibitor results mechanistically from synthetic lethality between the HR pathway and the
402 MMEJ pathway.
403
404
405

406 **DISCUSSION**

407 Despite the high sensitivity to DNA-damaging agents, EwS cells, expressing the EWS-
408 FLI1 fusion oncoprotein, have a remarkably low somatic mutation burden [30,50,51]. This
409 observation suggested that EwS cells are deficient in an error-prone DNA repair mechanism,
410 such as MMEJ. Indeed, CRISPR screens confirmed that the knockout of the EWSR1 gene
411 functionally resembles the knockout of known MMEJ genes, such as *POLQ*, *XRCC1*, *APEX2*,
412 and *RHNO1*, suggesting that EWSR1 protein cooperates with these other encoded proteins in the
413 MMEJ pathway. Moreover, EWSR1-deficient cancer cell lines and EwS tumors have a low ID6
414 mutational signature, indicating a low level of microhomology-mediated repair of double-strand
415 breaks. Since EWSR1 has a known function as a mRNA splicing factor [35,52-54], we hypothesized
416 that EWSR1 may regulate MMEJ indirectly through its splicing of the mRNA encoding a MMEJ
417 protein. EWSR1 is indeed required for the accurate splicing of the long mRNA encoding the
418 critical MMEJ polymerase, POLΘ, although it is not required for splicing of mRNAs encoding
419 other MMEJ proteins. Disruption of EWSR1 activity in EwS cells results in skipping of multiple
420 exons in the *POLQ* pre-mRNA, especially exon 25, leading to decreased POLΘ expression in
421 EwS cells and to a strong MMEJ defect.

422 In contrast to previous reports, our study indicates that EwS tumors are competent for
423 high-fidelity DNA repair pathways, such as the homologous recombination pathway, and the
424 tumors are PARP inhibitor-resistant. Other recent studies indicate that EwS cells are dependent
425 on the HR genes, BRCA1, BARD1, and PALB2 [55,56] for survival. Previous studies have also
426 demonstrated that HR deficiency is synthetic lethal in cells with a MMEJ deficiency [22,41,57].
427 Accordingly, the strong MMEJ defect in EwS cells could result in an increased reliance on HR
428 repair.

429 The chromosome 11/22 translocation in EwS cells and the generation of the EWS-FLI1
430 fusion oncoprotein appears to account, at least in part, for the cellular defect in EWSR1 splicing
431 activity. First, since one allele of EWSR1 is disrupted by the chromosome translocation, the
432 EwS cells already have a 50% reduction in EWSR1 protein expression. Second, the EWS-FLI1
433 oncoprotein heterodimerizes with EWSR1 and exerts a dominant negative effect on EWSR1
434 function [5]. Our studies indicate that loss of EWSR1 function can account for the decreased
435 expression of POLΘ protein, the elevated exon 25 skipping of the *POLQ* pre-mRNA, and the
436 defective MMEJ activity in EwS cells. Enhanced expression of the EWSR1 protein, or acute
437 knockdown of the EWS-FLI1 oncoprotein, can reverse these defects and restore MMEJ activity,
438 thereby reducing the cellular reliance on other DSB repair pathways, such as HR and NHEJ.

439 Splicing of specific mRNAs is regulated, at least in part, by RNA Binding Proteins
440 (RBPs) which function in membrane-less condensates. Condensates known as nuclear speckles
441 are required for splicing activity[58]. Many RNPs, including the EWSR1 protein, contain a prion-
442 like domain (PrLD), allowing the proteins to assemble with other RBPs contained in
443 condensates. We reasoned that EWSR1 might interact with other RBPs and function
444 cooperatively as a spliceosome for the *POLQ* pre-mRNA. Moreover, disruption of the PrLD of
445 EWSR1, through the generation of multiple Tyrosine to Serine (YS) mutations, disrupts the
446 assembly of functional spliceosomes. Indeed, the EWSR 37YS mutant, known to be defective in
447 condensate assembly [5], also fails to correct exon 25 skipping of the *POLQ* mRNA, and fails to
448 restore POLΘ protein expression. IP/Mass Spectrometry identified specific RBPs that interact
449 with EWSR1. Interestingly, multiple RBPs containing prion-like domains were identified in the
450 immune complexes, and these proteins did not coimmunoprecipitate with the EWSR1 37YS
451 mutant protein. Components of SWI/SNF complexes, including subunits of the cBAF complex

452 with prion-like domains, were also found to interact with EWSR1 and EWS-FLI1, consistent
453 with a previous report [5]. Unlike EWSR1, other FET proteins containing PrLD domains, such as
454 FUS and TAF15, were not required for accurate *POLQ* splicing, suggesting that EWSR1 forms
455 distinct RBP complexes, perhaps functioning in distinct condensates. Taken together, EWSR1
456 may act as a "hub" for spliceosomes, using its specific prion-like domain for binding to a distinct
457 set of RBPs and for splicing of the *POLQ* mRNA and probably other mRNAs. Expression of
458 EWS-FLI1 disrupts this splicing mechanism.

459 Some RNA binding proteins, including FUBP1 and KHSRP/FUBP2, specifically interact
460 with wildtype EWSR1, but not with the EWSR1 37YS mutant. FUBP1 and KHSRP have high
461 similarity in their protein sequence and exhibit functional redundancy in their splicing activity [59].
462 FUBP1 and KHSRP are multifunctional RNA binding proteins and are known to redundantly
463 regulate the splicing of the SMN2 mRNA [59]. A carboxy-terminal, tyrosine-rich region is present
464 in both FUBP1 and KHSRP/FUBP2 [60]. However, the biological functions of the tyrosine-rich
465 regions of FUBP1 and KHSRP have remained unclear. Since the tyrosine residues of the prion-
466 like domain are critical for liquid-liquid phase separation[61,62] and condensate formation, a YS
467 mutant of FUBP1 or KHSRP, may fail to form condensates with EWSR1 and may lead to
468 aberrant splicing events, such as *POLQ* exon skipping. FUBP1 is crucial for splicing long
469 introns [34] such as the long intron 24/25 in the *POLQ* pre-mRNA. Therefore, a condensate
470 formed by EWSR1-FUBP1/KHSRP may be required for the accurate splicing of exons trapped
471 between long introns. Interestingly, the dual knockout of FUBP1 and KHSRP, like the knockout
472 of EWSR1, results in exon 25 skipping of the *POLQ* mRNA and a reduction in POLΘ protein
473 expression and MMEJ. Re-expression of the wildtype FUBP1, but not of the FUBP1-YS
474 mutant, rescued these defects in the dual knockout cells. The RBPs, EWSR1, FUBP1, and

475 KHSRP therefore appear to functionally interact via their PrLD domains and to cooperate in a
476 EWSR1-initiated splicing pathway for the *POLQ* mRNA (**Fig. S10**).

477 Given that overexpression of EWS-FLI1 oncoprotein induces extensive DNA damage[63],
478 we reasoned that the EWS-FLI1 fusion oncoprotein could impair MMEJ activity in EwS cells.
479 Indeed, the acute degradation of the EWS-FLI1 oncoprotein rapidly rescued MMEJ, suggesting
480 an acute upregulation of POLΘ expression and POLΘ mitotic foci. While the EWS-FLI1
481 protein forms condensate with EWSR1, it disrupts the function of EWSR1, reduces POLΘ
482 expression, and inhibits MMEJ. The EWS-FLI1-37YS mutant fails to form condensates with
483 wild-type EWSR and fails to reduce MMEJ. While knockout of EWS-FLI1 restores MMEJ, loss
484 of the oncoprotein is also detrimental to EwS cell growth and results in a reduction in the
485 transcription of EWS-FLI1 target genes which contributes to EwS cell growth.

486 Previous studies on the pathogenesis of Ewing Sarcoma have focused primarily on the
487 transcriptional activity of the EWS-FLI1 oncoprotein, driven by the carboxy-terminal FLI1
488 transcriptional domain. Indeed, this oncoprotein upregulates the transcription of genes which in
489 turn promote R-loops and the neoplastic growth of the EwS tumor. Our study also provides new
490 insights into the pathogenesis of the cancer. While the chromosome 11/22 translocation results
491 in the formation of the EWS-FLI1 oncoprotein, it also simultaneously inactivates the EWSR1
492 *tumor suppressor* function. One allele of this EWSR1 tumor suppressor gene is inactivated by
493 the translocation itself, and the remaining EWSR1 suppressor function is inactivated by the
494 binding of the fusion oncoprotein to the remaining EWSR1 protein. Due to the loss of the
495 splicing activity of EWSR1, the tumor cells exhibit the characteristic MMEJ defect- namely,
496 radiation sensitivity, a defect in microhomology-mediated DSB repair, and a hypo-mutable
497 phenotype. The splicing defect may also result in the inactivation of other tumor suppressor

498 genes and a more direct role in the process of oncogenesis. For instance, the EWS-FLI1 fusion
499 protein may have additional direct oncogenic functions beyond its ability to promote
500 transcription, R-loops, and replication stress. Specifically, the EWS-FLI1 fusion can disrupt
501 PLK1-activated POLΘ mitotic foci [39] which are known sites of TOPBP1-mediated DSB repair.
502 Given that inhibition of MMEJ under replication stress leads to sensitization to PARPi and
503 ATRi[64], an MMEJ defect in Ewing sarcoma, despite its HR proficiency, may be responsible for
504 its sensitivity to these drugs. Accordingly, the EWS-FLI1 oncoprotein may further block the
505 repair of DSBs in mitosis, promote the formation of micronuclei, and enhance genomic
506 instability.

507 Taken together, *Ewing sarcoma is the first known cancer with loss of MMEJ activity.* The
508 impairment of the MMEJ pathway in EwS prompted us to target the FA, NHEJ, or HR pathways,
509 the three DNA repair pathways known to be synthetic lethal with MMEJ loss. Indeed, EwS cells
510 are sensitive to the RBM39 degraders, which lead to the disruption of the FA pathway. In
511 addition, EwS cells are sensitive to a NHEJ inhibitor, peposertib, as a monotherapy. Peposertib
512 is also synergistic with the genotoxic drug, Etoposide, in killing EwS cells. Accordingly, the use
513 of this drug combination could reduce the need for high doses of Etoposide for EWS patients and
514 thereby reduce its long-term toxicity, such as therapy-related leukemia[65]. EWS cells, due to
515 their MMEJ defect, are also sensitive to the HR inhibitor, THZ531, a CDK12 inhibitor. This
516 inhibitor is one of the first known inhibitors of the HR pathway. Exon 25 skipping of the *POLQ*
517 mRNA in fresh tumor samples may provide a biomarker for identifying tumors with an
518 underlying MMEJ defect which may in turn respond to targeted NHEJ inhibitors or HR
519 inhibitors through the mechanism of synthetic lethality.

520

521 **ACKNOWLEDGMENTS**

522 We thank members of the D'Andrea laboratory for their helpful suggestions and comments. We
523 thank Harvard Medical School and the Dana-Farber/Harvard Cancer Center in Boston, MA, for
524 the use of the Animal, Flowcytometry, and Taplin Mass Spectrometry core facilities. This work
525 was supported by U.S. National Institutes of Health grants R01HL052725 and R01CA296618
526 (A.D.D), the Breast Cancer Research Foundation (A.D.D.), the Ludwig Center at Harvard
527 (A.D.D.), the David Liposarcoma Research Initiative at Harvard (A.D.D.), and the Smith Family
528 Foundation (A.D.D.), and the Alex's Lemonade Stand Foundation (S.A.). This work was also
529 supported by U.S. National Institutes of Health grants P50 CA168504 (A.D.D, G.I.S.), P50
530 CA240243 (A.D.D., G.I.S.), the SENSHIN Medical Research Foundation (S.A.), the Japan
531 Society for the Promotion of Science Overseas Research Fellowships (S.A.), NCI K08 Career
532 Development Award (R.G.), the DoD PRCRP Fellow Career Development Award (R.G.), the
533 ASCO Career Development Award (R.G.), the Rally Foundation Career Development Award
534 (R.G.) and the Boston Children's Hospital TRP Mentored Career Development Award (R.G.).

535

536 **AUTHOR CONTRIBUTIONS**

537 S.A and A.D.D. conceived the study. S.A., G.Z., J.P.A., Y.H., D.R.I., S.M. and L.J. designed and
538 performed biological experiments and analyzed the data. S.A. and Y.H designed and performed
539 animal experiments. Y.T., H.N. and R.G. performed computational analysis. N.W.A. performed
540 AlphaFold analysis. M.D.B., J.J.T and S.I.R. performed IHC analysis using patient samples. K.P.,
541 E.M.V.A. and G.I.S. provided scientific inputs. S.A. and A.D.D. wrote the manuscript.

542

543

544 **FIGURE LEGENDS**

545 **Figure 1: *EWSR1* knock-out cells display MMEJ-deficient phenotypes through POLΘ**
546 **protein reduction.**

547 (A) Immunoblotting analysis for the detection of EWSR1 in RPE p53-/- clones edited with
548 CRISPR-Cas9.

549 (B, C) U2OS I-SceI-based (B, n=9) or Cas9-based (C, n=4) or were transduced lentivirally
550 transduced with control sgRNA or sgRNA targeting *EWSR1* or *POLQ* (co-expressing puromycin
551 resistance gene). Cells were treated with puromycin for 4 days, and then subjected to MMEJ
552 reporter analysis.

553 (D) Colony formation assay data of DLD1 *BRCA2* wild-type and *BRCA2* knockout cells
554 transduced with control, sg*POLQ* or sg*EWSR1* (n=3, left). Shown are representative images of the
555 colonies (right).

556 (E) RPE *TP53-/-* 3xFLAG-*POLQ* knock-in cells were lentivirally transduced with Cas9 and a
557 sgRNA targeting control (NT), *EWSR1* or *POLQ* (co-expressing puromycin resistance gene). After
558 puromycin selection, cells were subjected to immunoblotting analysis.

559 (F) HEK293T 3xFLAG-*POLQ* single knock-in cells and HEK293T 3xFLAG-*POLQ*/2xHA-
560 FKBP12 V36F *EWSR1* double knock-in cells are treated with DMSO or $dTAG^{V1}$ for indicated
561 time. Cell lysates were extracted and followed by immunoblotting analysis.

562 (G) Immunofluorescence analysis showing DNA damage-induced the foci formation of V5-tagged
563 endogenous POLΘ was decreased by EWSR1 depletion (scale bars = 2μm).

564 (H) U2OS MMEJ reporter cells (I-SceI based) were transduced with a control vector or POLQ
565 cDNA (co-expressing blasticidin resistance gene). After blasticidin selection, cells were
566 subsequently transduced with Cas9 and a sgRNA targeting control or EWSR1 (co-expressing

567 puromycin resistance gene). After puromycin selection, cells were subjected to MMEJ reporter
568 analysis (n=4).
569 (I) RPE *p53*-/- cells and RPE *p53*-/- *EWSR1* knockout cells were transduced with control, wildtype
570 *EWSR1* or *POLQ* cDNA. Colony formation assays were performed in the presence of Topotecan
571 (n=3).
572
573
574 **Figure 2: Disruption of MMEJ activity in Ewing sarcoma is driven by *POLQ* exon skipping.**
575 (A) Volcano plots showing alternatively spliced skipped exon (SE) in RPE *p53*-/- *EWSR1* knock-
576 out cells compared with RPE *p53*-/- cells defined by deep RNA-seq analysis.
577 (B) Sashimi plots of the alternative splicing events in control and *EWSR1* knock-out RPE *p53*-/-
578 cells: the region between exon24 and exon26 of the *POLQ* transcript.
579 (C) U2OS endogenous V5 tagged- POLΘ expressing cells were transduced with Cas9 and sgRNA
580 targeting the indicated exon of the *POLQ* gene. Cell lysates were extracted and followed by
581 immunoblotting analysis.
582 (D) U2OS MMEJ ver.2 (Cas9-based) cells were lentivirally transduced with control sgRNA or
583 sgRNA targeting different *POLQ* exons (co-expressing puromycin resistance gene). Cells were
584 treated with puromycin for 4 days, and then subjected to MMEJ reporter analysis (n=4).
585 (E) *POLQ* mRNA without exon 25 produces shorter POLΘ which is unstable. Blot showing
586 HEK293T cells transfected with FLAG-*POLQ* cDNA containing *POLQ* full-length CDS or CDS
587 lacking exon25. Cells were treated with CHX for 3–9 hr.
588 (F) HEK293T *POLQ* knockout cells were transfected with MMEJ reporter (ver.2) and sgRNA
589 targeting the reporter together with control vector or indicated *POLQ* cDNA. 48h after
590 transfection, cells were subjected to FACS analysis to measure the MMEJ activity (n=3).

591 (G) Schematic representation of the minigene reporter construct (left). K562 cells carrying the
592 minigene reporter were lentivirally transduced with Cas9 and sgRNA targeting the indicated genes.
593 Shown are relative frequencies of mNeonGreen positive fraction within mScarlet positive cells
594 (right, n=3).
595 (H) RT-PCR showing the exon 7 and exon 25 skippings of *POLQ* transcript in Ewing sarcoma cell
596 lines.
597 (I) Immunoblotting analysis showing the lower levels of POLΘ expression in Ewing sarcoma cell
598 lines compared to U2OS cells.
599 (J) rMATS analysis showing *POLQ* exon skipping events in primary samples from pediatric cancer
600 patients. n = 498 (EWS = 44, NBL = 131, OS = 88, WT = 110, RMS = 125).
601 (K) RNA-seq data from the patient sample shows the *POLQ* mRNA expression is significantly
602 lower in Ewing sarcoma patients compared with RMS/WT. n = 832 (EWS = 83, NBL = 195, OS
603 = 182, WT = 162, RMS = 210).
604 (L, M) Low somatic SNV and MMEJ deletion mutation burden in Ewing sarcoma tumors (ES; n
605 = 23) as compared to neuroblastoma tumors (NB; n = 47). Short somatic mutations were
606 determined from the whole genome sequencing data of tumors and matched normals. Each dot in
607 K represents the total number of somatic SNVs for each tumor. Each dot in L represents the
608 proportion of 3+-bp deletions with 2+-bp microhomology among all indels of each tumor.
609
610 **Figure 3: Formation of EWSR1 condensates through the prion-like domain is critical for**
611 **faithful splicing of *POLQ* transcript via interacting with FUBP1 and KHSRP/FUBP2.**
612 **(A)** Schematic representation of the individual domains of EWSR1 and the deletion mutants used
613 in Fig.3B, C.

614 (B, D) RPE *p53*-/- 3xFLAG-*POLQ*/2xHA-FKBP12 V36F *EWSR1* double knock-in cells were
615 retrovirally transduced with empty vector, wildtype EWSR1, or indicated EWSR1 mutants. After
616 transduction, cells were treated with blasticidin for four days. Then, cells were treated with DMSO
617 or 1μM $dTAG^{v1}$ for 24hr. After $dTAG^{v1}$ treatment, cell lysates were subjected to immunoblot
618 analysis.
619 (C, E) RT-PCR showing the *POLQ* exon 25 skipping in the indicated cells.
620 (F) U2OS MMEJ ver.2 (Cas9-based) cells were lentivirally transduced with control sgRNA or
621 sgRNA targeting *EWSR1* together with empty vector wild-type EWSR1 or the indicated EWSR1
622 mutants by retroviral transduction. Cells were treated with puromycin and blasticidin for 4days,
623 and then subjected to MMEJ reporter analysis (n=4).
624 (G) Volcano plots comparing detected protein levels by IP-MS between EWSR1 wildtype and the
625 EWSR1 37YS mutant.
626 (H) A ven diagram showing the frequency of all the genes and positive hits with a prion-like
627 domain identified by PLAAC.
628 (I) Immunoprecipitation followed by immunoblotting analysis showing wildtype EWSR1
629 preferentially bound to FUBP1, KHSRP, SMARCA4 and SMARCC1 compared to the EWSR1
630 mutants.
631 (J) FUBP1/KHSRP DKO cells exhibited POLΘ protein reduction (upper) and increased *POLQ*
632 exon 25 skipping (lower).
633 (K) MMEJ activity was profoundly decreased in FUBP1/KHSRP DKO cells measured by U2OS
634 MMEJ ver.2 cells (n=4).
635 (L) Schematic representation of wildtype and YS-mutated EWSR1 or FUBP1.

636 (M) Immunoblotting showing wildtype FUBP1 preferentially bound to EWSR1 compared to the
637 FUBP1 16YS mutant.
638 (N) U2OS MMEJ ver.2 cells were lentivirally and retrovirally transduced with indicated sgRNA(s)
639 (co-expressing puromycin resistance gene) and control or FUBP1 cDNA (co-expressing
640 blastidcidin resistance gene). Cells were treated with puromycin and blasticidin for 4days, and then
641 subjected to MMEJ reporter analysis (n=4).
642 (O) RPE *p53*-/- 3xFLAG-*POLQ*/2xHA-FKBP12 V36F *EWSR1* double knock-in cells were
643 lentivirally transduced with Cas9 and a sgRNA targeting control (NT) or sgRNAs targeting FUBP1
644 and KHSRP together with retrovirally transduced with a control vector, wildtype FUBP1 or the
645 FUBP1 16YS mutant. After puromycin and blasticidin selection, cells were subjected to
646 immunoblotting analysis.
647 (P) RT-PCR showing the *POLQ* exon25 skipping in the indicated cells.
648
649 **Figure 4: Expression of EWS-FLI1 perturbs POLΘ foci assembly, resulting in impairment**
650 **of MMEJ.**
651 (A) I-SceI-based MMEJ reporter cells were lentivirally transduced with an empty vector, wild-
652 type *EWS-FLI1* or the FKBP12 V36F-tagged *EWS-FLI1*. Cells were treated with 1uM dTAG^{V1}
653 for 18hr, and then adenovirally transduced with I-sceI. 48hr after I-sceI transduction, the
654 frequencies of GFP positive cells were assessed by FACS (n=6).
655 (B) Schematic representation of the EWS-FLI and mutant forms of EWS-FLI1 used in MMEJ
656 reporter assay (left). I-SceI-based MMEJ reporter cells were lentivirally transduced with an empty
657 vector, wild-type *EWS-FLI1* or indicated mutant forms of *EWS-FLI1* (co-expressing puromycin

658 resistance gene). After puromycin selection, cells were subjected to MMEJ reporter assay (right,
659 n=6).
660 (C) I-SceI based MMEJ reporter was lentivirally transduced with U2OS, A673, RH1 and RD-ES
661 cell lines. Cells were subsequently transduced with Cas9 together with control sgRNA or sgRNA
662 targeting FLI1. Cells were treated with puromycin for 4days, and then subjected to MMEJ reporter
663 analysis (n=3).
664 (D) EWS-FLI1 but not the EWS-FLI1 37YS mutant increased *POLQ* exon 25 skipping measured
665 by K562 minigene reporter cells (n=6).
666 (E) A673 and TC32 cells carrying the minigene reporter showing depletion of EWS-FLI1
667 decreased *POLQ* exon 25 skipping (n=3).
668 (F) Immunoprecipitation followed by immunoblotting analysis showing wildtype EWS-FLI11
669 preferentially bound to EWSR1 compared to the EWS-FLI1 37YS mutant.
670 (G) ChIP-qPCR assay showing expression of EWS-FLI1 perturbed POLΘ assembly to the DSB
671 loci induced by Isce-I (n=2).
672 (H) Immunofluorescence analysis showing endogenous V5-tagged POLΘ foci formation was
673 perturbed by EWS-FLI1 expression both asynchronous and mitotic arrested cells. Cells were
674 treated with 2Gy irradiation and then incubated for 4hr (scale bars = 2μm).
675 (I) Immunofluorescence analysis showing endogenous V5-tagged POLΘ foci formation was
676 restored by EWS-FLI1 depletion in V5-tagged-*POLQ* knock-in A673 cells. Cells were treated with
677 2Gy irradiation and then incubated for 4hr (scale bars = 2μm).
678
679 **Figure 5: Inhibition of FA, NHEJ or HR efficiently eliminates Ewing sarcoma cells.**
680

681 (A) Colony forming assay showing that the control A673 cells exhibited higher dependence on
682 *FANCA*, *FANCI*, *FANCL*, and *BRCA2* genes compared with the EWS-FLI1-depleted A673 cells
683 by sg*FLI*1.
684 (B) Immunofluorescence analysis showing FANCD2 foci formation was increased by EWS-FLI1
685 expression in A673 cells. Cells were treated with 10ng/ml MMC for 24hr. Shown are the number
686 of FANCD2 foci (left) and the representative images of the cells treated with MMC (right, scale
687 bars = 2um).
688 (C) Immunoblotting analysis of the cell lysates from A673 cells treated with DMSO, 250nM
689 E7820 or 250nM Indisulam for 72hr. Treatment with RBM39 degraders decreased FANCA and
690 FANCD2 protein expression.
691 (D, E) The CTG assay showing that compared with U2OS, Ewing sarcoma cells showed
692 hypersensitivity to RBM39 degraders, E7820 (D) and Indisulam (E).
693 (F, G) The CTG assay showing that depletion of EWS-FLI1 by sgFLI1 in TC32 cells led to
694 acquisition of resistance to RBM39 degraders, E7820 (F) and Indisulam (G).
695 (H, I) Xenograft model using TC32 showing therapeutic efficacy of a Peposertib and Etoposide.
696 NSG mice (n = 10 mice/group) bearing luciferized TC32 cells were treated with 100 mg/kg of
697 Peposertib (orally), 8 mg/kg etoposide (via IP), or both for 2 weeks. Tumor sizes were measured
698 every 2-3 days (H) and also monitored by bioluminescence images (I).
699 (J) Immunohistochemistry analysis from the patient samples of EwS (n=8) showing higher pDNA-
700 PKc activities compared with that of OS (n=9).
701 (K) Colony formation assay data of RPE *p53*-/- cells transduced with a control vector, EWS-FLI1
702 or EWS-FLI1 37YS together with or without BRCA2 depletion (n=3, top) and the representative
703 colony images (bottom).

704 (L, M) The CTG assay showing that compared with U2OS, Ewing sarcoma cells showed
705 hypersensitivity to CDK12 inhibitors, THZ531 (L) and MFH290 (M).
706 (N, O) The CTG assay showing that depletion of EWS-FLI1 by sg*FLI*1 in TC32 cells led to
707 acquisition of resistance to CDK12 inhibitors, THZ531 (N) and MFH290 (O).

708 **Supplementary Figure 1: *EWSR1* loss is synthetic lethal with BRCA1/2 deficiency.**

709 (A) A Venn diagram showing overlap between genes identified in the previously reported CRISPR
710 screens to identify synthetic *BRCA2* lethality and genes whose dependence is positively correlated
711 with *POLQ* in the Depmap analysis.

712 (B-F, I) Colony formation assay data of RPE *p53*-/- cells and RPE *p53*-/- *EWSR1* knock-out clones
713 treated with X-ray (B), VE822 (C), Topotecan (D), Etoposide (E), Olaparib (F) and Novobiocin (I
714 4) (n=4).

715 (G) U2OS DR-GFP reporter cells (I-SceI based) were transduced lentivirally transduced with
716 control sgRNA or sgRNA targeting EWSR1, BRCA1 or BRCA2 (co-expressing puromycin
717 resistance gene). Cells were treated with puromycin for 4days, and then subjected to reporter
718 analysis (n=3).

719 (H) Schematic representation of the Cas9-based MMEJ reporter assay (ver.2).

720 (J, K) Colony formation assay data of MDA-MB-436 (J, n=3) and HCC1937 (K, n=3) cells and
721 the cells complemented with BRCA1 cDNA transduced with control, sg*POLQ* or sg*EWSR1* (left).
722 Shown are representative images of the colonies (right).

723 (L) RPE *p53*-/- cells were lentivirally transduced Cas9 (expressing balasticidin resistance gene).
724 After balasticicin selection, cells were lentivirally transduced with a sgRNA targeting control,
725 *POLQ* or *EWSR1* (co-expressing GFP) together with with a sgRNA targeting control, *BRCA1* or
726 *BRCA2* (co-expressing tRFP657). 72hr after the sgRNA transduction, the frequency of the
727 GFP/tRFP657 cells was traced by FACS (n=3).

728

729 **Supplementary Figure 2: Subacute depletion of EWSR1 results in POLΘ protein loss.**

730 **(A)** RPE *TP53-/-* 3xFLAG-POLQ knock-in cells were transduced with Cas9 and a sgRNA
731 targeting *EWSR1* by electroporation. Single clones are isolated 7days after electroporation. Shown
732 are immunoblotting analyses for FLAF- POLΘ, EWSR1 and GAPDH in control cells and *EWSR1*
733 knockout clones.
734 (B) Colony formation assay data of RPE *p53*-/- 3xFLAG-*POLQ* knock-in cells and RPE *p53*-/-
735 *EWSR1* knock-out 3xFLAG-*POLQ* knock-in clones treated with X-ray (n=3).
736 (C) RPE *p53*-/- 2xHA-FKBP12 V36F *EWSR1* cells were treated with DMSO, 1μM $dTAG^{13}$ or
737 1μM $dTAG^{v1}$ for 24hr. The cell lysates were extracted and then analyzed by immunoblotting.
738 $dTAG^{v1}$ but not $dTAG^{13}$ efficiently degraded endogenous EWSR1 protein.
739 (D) RPE *p53*-/- 3xFLAG-*POLQ*/2xHA-FKBP12 V36F *EWSR1* double knock-in cells are treated
740 with 1μM $dTAG^{V1}$ for the indicated time. The cell lysates were extracted and then analyzed by
741 immunoblotting.
742 (E) RPE *p53*-/- 3xFLAG-*POLQ*/2xHA-FKBP12 V36F *EWSR1* double knock-in cells are treated
743 with $dTAG^{V1}$ at the indicated concentration for 24hr. The cell lysates were extracted and then
744 analyzed by immunoblotting.
745 (F) RPE *p53*-/- 3xFLAG-*POLQ* single knock-in cells and RPE *p53*-/- 3xFLAG-*POLQ*/2xHA-
746 FKBP12 V36F *EWSR1* double knock-in cells are treated with $dTAG^{V1}$ for indicated time. The cell
747 lysates were extracted and then analyzed by immunoblotting.
748 (G) Immunoblotting analyses showed that BRCA1, BRCA2 and other MMEJ proteins, except for
749 POLΘ, were not affected by *EWSR1* knockout in RPE *p53*-/- cells.
750 (H) RPE *p53*-/- 3xFLAG-*POLQ* knock-in cells were lentivirally transduced with control sgRNA
751 or sgRNA targeting *EWSR1, FUS* or *TAF15* (co-expressing puromycin resistance gene). Cells

752 were treated with puromycin for 4days, and then the cell lysates were extracted and then analyzed
753 by immunoblotting.
754 (I) K562 MMEJ ver.2 (Cas9-based) cells were lentivirally transduced with control sgRNA or
755 sgRNA targeting *EWSR1, FUS* or *TAF15* (co-expressing puromycin resistance gene). Cells were
756 treated with puromycin for 4days, and then cells were subjected to MMEJ reporter analysis (n=3).
757 (J) RPE *p53*-/- cells and RPE *p53*-/- *EWSR1* knockout cells were transduced with control, wildtype
758 *EWSR1* or *POLQ* cDNA. Colony formation assays were performed in the presence of Etoposide
759 (n=3).
760 (K) MDA-MB-436 cells and the cells complemented with BRCA1 were transduced with Cas9 and
761 a sgRNA targeting control or *EWSR1*. Cells were subjected to comet assay to measure unrepaired
762 DNA damage.
763 (L) RPE *p53*-/- cells and RPE *p53*-/- *EWSR1* knockout cells were transduced with Cas9 and a
764 sgRNA targeting control or *BRCA2*. Cells were treated with or without synchronization by 8μM
765 RO3306. 1 hour after removal of RO3306, cells were treated with 2 Gy irradiation and then
766 incubated for 24 hours. The frequency of micronuclei positive cells is shown.
767
768 **Supplementary Figure 3: EWSR1 prevents multiple exon skipping events of the *POLQ***
769 **transcript.**
770 (A) U2OS MMEJ reporter cells (I-SceI based) were transduced with *POLQ* cDNA (co-expressing
771 blasticidin resistance gene). After blasticidin selection, cells were subsequently transduced with
772 Cas9 and a sgRNA targeting control or *EWSR1* (co-expressing puromycin resistance gene). After
773 puromycin selection, cell lysates were extracted and then analyzed by immunoblotting. See also
774 Fig.2C.

775 (B) RPE *p53*-/- 3xFLAG-*POLQ* knock-in cells were transduced with Cas9 and a control sgRNA
776 or sgRNA targeting *EWSR1* by electroporation. 72hr after electroporation, cells were treated with
777 MG132 or Chloroquine for 4hr. After the treatment, cell lysates were extracted and then analyzed
778 by immunoblotting.
779 (C) A pie chart summarizing alternative splicing event types in RPE *p53*-/- *EWSR1* knock-out cells
780 obtained by MISO analysis.
781 (D-G) Volcano plots showing retained introns (RI) (D), alternatively spliced 5' splice cites (A5SS)
782 (E), alternatively spliced 3' splice cites (A3SS) (F), mutually exclusive exons (MXE) (G) in RPE
783 *p53*-/- *EWSR1* knock-out cells compared with RPE *p53*-/- cells.
784 (H) Volcano plots showing alternatively spliced skipped exon (SE) in HEK293T si*EWSR1*
785 transduced cells compared with control cells defined by RNA-seq analysis (GSE154944).
786 (I) Sashimi plots of the alternative splicing events in control and *EWSR1* knock-out RPE *p53*-/-
787 cells: the region between exon 23 and exon 26 of *POLQ* transcript.
788 (J) RT-PCR showing the exon 7, 21, 22 and 25 skipping of *POLQ* transcript in *EWSR1* knock-out
789 cells derived from RPE *p53*-/- (top) and from RPE *p53*-/-3xFLAG-*POLQ* knock-in cells (bottom).
790 (K) The schematics illustrates the location of protein domains with the primary sequence POLΘ.
791 Numbers refer to amino acid residues. Exo = exonuclease, T = thumb, P = palm, F = fingers. The
792 ribbon illustrations are AlphaFold 3-generated predictions of the WT and truncated form of the
793 POLΘ polymerase domain. The two views represent 180º rotation around the y-axis. Colors
794 illustrate the sub-domain architecture.
795
796 **Supplementary Figure 4: Exon 25 skipping of the *POLQ* transcript decreased POLΘ protein,**
797 **resulting in profound MMEJ deficiencies.**

798 (A) Schematics of the *POLQ* exon 25, intron 24/25 and the design of ASO and sgRNAs targeting
799 the splice sites.
800 (B) Immunoblotting (upper) and RT-PCR (lower) analysis showing that transduction of two ASOs
801 efficiently induced exon 25 skipping and POLΘ protein loss in RPE *p53*-/- 3xFLAG-*POLQ* knock-
802 in cells.
803 (C) U2OS MMEJ ver.2 (Cas9-based) were transduced control or two ASOs targeting *POLQ* exon
804 25 splice sites. 48h after ASO transduction, cells were subjected to MMEJ reporter analysis (n=4).
805 (D) Schematic representation of the endogenous *POLQ* exon 25 and intron 24/25 and the minigene
806 constructs.
807 (E) HEK293T 2xHA-FKBP12 V36F *EWSR1* dknock-in cells were transfected with the indicated
808 minigene construct and then treated with DMSO or $dTAG^{V1}$. 48h after transfection, cells were
809 subjected to assess the endogenous- and minigene- derived *POLQ* exon 25 skipping (left) and
810 FACS analysis to measure the reporter activity (right).
811 (F-H) Binding of EWSR1 to *POLQ* pre-mRNA evaluated using the RNA immuno-precipitation
812 (RIP) assay, performed using an anti-EWS antibody and an anti-HA antibody (N=2). The assay
813 was performed in HEK293T 3xFLAG-POLQ/2xHA-FKBP12 V36F *EWSR1* double knock-in cells
814 in the presence of DMSO or $dTAG^{v1}$. qPCR was performed with primers targeting *POLQ* pre-
815 mRNA around exon 7 and 25, *POLQ* mature mRNA and *GAPDH* (bottom). Shown were
816 immunoblotting for cell lysates with or without immunoprecipitation (F), RIP-qPCR assay for the
817 samples with EWS-IP (G) and HA-IP (H).
818 (I) Binding of multiple EWSR1 mutants to *POLQ* pre-mRNA evaluated using the RNA immuno-
819 precipitation (RIP) assay, performed using anti-EWS antibody. The assay was performed in
820 HEK293T 3xFLAG-*POLQ*/2xHA-FKBP12 V36F *EWSR1* double knock-in cells transduced with

821 a control vector, EWSR1 WT, EWSR1 7YS mutant or EWSR1 37YS mutant in the presence of
822 DMSO or dTAG^{v1}. qPCR was performed with primers targeting *POLQ* pre-mRNA around exon
823 7 and 25 and *GAPDH* (bottom).
824
825 **Supplementary Figure 5: Samples from Ewing sarcoma patients show no HRD genomic**
826 **signatures.**
827 (A-C) Contribution of COSMIC indel (ID)-signature (A) and stacked bar plots of the numbers of
828 indels attributed to COSMIC ID signatures for Ewing sarcoma tumors (ES) (in B), and
829 neuroblastoma tumors (NB) (in C). Short somatic mutations were determined from whole genome
830 sequencing data of tumors and matched normals using GATK4, and SigProfilerAssignment was
831 used to estimate the COSMIC ID signatures from the mutations. Each bar contains relative
832 numbers of indels attributed to specific ID signatures, which are shown in different colors. There
833 are no ES tumors with MMEJ-related ID6 indels (B). In contrast, there are several NB tumors with
834 ID6 indels (C).
835 (D-F) Contribution of COSMIC SNV-signature 3 (D) and stacked bar plots of the number of SNVs
836 attributed to COSMIC SNV signatures for Ewing sarcoma tumors (ES) (in E), and neuroblastoma
837 tumors (NB) (in F). Short somatic mutations were determined from whole genome sequencing
838 data of tumors and matched normals using GATK4, and SigProfilerAssignment was used to
839 estimate the COSMIC SNV signatures from the mutations. Each bar represents estimated numbers
840 of SNVs attributed to specific SNV signatures, which are shown in different colors. There are no
841 ES tumors with MMEJ-related Signature 3 SNVs (E). In contrast, there are several NB tumors
842 with Signature 3 SNVs (F).

843 (G-H) Distribution of insertions and deletions by size in Ewing sarcoma tumors (ES; n = 23), and
844 neuroblastoma tumors (NB; n = 47). Short somatic mutations were determined from the whole
845 genome sequencing data of tumors and matched normals. Each bar represents the proportion of
846 deletions (G) or insertions (H) of a particular size among all deletions or all insertions, respectively,
847 of each cohort.
848 (I) Low templated insertions in Ewing sarcoma tumors (ES; n = 23) as compared to neuroblastoma
849 tumors (NB; n = 47).
850 (J, K) The bar graphs show the length of microhomology at canonical translocation breakpoints in
851 Ewing sarcoma samples from GMKF (J, n=46) and St. Jude (K, N=43) cohorts. All translocations
852 were called using the Manta structural variant caller. Canonical translocations are defined as those
853 impacting one of the following genes: EWSR1, FLI1, ETV1, FEV, FUS, ERG.
854
855 **Supplementary Figure 6: The prion-like domain of EWSR1 is critical for the faithful splicing**
856 **of *POLQ* transcript.**
857 (A) RPE *p53*-/- 3xFLAG-*POLQ* knock-in cells were retrovirally transduced with empty vector,
858 wildtype *EWSR1*, or indicated *EWSR1* mutants (co-expressing blasticidin resistance gene)
859 together with lentivirally Cas9 and a control sgRNA or sgRNA targeting *EWSR1* (co-expressing
860 puromycin resistance gene). Cells were treated with puromycin and blasticidin for 4days, and
861 then cell lysates were extracted and then analyzed by immunoblotting.
862 (B) U2OS MMEJ ver.2 (Cas9-based) cells were lentivirally transduced with control sgRNA or
863 sgRNA targeting *EWSR1* together with empty vector wild-type EWSR1 or the indicated EWSR1
864 mutants by retroviral transduction. Cells were treated with puromycin and blasticidin for 4days
865 and then subjected to MMEJ reporter analysis (n=4).

866 (C-E) Colony formation assay data of RPE *p53*-/- cells and RPE *p53*-/- *EWSR1* knock-out clones
867 transduced with an empty vector, wild-type *EWSR1* or the indicated *EWSR1* mutants by
868 retroviral transduction in the presence of 10nM Topotecan (C), 62.5nM Etoposide (D), or 100nM
869 VE822 (E), respectively. The data is normalized to the DMSO control (n=3).
870 (F, G) K562 cells were lentivirally transduced with sgRNAs targeting control or *EWSR1* (co-
871 expressing puromycin resistance gene) and control or *BRCA2* (co-expressing blasticidin resistance
872 gene). Cells were treated with puromycin and blasticidin for 4days, and then retrovirally
873 transduced with indicated constructs (co-expressing GFP). 72hr after retroviral transduction, the
874 change of frequency of GFP positive fraction was traced by FACS (n=3).
875 (H) Schematic representation of the deletion mutants within the prion-like domain used in Fig. S6I.
876 (I) RPE *p53*-/- 3xFLAG-*POLQ*/2xHA-FKBP12 V36F *EWSR1* double knock-in cells were
877 retrovirally transduced with empty vector, wildtype EWSR1, or indicated EWSR1 mutants. After
878 transduction, cells were treated with blasticidin for four days. Then, cells were treated with DMSO
879 or 1μM $dTAG^{v1}$ for 24hr. After $dTAG^{v1}$ treatment, cell lysates were subjected to immunoblot
880 analysis.
881 (J) Wildtype EWSR1 but not the EWSR1 7YS or 37YS mutant rescued POLΘ protein expression
882 in RPE *p53*-/- 3xFLAG-*POLQ* knock-in cells.
883 (K) Wildtype EWSR1 but not the EWSR1 7YS or 37YS mutant prevented *POLQ* exon 25 skipping
884 measured by K562 minigene reporter cells (n=3).
885
886 **Supplementary Figure 7: Exon skipping in *EWSR1* KO cells was typically observed for exons**
887 **that are flanked by longer introns.**

888 (A) Volcano plots comparing detected protein levels by IP-MS between EWSR1 wildtype and
889 control.
890 (B) The length of introns surrounding included, excluded or background exons in *EWSR1*
891 knockout cells identified by RNA-seq analysis.
892 (C) Dual depletion of FUBP1 and KHSRP increased *POLQ* exon 25 skipping measured by K562
893 minigene reporter cells (n=3).
894 (D) The FUBP1 16YS mutant failed to rescue *POLQ* exon 25 skipping induced by FUBP1/KHSRP
895 dual depletion measured by K562 minigene reporter cells (n=3).
896 (E) RPE *p53*-/- 3xFLAG-*POLQ*/2xHA-FKBP12 V36F *EWSR1* double knock-in cells were
897 lentivirally transduced with Cas9 and a sgRNA targeting control (NT) or sgRNAs targeting
898 FUBP1 and KHSRP together with retrovirally transduced with a control vector, wildtype
899 KHSRP or the KHSRP 16YS mutant. After puromycin and blasticidin selection, cells were
900 subjected to immunoblotting analysis.
901 (F) RT-PCR showing the *POLQ* exon25 skipping in the indicated cells.
902 (G) U2OS MMEJ ver.2 (Cas9-based) cells were lentivirally transduced with indicated sgRNA(s)
903 (co-expressing puromycin resistance gene). Cells were treated with puromycin for 4days, and
904 then subjected to MMEJ reporter analysis (n=4).
905 (H) The KHSRP 17YS mutant failed to rescue *POLQ* exon 25 skipping induced by
906 FUBP1/KHSRP dual depletion measured by K562 minigene reporter cells (n=3).
907
908 **Supplementary Figure 8: Depletion of EWS-FLI1 ameliorates MMEJ activity in Ewing**
909 **sarcoma cells.**

910 (A) The cell lysates were extracted from an Osteosarcoma cell line U2OS and Ewing Sarcoma cell
911 lines (A673, TC32, TC71, RH1, and RD-ES, and then analyzed by immunoblotting.
912 (B) Cas9-based MMEJ reporter cells were lentivirally transduced with an empty vector, wild-type
913 *EWS-FLI1* or indicated mutant forms of *EWS-FLI1* (co-expressing puromycin resistance gene).
914 After puromycin selection, cells were subjected to MMEJ reporter assay (n=3).
915 (C, D) the CellTiter-Glo® (CTG) assay showing Ewing sarcoma cells showed resistance to POLΘ
916 inhibitors, Novobiocin (C) and ART558 (D).
917 (E, F) Colony formation assay data of RPE *p53*-/- cells lentivirally transduced with control vector,
918 EWS-FLI WT or the EWS-FLI1 37YS mutant treated with Etoposide (E) and Topotecan (F) (n=2).
919 (G) The cell lysates used in Fig.4C were extracted and then analyzed by immunoblotting. The
920 black and red arrows showing EWS-FLI1 and FLI1, respectively.
921 (H) The CTG assay shows that depletion of EWS-FLI1 in A673 cells sensitized to ART558.
922 (I) U2OS I-SceI-based MMEJ reporter cells were transduced with control or EWS-FLI1 together
923 with an empty vector, RNaseH1 WT, the RNaseH1 DN, or the RNaseH1 WKKD mutant. Cells
924 were treated with puromycin and blasticidin for 4days and then subjected to MMEJ reporter
925 analysis (n=6).
926 (J) A673 carrying the Isce-I-based MMEJ reporter were transduced with an empty vector,
927 RNaseH1 WT, the RNaseH1 DN, or the RNaseH1 WKKD mutant. Cells were treated with
928 blasticidin for 4days and then subjected to MMEJ reporter analysis (n=3).
929
930 **Supplementary Figure 9: Combination of Peposertib and Etoposide efficiently killed Ewing**
931 **sarcoma cells in vivo.**

932 (A, B) Immunofluorescence analysie showing FANCD2 foci formation was increased by EWS-
933 FLI1 expression in TC32 cells (A) but not by sgFLI1 in U2OS cells (B). Cells were treated with
934 10ng/ml MMC for 24hr. Shown are the number of FANCD2 foci (left) and the representative
935 images of the cells treated with MMC (right, scale bars = 2um).
936 (C, D) The CTG assay showing that depletion of EWS-FLI1 by sg*FLI1* in A673 cells led to
937 acquisition of resistance to RBM39 degraders, E7820 (C) and Indisulam (D).
938 (E) The CTG assay showing that compared with U2OS, Ewing sarcoma cells showed
939 hypersensitivity to Peposertib.
940 (F) Immunoblot analysis showing phospho-DNAPK, DNAPK and GAPDH protein level in U2OS
941 and Ewing sarcoma cell lines.
942 (G, H) The CTG assay showing that compared with U2OS, Ewing sarcoma cells showed
943 hypersensitivity to Topotecan (G) and Etoposide (H).
944 (I, J) The CTG assay showing that a combination of Peposertib and Etoposide showed a strong
945 synergistic effect on Ewing sarcoma cell lines A673 (I) and TC32 (J).
946 (K) Overall survivals showing a therapeutic efficacy of a combination of Etoposide and Peposertib
947 in a TC32 xenograft model (n=10, each group).
948 (L) The changes of the body weight of the treated mice.
949 (M, N) The CTG assay showing that depletion of EWS-FLI1 in A673 cells led to acquisition of
950 resistance to CDK12 inhibitors, THZ531 (M) and MFH290 (N).

951 **Supplementary Figure 10:** The schematic representation of the findings of this study.

952

953 **EXPERIMENTAL MODEL AND SUBJECT DETAILS**

954 **Cell cultures**

955 RPE *p53*-/- cells generated previously[66] were grown in DMEM/F12 containing GlutaMAX
956 (Gibco) and supplemented with 10% fetal bovine serum (FBS) (Sigma-Aldrich). HEK293T
957 (ATCC, CRL-3216) cells were grown in DMEM (Gibco) supplemented with 10%FBS. TC32 and
958 TC71 cell lines were obtained from children cancer repository and grown in RPMI (Gibco)
959 supplemented with 10%FBS. RH-1 (DSMZ, ACC493) cell grown in RPMI 1640 supplemented
960 with 10%FBS, 1% P/S. RD-ES (ATCC, HTB-166) cells were grown in RPMI 1640 supplemented
961 with 20%FBS, 1% P/S. SK-ES1 (ATCC, HTB-86) and SK-PN-DW (ATCC, CRL-2139) cells
962 were cultured in DMEM (Gibco) supplemented with 10%FBS. U2OS parental (ATCC, HTB-96)
963 and carrying a DNA repair template cells were grown in DMEM (Gibco) supplemented with
964 10%FBS. The BRCA1-deficient cell lines HCC1937 (ATCC, CRL-2336) and HCC1954 (ATCC,
965 CRL-2338) and BRCA1-complemented cells were grown in RPMI (Gibco) supplemented with
966 10%FBS. RH-1 (DSMZ, ACC493). K562 (ATCC, CCL-243) cells were grown in RPMI 1640
967 supplemented with 20%FBS, 1% P/S. MDA-MB-436 and MDA-MB-436+BRCA1 cells were a
968 kind gift from Dr. Geoffrey Shapiro (Dana Farber Cancer Institute) and grown in RPMI (GIBCO)
969 supplemented with 10% fetal bovine serum. DLD1 BRCA2 -/- and DLD1 Parental were obtained
970 from Horizon discovery, Waterbeach, UK. U2OS cells with HR reporter (DR-GFP) was a kind
971 gift from Dr. Jeremy Stark (City of Hope).

972 To establish the U2OS-MMEJ reporter cells, U2OS cells were lentivirally transduced with the
973 Isce-I-based (ver.1) or Cas9-based (ver.2) MMEJ reporter and then incubated with puromycin.
974 After selection with puromycin, a single clone was isolated and subsequently the clones were
975 validated.

976 All cells were cultured in an incubator maintained at 37°C, 5% CO_2 and a relative humidity of
977 95%.
978
979 **Compounds and antibodies**
980 Chemical compounds, including Olaparib (#S1060), Novobiocin (#S2492), Etoposide (#S1225),
981 VE822 (#S7102), Ro-3306 (#S7747), E7820 (#S6628), Indisulam (#S9742), M3814 (#S8586) and
982 THZ0531 (#$6595) were purchased from Selleckchem. ART558 (#HY-141520) and MFH-290
983 (#HY-153244) were purchased from MedChemExpress. Nocodazole (#1404) was purchased from
984 Sigma Aldrich. Chemicals were dissolved in DMSO and kept in small aliquots at −20°C or 80°C.
985 The key sources of antibodies are: POLθ (Cell Signaling Technology, #64708), γH2AX (Millipore
986 #05–636), LIG3 (BD Biosciences, #611876), HMCES (Santa Cruz Biotechnology, SC-514238),
987 HMCES (Atlas Antibodies #HPA044968), APEX2 (Cell Signaling Technology, #74728),
988 PARP1(Cell Signaling Technology, #9542), CIP2A (Abcam, ab128179), DNA-PK (Cell
989 Signaling Technology, #12311), Phospho-DNA-PKcs (Ser2056) (Cell Signaling Technology,
990 #68716), TOPBP1 (Abcam, ab2402), XRCC1 (Cell Signaling Technology, #76998), FEN1 (Cell
991 Signaling Technology, #82354), EWSR1 (Cell Signaling Technology, #11910 for WB), EWSR1
992 (Santa Cruz Biotechnology, sc-28327 for WB), EWSR1 (Life Technologies, A300417A for IP and
993 RIP), BRCA1 (Merck Millipore, OP92), BRCA2 (Cell Signaling Technology, #10741), FLI1
994 (Abcam, ab133485), FUS (Cell Signaling Technology, #67840), TAF15(Cell Signaling
995 Technology, #28409), Vinculin (Cell Signaling Technology, #4650), FLAG (Sigma, F1804), HA
996 (Cell Signaling Technology, #3724 for WB), HA (Roche, #11867431001 for IP and RIP), V5 (Cell
997 Signaling Technology, #13202 for WB and IF), V5(Abcam, ab15828 for ChIP), V5(Abcam,
998 ab27671 for IP and WB), GAPDH (Cell Signaling Technology, #5174), Histone H3 (Cell

999 Signaling Technology, #9715), FUBP1 (Abcam ab181111), KHSRP (Cell Signaling Technology,
1000 #13398), SMARCA4/BRG1 (Cell Signaling Technology, #3508), SMARCC1 (Cell Signaling
1001 Technology, #11956), MYC (Santa Cruz Biotechnology, SC-40), FANCA (Cell Signaling
1002 Technology, #14657), FANCD2 (Novus Biologicals, NB100-182).
1003

1004 **Generation of CRISPR engineered cell lines**

1005 For generating *EWSR1* knock-out clones in HEK293T and RPE *p53*-/- cells, a ribonucleoprotein
1006 (RNP) complex was formed by Alt-R™ S.p. HiFi Cas9 and CRISPR-Cas9 sgRNA targeting
1007 *EWSR1* (Integrated DNA Technologies). For generating endogenously 3xFLAG-tagged *POLQ*
1008 knock-in HEK293T and RPE *p53*-/- cells, 3xFLAG-tagged *POLQ* HEK293T *EWSR1*-FKBP12
1009 V36F double knock-in cells or V5-tagged *POLQ* knock-in U2OS and A673 cells, the Cas9/sgRNA
1010 RNP complex together with a template was delivered. Cells were resuspended in SE (U2OS cells),
1011 SF (HEK293T and A673 cells) or P3 (RPE *p53*-/- cells) Nucleofector Solution with supplement
1012 (Lonza) and then mixed with the Cas9/sgRNA RNP complex and Alt-R™ Cas9 Electroporation
1013 Enhancer (Integrated DNA Technologies), respectively. The Cas9/sgRNA RNP complex was
1014 delivered to the cells by 4D-Nucleofector™ (Lonza). Media was changed the following day, and
1015 then 2 days after cells were seeded in a 96-well plate to isolate single clones. Individual clones
1016 were tested for genomic editing analyses using immunoblotting and genomic PCR with subsequent
1017 Sanger sequencing.
1018

1019 **Plasmids**

1020 psPAX2 and pMD2.G (Addgene #12260 and #12259) were gifts from Dr. Didier Trono. pLV-
1021 EF1a-IRES-Blast (pLV-Blast) (Addgene #85133) was a gift from Dr. Tobias Meyer.[67]

1022 pCDH-puro-EWS-FLI1 was a gift from Jialiang Wang (Addgene plasmid # 102813). pLenti
1023 CMV Puro LUC (w168-1) was a gift from Eric Campeau & Paul Kaufman (Addgene plasmid #
1024 17477). pCVL.SFFV.d14GFP.EF1a.HA.NLS.Sce(opt).T2A.TagBFP was a gift from Andrew
1025 Scharenberg (Addgene plasmid # 32627). EWS-FLI1 37YS mutant was cloned into pCDH-puro
1026 vector. EWSR1, FUBP1, KHSRP, RNaseH1 and its mutant forms were cloned into pMYs-IRES-
1027 Blastcidin vector, respectively. sgRNAs were cloned into a lentiCRISPR-v2 construct as
1028 previously described[68]. Of note, sgEWSR1 #2, sgFUBP1 #2 or sgKHSRP #2 target genomic
1029 DNA but not cDNA, so that endogenous knockout and ectopic cDNA expression are possible
1030 simultaneously. All the sgRNA sequences used in this study were provided in Supplemental
1031 Table 1.
1032
1033 **Virus generation**
1034 Lentivirus was generated by co-transfecting lentiviral constructs with packaging vectors, psPAX2
1035 and pMD2.G, into HEK293T cells using CalPhos Mammalian Transfection Kit (Takara Bio). Two
1036 days after transfection, supernatant containing virus was harvested and filtered through 0.45 μm
1037 filter. Viral transductions were performed in the presence of 8 μg/ml (for RPE *p53*-/-, MDA-MB
1038 436, DLD1, HCC1937, and HCC1954 cells) or 4 μg/ml (for K562 cells) polybrene (Sigma-
1039 Aldrich). For all virus generations and transductions media supplemented with heat inactivated
1040 FBS was used. Retrovirus was generated by co-transfecting retroviral constructs with packaging
1041 vectors, and, into HEK293T cells using CalPhos Mammalian Transfection Kit (Takara Bio). Two
1042 days after transfection, supernatant containing virus was harvested and filtered through 0.45 μm
1043 filter. Viral transductions were performed in the presence of 8 μg/mL polybrene (Sigma-Aldrich).
1044 Puromycin dihydrochloride (Sigma-Aldrich) or Blasticidin S HCl (Thermo Fisher Scientific) was
1045 used after infection of retrovirus or lentivirus.

1046

1047 **Colony formation assay**

1048 Cells were seeded in 6-well plates at 500-10,000 cells/well. The day after seeding, cells were
1049 exposed to each drug or x-ray. X-ray irradiation was performed using RS-2000 Irradiator (Rad
1050 Source Technologies). After incubation, cells were washed with PBS and then fixed in a mixture
1051 of 50% methanol, 10% acetic acid, and 40% water for 20 minutes. The fixed cells were stained
1052 with 0.5% crystal violet (Sigma-Aldrich) in 20% methanol for 2–6 h and then washed with water
1053 twice. The plates were imaged on GE Amersham Imager 600 using colorimetric transillumination
1054 setting. The area fraction of the colonies in each well was estimated using ImageJ.

1055

1056 **CellTiter-Glo assay**

1057 To test drug sensitivity, U2OS or Ewing sarcoma cells were seeded in 96-well plates at 1000–3000
1058 cells/well. The day after seeding, drug was added to the wells, and then the plates were incubated
1059 for 3-5 days. After incubation, ATP in each well was quantified using CellTiter-Glo Luminescent
1060 Cell Viability Assay (Promega). CellTiter-Glo assays were performed in technical duplicate if not
1061 otherwise specified in a figure legend.

1062

1063 **Immunofluorescence**

1064 Mitotic synchronization was achieved using Ro-3306 (8 μM, 16 hours) followed by 30min release
1065 in fresh medium. Then cells were incubated with 100ng/ml nocodazole and subsequently
1066 irradiated. 4h after irradiation or in the absence of treatment, cells were fixed with 4%
1067 paraformaldehyde for 15 minutes at room temperature. For FANCD2 foci evaluation, cells were
1068 treated with 10ng/ml MMC for 24hr. Cells were then permeabilized with 0.3% Triton X-100 for

1069 10 minutes on ice, followed by blocking with 3% non-fat milk for 1 hour at room temperature.
1070 The slides were stained with primary antibodies at 4℃ overnight. Afterward, they were stained
1071 with secondary antibodies for 1 hour at room temperature. The slides were scanned using
1072 fluorescence microscope. At least 100 cells were counted for each sample. Foci quantification was
1073 performed using software CellProfiler version 4.2.6.
1074
1075 **Immunoblotting**
1076 Whole cell lysate was prepared by lysing cells in ice-cold RIPA buffer (Cell Signaling
1077 Technology) supplemented with Protease/Phosphatase inhibitor Cocktail (Cell Signaling
1078 Technology). Cell lysate was cleared by centrifuging the samples at 12000 rpm, 4°C for 20
1079 minutes. Supernatant was recovered and protein concentration was estimated using BCA assay kit
1080 (Thermo Fisher Scientific). Protein samples were boiled in 2X Laemmli sample buffer (Bio-rad)
1081 supplemented with 5% 2-mercaptoethanol or NuPAGE LDS sample buffer (Thermo Fisher
1082 Scientific) supplemented with NuPAGE sample reducing agent (Thermo Fisher Scientific).
1083 Samples were run in NuPAGE 4-12% Bis-Tris gels (Thermo Fisher Scientific) using NuPAGE
1084 MES SDS Running Buffer (Thermo Fisher Scientific) or NuPAGE 3-8% Tris-Acetate Gel
1085 (Thermo Fisher Scientific) using NuPAGE Tris-Acetate SDS Running Buffer (Thermo Fisher
1086 Scientific). After electrophoresis, samples were transferred onto a nitrocellulose membrane
1087 (Amersham). Membranes were blocked for 1 h with Blocking Buffer, which was prepared by
1088 diluting Fish Serum Blocking Buffer (Thermo Fisher Scientific) with Tris-buffered saline
1089 containing 0.1% Tween20 (TBST). Membranes were incubated with primary antibodies diluted in
1090 Blocking Buffer overnight at 4°C. Membranes were washed with TBST three times, 5 minutes
1091 each, incubated with secondary antibodies diluted in blocking buffer for 1h, which either

1092 horseradish peroxidase (HRP)-conjugated for chemiluminescent detection or fluorophore-
1093 conjugated for visualization using the LI-COR imaging system. After secondary antibody
1094 incubation, membranes were washed with TBST and imaged using chemiluminescence setting on
1095 GE Amersham Imager 600 or the LI-COR imaging system.
1096
1097 **DNA repair template assay**
1098 DR-GFP and EJ5-GFP cells were kind gifts from Dr. Jeremy Stark. MMEJ-GFP cells (ver.1 and
1099 ver.2) were generated by lentivirally transducing a cassette into U2OS or Ewing sarcoma cells
1100 using a pLV-EF1a-IRES-puro vector (addgene #85132) as previously described [20]. U2OS cells
1101 carrying a DNA repair template reporter (DR-GFP, EJ5-GFP, and MMEJ-GFP) or Ewing sarcoma
1102 cells carrying a MMEJ reporter were lentivirally transduced with Cas9 and sgRNA (co-expressing
1103 puromycin resistance gene). After puromycin or blasticidin selection, 40,000 DNA repair template
1104 reporter cells were seeded in 12-well plates and adenovirally (for U2OS) or lentivirally (co-
1105 expressing BFP, for Ewing sarcoma cells) transduced with Isce-I the following day. 48h after Isce-
1106 I transduction, GFP signals were analyzed by CytoFLEX (Beckman). The signals were normalized
1107 to control cells. For U2OS Cas9-based MMEJ reporter assay, the cells were subsequently
1108 transduced with Cas9 and sgRNA targeting the reporter (co expressing BFP). 72h after
1109 Cas9/sgRNA transduction, GFP signals within BFP positive fraction were analyzed by CytoFLEX
1110 (Beckman). For Cas9-based MMEJ reporter assay using HEK293T *POLQ* WT or knockout cells,
1111 the MMEJ reporter, Cas9 and sgRNA targeting the reporter (co expressing BFP) together with a
1112 control vector, *POLQ* WT cDNA or *POLQ* mutant cDNA were transduced using Lipofectamine
1113 LTX with Plus reagent (Thermo Fisher Scientific). After 72 h incubation, GFP signals within BFP
1114 positive fraction were analyzed by CytoFLEX (Beckman).

1115

1116 **Comet assay**

1117 The alkaline comet assays were performed to detect both single and double-stranded DNA breaks.
1118 1000 cells, suspended in PBS, were mixed with 50µl melted low melting agarose and pipetted onto
1119 the Cometslides (R&D Systems). Once the agarose solidified, the slides were immersed in a lysis
1120 solution for 18 hours to facilitate cell lysis. Following lysis, the slides were incubated in an alkaline
1121 unwinding solution for 1 hour to denature the DNA. Electrophoresis was performed at 21 V for 45
1122 minutes in an alkaline electrophoresis solution. The slides were stained with SYBR green solution,
1123 scanned by fluorescence microscope, and analyzed using CometScore 2.0 software.

1124

1125 **Chromatin immunoprecipitation (ChIP) assay**

1126 U2OS biallelic endogenous V5-*POLQ* expressing cells carrying an Isce-I based MMEJ reporter
1127 were adenovirally transuduced with Isce-I in the presence or absence of 100ng/ml nocodazole.
1128 12h after Isce-I trunscduction, chromatin immunoprecipitation was performed using SimpleChIP
1129 Enzymatic Chromatin IP Kit (Magnetic Beads) (Cell Signaling Technology). Protein-DNA
1130 cross-linking was performed with 1% formaldehyde and glycine solution. Chromatin was
1131 fragmented with Micrococcal Nuclease. The digested chromatin was incubated at 4°C with each
1132 antibody for 4 h. After the antibody reaction, ChIP-Grade Protein G Magnetic Beads were added
1133 to the samples, and the samples were incubated at 4°C for 1–2 h. For crosslinking reversal, each
1134 sample was incubated at 65°C with Proteinase-K overnight. After DNA purification,
1135 immunoprecipitated DNA was analyzed by qPCR using a primer set targeting the integrated
1136 MMEJ reporter locus. ChIP-qPCR was performed in technical triplicate. All the primer
1137 sequences for ChIP-qPCR used in this study were provided in Supplemental Table 1.

1138

1139 **Reverse transcription PCR (RT-PCR)**

1140 Total RNA was extracted using RNeasy Mini Kit (QIAGEN). Complementary DNA synthesis
1141 was performed using SuperScript IV First-Strand cDNA Synthesis Reaction (Thermo Fisher
1142 Scientific). The PCR products were separated in 2% agarose gel stained with SYBR Safe
1143 (Thermo Fisher Scientific) and imaged using ChemiDoc MP Imaging System (Bio-rad). All the
1144 primer sequences for RT-PCR used in this study were provided in Supplemental Table 1.

1145

1146 **ASO transfection**

1147 ASO was designed to target near the splice sites of the *POLQ* exon 25. The ASO was synthesized
1148 using 2′-O-methoxyethyl-phosphorothioated bases by Integrated DNA Technologies (IDT). Prior
1149 to ASO transfection, cells were seeded in a 6-well plate and cultured overnight. ASO was
1150 transfected at a final concentration of 0.1 μM using Lipofectamine LTX with Plus reagent (Thermo
1151 Fisher Scientific). After 48 h incubation, cells were harvested and analyzed by RT-PCR and
1152 western blotting. All the sequences for ASO used in this study were provided in Supplemental
1153 Table 1.

1154

1155 **Splicing minigene reporter assay**

1156 A mini-gene reporter carrying mNeongreen split by synthetic intronic sequence derived from
1157 *POLQ* intron 24/25 and exon 25 was generated as previously described [28]. The synthetic intron
1158 was made up of 250 bp of the start of the *POLQ* intron 24, 250 bp or 1000bp of the end of the
1159 *POLQ* intron 24, the *POLQ* exon 25, 250 bp or 1000bp of the start of the *POLQ* intron 25m and
1160 250 bp of the end of the *POLQ* intron 25. The synthetic introns and exon so generated were

1161 placed between the sequences encoding the N-terminus and C-terminus of split mNeongreen.
1162 The mScarlet-P2A-split mNeongreen (N-terminus)-synthetic introns/exon-split mNeongreen (C
1163 terminus) construct was integrated into a pLV-EF1a-IRES-Neo vector (Addgene #85139) to
1164 generate the mini-gene reporter. K562 cells or Ewing sarcoma cell lines were lentivirally
1165 transduced with the mini-gene reporter. 48hr after lentiviral transduction, the cells were enriched
1166 by using G418 (0.8mg/ul) for seven days. After antibiotic selection, mScarlet and mNeongreen
1167 signals in the reporter cells were analyzed by CytoFLEX (Beckman). For the flow cytometry
1168 analyses, mScarlet positive fractions within living cells were gated. Thereafter, the frequency of
1169 the mNeongreen positive cells within mScarlet expressing cells was analyzed by using Flowjo
1170 ver.10.9.0.
1171
1172 **Mass spectrometry analysis**
1173 HEK293T EWSR1-FKBP12 V36F knock-in cells were seeded into 15cm dishes and cultured
1174 overnight. The cells were transfected with pMYS-IB empty vector (EV) or pMYs-IB-EWSR1
1175 wildtype or pMYs-IB-EWSR1 37YS plasmid. Cells were transfected with 30 µg of vector /dish
1176 using Lipofectamine LTX with Plus reagent. 16h after transfection, media was changed with 1uM
1177 dTAG^{v1}. The cells were harvested 40 h after transfection and then were lysed with 40 mM Tris-
1178 HCl pH 8 buffer supplemented with 0.5% NP-40, 200 mM NaCl, 2 mM EDTA,
1179 Protease/Phosphatase inhibitor Cocktail (Cell Signaling Technology), and MG-132. The lysate
1180 was centrifuged, and the pellet was resuspended with 20 mM Tris-HCl pH 7.5 supplemented with
1181 100 mM KCl, 2 mM MgCl2, 1 mM CaCl2, and Protease/Phosphatase inhibitor Cocktail and treated
1182 with Micrococcal Nuclease (Thermo Fisher Scientific) for approximately 30 minutes, followed by
1183 addition of 5 mM EGTA (final concentration) to stop digestion. After three pulses of sonication

1184 (30 s each), samples were centrifuged to collect the supernatants as chromatin fractions.
1185 Immunoprecipitation was performed using Anti-FLAG M2 antibody (Sigma-Aldrich) conjugated
1186 with Dynabeads Protein G for Immunoprecipitation (Thermo Fisher Scientific). Beads were
1187 washed with TGN-150 wash buffer containing 20 mM Tris-HCl pH 7.6, 150 mM NaCl, 3 mM
1188 MgCl2, 10% glycerol, and 0.01% NP-40. Beads were then boiled at 70□C for 20 minutes in 1:1
1189 diluted NuPAGE LDS Sample buffer (4X) (Thermo Fisher Scientific) to elute the proteins. The
1190 eluted proteins were applied to SDS-PAGE, and Coomassie stained gel band samples were used
1191 for the analyses. Two independent biological replicate samples were analyzed by mass
1192 spectrometry.
1193 The gel bands were cut into approximately 1 mm3 pieces. Gel pieces were then subjected to a
1194 modified in-gel trypsin digestion procedure. Gel pieces were washed and dehydrated with
1195 acetonitrile for 10 minutes and completely dried in a SpeedVac (Thermo Fisher Scientific). The
1196 gel pieces were rehydrated with 50 mM ammonium bicarbonate containing 12.5 µg/mL modified
1197 sequencing-grade trypsin (Promega) at 4°C. After rehydration, the excess trypsin solution was
1198 removed and replaced with 50 mM ammonium bicarbonate solution. Samples were then incubated
1199 at 37°C overnight. Peptides were later extracted with a solution containing 50% acetonitrile and
1200 1% formic acid and dried in a SpeedVac. The samples were reconstituted in 5–10 µL of HPLC
1201 solvent A (2.5% acetonitrile, 0.1% formic acid). A nano-scale reverse-phase HPLC capillary
1202 column was created by packing 2.6 µm C18 spherical silica beads into a fused silica capillary (100
1203 µm inner diameter x ~30 cm length) with a flame-drawn tip. After equilibrating the column each
1204 sample was loaded via an EASY-nLC (Thermo Fisher Scientific). A gradient was formed, and
1205 peptides were eluted with increasing concentrations of solvent B (90% acetonitrile, 0.1% formic
1206 acid). As peptides eluted, they were subjected to electrospray ionization and then entered into a

1207 Orbitrap Exploris480 mass spectrometer (Thermo Fisher Scientific). Peptides were detected,
1208 isolated, and fragmented to produce a tandem mass spectrum of specific fragment ions for each
1209 peptide. Peptide sequences were determined by matching protein databases with the acquired
1210 fragmentation pattern by the software program, Sequest (Thermo Fisher Scientific). All databases
1211 include a reversed version of all the sequences and the data was filtered to between a one and two
1212 percent peptide false discovery rate. Perseus (version 2.0.11.0) [69] was used to preprocess the
1213 protein data. The protein intensities were normalized by the median and log2-transformed. Proteins
1214 with only one intensity value or with a sum of all total peptide counts of less than 5 were filtered
1215 out. For each sample, missing log2-intensity values were imputed using the normal distribution
1216 with width of 0.3 and down shift of 1.8. Histograms of log2-instensity values were inspected to
1217 confirm that the imputed values were at the lower end. Finally, limma analysis (version 3.54.2) [70]
1218 was performed on the log2-instensity values to determine enriched and depleted proteins. Volcano
1219 plots were generated using ggplot2 and ggrepel R packages.
1220

1221 **RNA immuno-precipitation (RIP) assay**

1222 Protocol for RIP assay was adapted from Nicholson-Shaw et al., 2022[29]. HEK293T EWSR1-
1223 FKBP12 V36F knock-in cells were cultured in 15 cm dishes and 2-3 plates were used per cell line
1224 for each assay. 16hr after transfection, media was changed with 1uM dTAG^{v1}. Cells were harvested
1225 40hr after transfection, washed with ice-cold PBS 2X times, cross-linked with 0.2% PFA for 15
1226 min. and then quenched by adding glycine to a final concentration of 125mM. Cells were lysed in
1227 iCLIP buffer (50mM Tris-HCl pH 7.4, 100mM NaCl, 1% NP-40, 0.1% SDS, 0.5% sodium
1228 deoxycholate) supplemented with protease, phosphatase and RNase inhibitor cocktail. The
1229 samples were rotated at 4°C for 10 min. and then sonicated on 'light' setting twice. The lysate was

1230 incubated with Protein A beads on a rotor for 10 min. at 4°C to pre-clear the extract. The lysate
1231 was centrifuged at max speed for 10 min. and the supernatant was recovered and incubated for 2
1232 hrs on a rotor at 4°C with Protein A beads coupled to EWSR1 Ab (Life Technologies). A part of
1233 the lysate (0.4-0.6%) was kept aside as input. After 2 hrs the beads were washed twice with iCLIP
1234 buffer. The input and the IP samples were all subjected to TURBO DNase treatment (Thermo
1235 Fisher Scientific) for 30 min. at 37°C to get rid of the genomic DNA and the cross-links were
1236 reversed by digesting with Proteinase K (NEB) for 30 min. at 37°C and further digestion and
1237 denaturation of proteins was achieved by adding urea to a final concentration of 2.5M and
1238 incubating the samples at 37°C for additional 20 min. After digestion of the DNA and protein from
1239 the samples, the RNA was purified by adding Trizol and processing the samples through Directzol
1240 RNA mini-prep kit (Zymo Research). The eluted RNA from the input and IP samples were
1241 converted to cDNA using the High-capacity RNA-to-cDNA kit (Thermo Fisher Scientific). The
1242 reverse transcription was performed with and without adding the reverse transcriptase enzyme.
1243 qPCR was set up with primers targeting *POLQ* pre-mRNA, *POLQ* mature mRNA, and GAPDH
1244 in technical replicates for each assay. Ct values were normalized to that from the control samples. .
1245 All the sequences for RIP-qPCR used in this study were provided in Supplemental Table 1.
1246

1247 **Next generation sequencing**

1248 Library preparation and sequencing reactions were conducted at GENEWIZ, Lin/Azenta US, Inc.
1249 Deep RNA-seq (300 million reads/sample, N = 3 for each cell line) was performed for RPE *p53-*
1250 */-* (parental control) and *p53-/-EWSR1* knock-out cells. RNA samples were prepared using RNeasy
1251 Mini Kit and RNase-Free DNase Set (QIAGEN). RNA samples were quantified using Qubit 2.0
1252 Fluorometer, and the RNA integrity was checked with 4200 TapeStation. NEBNext Ultra II RNA

1253 Library Prep Kit for Illumina was used following the manufacturer's recommendations (New
1254 England BioLabs). Briefly, mRNAs were initially enriched with Oligo d(T) beads. Enriched
1255 mRNAs were fragmented for 15 minutes at 94°C. First strand and second strand cDNA were
1256 subsequently synthesized. cDNA fragments were end repaired and adenylated at 3´ends, and
1257 universal adapters were ligated to cDNA fragments, followed by index addition and library
1258 enrichment by PCR with limited cycles. The sequencing libraries were validated using Agilent
1259 TapeStation and quantified using Qubit 2.0 Fluorometer as well as by quantitative PCR (KAPA
1260 Biosystems). The sequencing libraries were clustered on flowcell lanes. After clustering, the
1261 flowcell was loaded on the Illumina NovaSeq instrument according to manufacturer's instructions.
1262 The samples were sequenced using a 2x150 Paired End configuration. Image analysis and base
1263 calling were conducted by the Control Software (NCS). Raw sequence data (.bcl files) generated
1264 from the Illumina instrument was converted into fastq files and de-multiplexed using Illumina's
1265 bcl2fastq (version 2.17) software. One mismatch was allowed for index sequence identification.
1266 Several bioinformatics analyses were performed on the RNA-seq data to identify differentially
1267 expressed genes, differentially used exons, and differentially spliced events between RPE *p53-/-*
1268 control cells and *p53-/-EWSR1* knock-out cells.
1269 For differential gene expression analysis, Kallisto (version 0.48.0) [71] was used to map the raw
1270 RNA-seq reads against the GENCODE human reference gene annotation (Release 44) [72] and
1271 generate raw transcript abundance estimates, and the *tximport* Bioconductor R package [73] was used
1272 to summarize the transcript abundance estimates to produce gene-level estimated counts.
1273 Differentially expressed genes between control and *EWSR1* knock-out cell samples (N = 3) were
1274 determined using both edgeR (version 3.40.2) [74] and DESeq2 (version 1.38.3) [75] Bioconductor

1275 packages. The high concordance between the estimated $\log_2$ foldchange of the two algorithms was
1276 verified.
1277 For both differential exon usage and differential splicing analyses, STAR (version 2.7.10b) [76] was
1278 used to map RNA-seq reads and generate BAM files. Specifically, the 2-pass STAR was used to
1279 map the raw RNA-seq reads against the GRCh38/hg38 human reference genome, with the
1280 GENCODE human reference gene annotation (Release 44) [72]. The first round of the 2-pass STAR
1281 was run to identify splice junctions, and more confidence junctions then were filtered by requiring
1282 them to have at least 5 total mapped reads. The second round of the 2-pass STAR was run using
1283 the filtered junctions to generate BAM files.
1284 For differential exon usage analysis, DEXSeq (version 1.46.0) [77] was used. In brief, a list of unique
1285 exonic regions was initially generated using the Python script *dexseq_prepare_annotation.py.* This
1286 script "collapsed" exonic regions from different transcripts to be used as exon counting bins. Next,
1287 the *dexseq_count.py* Python script was used to count reads for each sample. Finally, differentially
1288 used exons between control and *EWSR1* knock-out cells (N = 3) were determined using DEXSeq.
1289 For the differential splicing analysis, MISO (version 0.5.4) [26] and other tools were used as
1290 discussed below. The exon-centric splicing event annotations were generated using the *rnaseqlib*
1291 Python package (http://github.com/yarden/rnaseqlib). These annotations were derived
1292 considering all transcripts from Ensembl, UCSC RefSeq and NCBI RefSeq gene annotations,
1293 which were obtained from https://hgdownload.soe.ucsc.edu/goldenPath/hg38/database, in files
1294 *knownGene.txt*, *refGene.txt*, and *ncbiRefSeq.txt*. Each annotation event belongs to one of these 5
1295 types: skipped exons (SE), alternative 3′ splice sites (A3SS), alternative 5′ splice sites (A5SS),
1296 mutually exclusive exons (MXE), and retained introns (RI). These annotated events were linked
1297 to representative overlapping exons or introns of the GENCODE human reference gene

1298 annotation (Release 44) using the intersect function of the *bedtools* toolset (version 2.31.0). The
1299 representative exons and introns were prioritized with a high overlapping percentage (95%),
1300 followed by good transcript quality information including whether they were annotated as
1301 canonical and basic, and with better transcript support level. MISO was performed to quantify
1302 the isoforms and compute percent-spliced-in values (PSIs) of each alternative splicing event
1303 from the sorted BAM of each sample. Lower quality events were filtered out as follows. For each
1304 replicate sample pair, the *compare_miso* program was used to compare the results of the control
1305 and the *EWSR1* knock-out samples. The *filter_events* program was then used to filter the
1306 comparison results, by requiring each sample to have at least 35 total isoform-identifying reads.
1307 Finally, *limma* analysis (version 3.54.2) was performed on the PSI values of the filtered events to
1308 determine differential splicing events between control and *EWSR1* knock-out cells (N = 3).
1309 Significant differential alternative splicing events were called if they had *FDR* smaller than 0.05
1310 and absolute delta PSI of at least 0.05. Events that had significant FDR (<0.05) but small
1311 absolute delta PSI (<0.05) were likely to be artifacts and thus were excluded from *limma* results.
1312 Volcano plots were generated using ggplot2.
1313 To have more confidence in the MISO results, we also independently analyzed differential
1314 splicing using rMATS (version v4.2.0) [27]. Since SE events were the most frequent event type,
1315 we focused on analyzing the concordance of SE events between MISO and rMATS. First,
1316 rMATS was run using all sorted BAMs as inputs and the GENCODE human reference gene
1317 annotation (Release 44). Lower quality events were filtered out by requiring each sample to
1318 have at least 35 total isoform-identifying reads. Then, the shared events that were highly similar
1319 between MISO and rMATS were identified if their target regions overlapped by at least 95%.
1320 Since one MISO event could be linked to multiple slightly different rMATS events, for each

1321 MISO event, a representative rMATS event was chosen that had the largest absolute difference
1322 in inclusion level. Finally, we assessed the concordance between MISO and rMATS by
1323 comparing their inclusion differences (delta PSI values and differences in inclusion levels,
1324 respectively) from these shared events. We observed that a great majority of significant MISO
1325 events had a shared rMATS event. Furthermore, we observed that the inclusion differences of
1326 MISO and rMATS were positively correlated with R^2 of 0.32. The scatterplot comparing the
1327 inclusion differences of the two algorithms was generated using ggplot2. Sashimi plots were
1328 generated using the *rmats2sashimiplot* program (https://github.com/Xinglab/rmats2sashimiplot/).
1329

1330 **AlphaFold analysis**

1331 AlphaFold3 and the AlphaFold Server [78] were used to model full-length (POLQ aa 1824-2579)
1332 and truncated (POLQ aa 1824-2390) POLQ polymerases domains in complex with two
1333 complementary 9 bp DNA molecules (5'-CCAATGACA-3' and 5'-TGTCATTGG-3'). Models
1334 were visualized in Pymol V3.0.4 (Schrödinger) using the top-ranking predictions per seed. The
1335 full-length model was compared with a published crystal structure of the POLQ polymerase
1336 domain (PDB 6XBU) [79] to ensure its accuracy.
1337

1338 **Mouse xenograft study**

1339 All animal experiments were conducted in accordance with Institutional Animal Care and Use
1340 Committee-approved protocol (#08-036) at Dana-Farber Cancer Institute. TC32 cells were
1341 lentivirally transduced with luciferase by using a pLenti CMV Puro LUC (w168-1) vector. Two
1342 million TC32 cells expressing luciferase were subcutaneously injected into 7-week-old male and
1343 female NOD.Cg-*Prkdc*^{scid} Il2rg^{tm1Wjl}/SzJ mice. After confirming tumor engraftment, mice were

1344 treated with Peposertib (100 mg/kg) or vehicle control once a day via oral administration together
1345 with Etoposide (8mg/kg) or vehicle control via intraperitoneal injection (IP injection) twice a week
1346 for 2 weeks. Tumors were measured every 2 to 3 days using an electronic caliper, and tumor
1347 volumes were calculated by using the formula L×W×W/2. For immunohistochemistry analysis,
1348 tumors were excised and fixed with formaldehyde. Mice with a tumor of more than 20 mm in
1349 length or width were euthanized.
1350

1351 **Data acquiring and processing of transcriptomic sequencing from patient tumor samples**

1352 Patient tumor sample bulk transcriptomic sequencing data were obtained from St. Jude's Cloud [80].
1353 For expression analysis, we used the mapped expression counts data; for the exon splicing data,
1354 we used the BAM files provided. For the expression counts data, all of the samples were uniformly
1355 processed and mapped to the same reference genome as part of the St. Jude's Cloud resource, and
1356 as such, no correction between samples or cancer types was performed. To evaluate the *POLQ*
1357 expression, we first computed the TPM (transcript-per-million) counts for all samples. In this
1358 computation, we omitted genes annotated as pseudogenes in GENCODE v.31, and used the
1359 median gene length as the gene length for each gene symbol.
1360

1361 **Computation of exon skipping rates in primary patient samples**

1362 To compute the proportions of reads with exons skipped in the sequencing reads data obtained
1363 from St. Jude's Cloud [81], rMATS-turbo, a computational tool to quantify alternative splicing
1364 patterns from RNA sequencing data, was applied. To compute the proportion of reads that each
1365 exon was skipped in, the rMATS-turbo results inclusive of supporting reads from counted from
1366 both junction and exon reads were used. Of note, for each individual exon, any sample that had no

1367 supporting reads for both the inclusive and skipped cases was omitted. All comparisons between
1368 distributions of skipped read proportions were performed using Mann-Whitney U tests.
1369

1370 **Mutational Analysis of Tumors**

1371 Mutational analysis was performed on the whole genome sequencing (WGS) data of Ewing
1372 sarcoma and neuroblastoma tumors obtained from St. Jude Cloud (https://www.stjude.cloud/).
1373 The samples include 23 Ewing sarcoma (ES) and 48 neuroblastoma (NB) tumor and matched-
1374 normal pairs. Somatic variants were determined as follows. First, for each cohort, short variants
1375 were called from the HG38 Genomic Variant Call Format (gVCF) data using the GATK joint
1376 genotyping workflow (version 4.2.4). Second, bcftools (version 1.14) was used to filter out low-
1377 quality variants with these hard filters: QD < 7.5, MQ < 59.9, -g3, and -G10. Only biallelic SNPs
1378 and INDELs were selected. Third, cohort-level singleton variants were selected if there was only
1379 one sample with read depth (DP) between 17 and 300, and variant allele fraction (VAF) of at
1380 least 0.1. And finally, a variant was considered somatic if both the tumor and matched-normal
1381 had SOR <= 3, MQ > 59.9, and DP > 17, and either, tumor VAF >= 0.175 and matched normal
1382 VAF = 0, or tumor VAF <= 0.825 and matched normal VAF = 1.
1383 Profiles of SNV mutations and INDELs were generated using SigProfilerMatrixGenerator
1384 (version 1.2.13; https://github.com/AlexandrovLab/SigProfilerMatrixGenerator). Mutational
1385 signature analysis was performed using SigProfilerAssignment (version 0.0.21;
1386 https://github.com/AlexandrovLab/SigProfilerAssignment). This involved fitting the mutational
1387 profiles to the COSMIC (https://cancer.sanger.ac.uk/signatures/) SNV signatures (SBS version 2)
1388 and INDEL signatures (ID version 3.3).

1389 The MMEJ signature was characterized by the presence of microhomologies at the
1390 boundaries of deletions and the presence of nearby template sequences in insertions, or templated
1391 insertions [82,83]. The presence of microhomologies in deletions was also independently determined
1392 using the method described by Taheri-Ghahfarokhi *et al* [82,83]. This method essentially finds the
1393 longest possible complementary subsequence between one end of the deleted sequence and the
1394 flanking sequence at the other end. In brief, for each deletion, 50-bp flanking sequences around
1395 the deleted sequence were first retrieved from the reference human genome (HG38) using
1396 bedtools (version 2.27.1; https://bedtools.readthedocs.io/). The deletion was then repeatedly
1397 shifted leftward by one base whenever its rightmost base matched the reference base
1398 immediately to its left. Finally, the microhomology sequence was the longest matching
1399 subsequence between the deleted sequence and the right flanking sequence starting from their
1400 leftmost bases. Deletions with length of at least 3bp with GATK ReadPosRankSum of greater
1401 than -5 and with microhomology of at least 2 bp were designated as MMEJ events [82]. For
1402 comparison between ES and NB, tumors with at least 15 deletions and the proportions of MMEJ
1403 deletions among all indels were used. Local templated insertions were characterized by the
1404 presence of subsequences in the inserted sequence that were identical to the flanking sequences
1405 (templated inserts) [15,84,85]. The templated inserts were detected by aligning the inserted sequence
1406 with the 50bp-flanking sequences around the insertion site using the Smith–Waterman local
1407 alignment algorithm [86]. The analysis was restricted to insertions with GATK ReadPosRankSum
1408 of greater than -5 and with length of at least 5bp. The insertions with templates adjacent to the
1409 insertion position were excluded. The remaining insertions with templates covering at least 60%
1410 of the inserted sequence were designated as MMEJ events. For comparison between ES and NB,

1411 tumors with at least 2 insertions, and the proportions of MMEJ templated insertions among all
1412 insertions were used.
1413
1414 **Immunohistochemistry (IHC)**
1415 Primary patient samples for IHC analysis were obtained from the Mayo Clinic (IRB approval #24-
1416 007702). IHC was performed using a Parhelia autostainer. Slides were deparaffinized using Slide
1417 Brite xylene substitute (23401-01) followed by rehydration in ethyl alcohol. Endogenous blocking
1418 was performed using methanol hydrogen peroxide solution. Slides were heated for 30 minutes in
1419 citrate solution for epitope retrieval. Slides were incubated for 30minutes in anti-DNAPKcs
1420 phosphor S2056 antibody at 1:150 followed by washing in wash buffer (Dako S3006) and
1421 inbubation for 30minutes in Mach 3 rabbit HRP (Buocare Medical RP531L). Primary staining was
1422 performed by incubation in DAB (Dako K3468) for 10minutes. Counterstaing was performed
1423 using hematoxylin (Sigma-Aldrich MHS16) and bluing buffer (Dako C5702). Slides were then
1424 dehydrated in ethyl alcohol before coverslipping using Permount mounting mediun (Fisher
1425 Scientific SP15-100). Slides were digitally imaged using a Motic Easyscan Pro 6.
1426 Histological image analysis was performed using QuPath (version 0.5.1). Whole-slide images
1427 (WSIs) were imported into QuPath, and automated color deconvolution was applied to separate
1428 the hematoxylin and DAB (3,3′-diaminobenzidine) staining channels. The mean optica l density
1429 (OD) of the DAB-positive areas was measured to assess staining intensity. For patients with
1430 multiple tissue sections, and the mean OD across all sections for the same patient was used to
1431 represent the patient's staining intensity.
1432
1433 **Statistical analysis**

Data were analyzed and visualized using GraphPad Prism (Version 10.2.2, GraphPad Software, LLC). For comparisons between two groups, either a two-tailed Student's t-test or a Mann-Whitney U test was used. For comparisons involving more than two groups, one-way analysis of variance (ANOVA) was performed. For *in vivo* survival analysis study, a log-rank test was performed. A p-value of less than 0.05 ($p < 0.05$) was considered statistically significant.

1448

1449 **REFERENCES**

1450 1. Riggi, N., Suva, M.L., and Stamenkovic, I. (2021). Ewing's Sarcoma. N Engl J Med *384*,
1451 154-164. 10.1056/NEJMra2028910.
1452 2. Grunewald, T.G.P., Cidre-Aranaz, F., Surdez, D., Tomazou, E.M., de Alava, E., Kovar,
1453 H., Sorensen, P.H., Delattre, O., and Dirksen, U. (2018). Ewing sarcoma. Nat Rev Dis
1454 Primers *4*, 5. 10.1038/s41572-018-0003-x.
1455 3. Gorthi, A., Romero, J.C., Loranc, E., Cao, L., Lawrence, L.A., Goodale, E., Iniguez,
1456 A.B., Bernard, X., Masamsetti, V.P., Roston, S., et al. (2018). EWS-FLI1 increases
1457 transcription to cause R-loops and block BRCA1 repair in Ewing sarcoma. Nature *555*,
1458 387-391. 10.1038/nature25748.
1459 4. Choy, E., Butrynski, J.E., Harmon, D.C., Morgan, J.A., George, S., Wagner, A.J.,
1460 D'Adamo, D., Cote, G.M., Flamand, Y., Benes, C.H., et al. (2014). Phase II study of
1461 olaparib in patients with refractory Ewing sarcoma following failure of standard
1462 chemotherapy. BMC Cancer *14*, 813. 10.1186/1471-2407-14-813.
1463 5. Boulay, G., Sandoval, G.J., Riggi, N., Iyer, S., Buisson, R., Naigles, B., Awad, M.E.,
1464 Rengarajan, S., Volorio, A., McBride, M.J., et al. (2017). Cancer-Specific Retargeting of
1465 BAF Complexes by a Prion-like Domain. Cell *171*, 163-178 e119.
1466 10.1016/j.cell.2017.07.036.
1467 6. Davis, R.B., Supakar, A., Ranganath, A.K., Moosa, M.M., and Banerjee, P.R. (2024).
1468 Heterotypic interactions can drive selective co-condensation of prion-like low-complexity
1469 domains of FET proteins and mammalian SWI/SNF complex. Nat Commun *15*, 1168.
1470 10.1038/s41467-024-44945-5.
1471 7. Chong, S., Graham, T.G.W., Dugast-Darzacq, C., Dailey, G.M., Darzacq, X., and Tjian,
1472 R. (2022). Tuning levels of low-complexity domain interactions to modulate endogenous
1473 oncogenic transcription. Mol Cell *82*, 2084-2097 e2085. 10.1016/j.molcel.2022.04.007.
1474 8. Zuo, L., Zhang, G., Massett, M., Cheng, J., Guo, Z., Wang, L., Gao, Y., Li, R., Huang,
1475 X., Li, P., and Qi, Z. (2021). Loci-specific phase separation of FET fusion oncoproteins
1476 promotes gene transcription. Nat Commun *12*, 1491. 10.1038/s41467-021-21690-7.
1477 9. Chong, S., Dugast-Darzacq, C., Liu, Z., Dong, P., Dailey, G.M., Cattoglio, C., Heckert,
1478 A., Banala, S., Lavis, L., Darzacq, X., and Tjian, R. (2018). Imaging dynamic and
1479 selective low-complexity domain interactions that control gene transcription. Science
1480 *361*. 10.1126/science.aar2555.
1481 10. Selvanathan, S.P., Graham, G.T., Grego, A.R., Baker, T.M., Hogg, J.R., Simpson, M.,
1482 Batish, M., Crompton, B., Stegmaier, K., Tomazou, E.M., et al. (2019). EWS-FLI1
1483 modulated alternative splicing of ARID1A reveals novel oncogenic function through the
1484 BAF complex. Nucleic Acids Res *47*, 9619-9636. 10.1093/nar/gkz699.
1485 11. Wang, Z., Song, Y., Li, S., Kurian, S., Xiang, R., Chiba, T., and Wu, X. (2019). DNA
1486 polymerase theta (POLQ) is important for repair of DNA double-strand breaks caused by
1487 fork collapse. J Biol Chem *294*, 3909-3919. 10.1074/jbc.RA118.005188.
1488 12. Goff, J.P., Shields, D.S., Seki, M., Choi, S., Epperly, M.W., Dixon, T., Wang, H.,
1489 Bakkenist, C.J., Dertinger, S.D., Torous, D.K., et al. (2009). Lack of DNA polymerase
1490 theta (POLQ) radiosensitizes bone marrow stromal cells in vitro and increases
1491 reticulocyte micronuclei after total-body irradiation. Radiat Res *172*, 165-174.
1492 10.1667/RR1598.1.

1493 13. Mengwasser, K.E., Adeyemi, R.O., Leng, Y., Choi, M.Y., Clairmont, C., D'Andrea,
1494 A.D., and Elledge, S.J. (2019). Genetic Screens Reveal FEN1 and APEX2 as BRCA2
1495 Synthetic Lethal Targets. Mol Cell *73*, 885-899 e886. 10.1016/j.molcel.2018.12.008.
1496 14. Adam, S., Rossi, S.E., Moatti, N., De Marco Zompit, M., Xue, Y., Ng, T.F., Alvarez-
1497 Quilon, A., Desjardins, J., Bhaskaran, V., Martino, G., et al. (2021). The CIP2A-TOPBP1
1498 axis safeguards chromosome stability and is a synthetic lethal target for BRCA-mutated
1499 cancer. Nat Cancer *2*, 1357-1371. 10.1038/s43018-021-00266-w.
1500 15. Chan, S.H., Yu, A.M., and McVey, M. (2010). Dual roles for DNA polymerase theta in
1501 alternative end-joining repair of double-strand breaks in Drosophila. PLoS Genet *6*,
1502 e1001005. 10.1371/journal.pgen.1001005.
1503 16. Della-Maria, J., Zhou, Y., Tsai, M.S., Kuhnlein, J., Carney, J.P., Paull, T.T., and
1504 Tomkinson, A.E. (2011). Human Mre11/human Rad50/Nbs1 and DNA ligase
1505 IIIalpha/XRCC1 protein complexes act together in an alternative nonhomologous end
1506 joining pathway. J Biol Chem *286*, 33845-33853. 10.1074/jbc.M111.274159.
1507 17. Fleury, H., MacEachern, M.K., Stiefel, C.M., Anand, R., Sempeck, C., Nebenfuehr, B.,
1508 Maurer-Alcala, K., Ball, K., Proctor, B., 3rd, Belan, O., et al. (2023). The APE2 nuclease
1509 is essential for DNA double-strand break repair by microhomology-mediated end joining.
1510 Mol Cell *83*, 1429-1445 e1428. 10.1016/j.molcel.2023.03.017.
1511 18. Brambati, A., Sacco, O., Porcella, S., Heyza, J., Kareh, M., Schmidt, J.C., and Sfeir, A.
1512 (2023). RHINO directs MMEJ to repair DNA breaks in mitosis. Science *381*, 653-660.
1513 10.1126/science.adh3694.
1514 19. Hussmann, J.A., Ling, J., Ravisankar, P., Yan, J., Cirincione, A., Xu, A., Simpson, D.,
1515 Yang, D., Bothmer, A., Cotta-Ramusino, C., et al. (2021). Mapping the genetic landscape
1516 of DNA double-strand break repair. Cell *184*, 5653-5669 e5625.
1517 10.1016/j.cell.2021.10.002.
1518 20. Truong, L.N., Li, Y., Shi, L.Z., Hwang, P.Y., He, J., Wang, H., Razavian, N., Berns,
1519 M.W., and Wu, X. (2013). Microhomology-mediated End Joining and Homologous
1520 Recombination share the initial end resection step to repair DNA double-strand breaks in
1521 mammalian cells. Proc Natl Acad Sci U S A *110*, 7720-7725. 10.1073/pnas.1213431110.
1522 21. Pierce, A.J., Johnson, R.D., Thompson, L.H., and Jasin, M. (1999). XRCC3 promotes
1523 homology-directed repair of DNA damage in mammalian cells. Genes Dev *13*, 2633-
1524 2638. 10.1101/gad.13.20.2633.
1525 22. Zhou, J., Gelot, C., Pantelidou, C., Li, A., Yucel, H., Davis, R.E., Farkkila, A.,
1526 Kochupurakkal, B., Syed, A., Shapiro, G.I., et al. (2021). A first-in-class Polymerase
1527 Theta Inhibitor selectively targets Homologous-Recombination-Deficient Tumors. Nat
1528 Cancer *2*, 598-610. 10.1038/s43018-021-00203-x.
1529 23. Nabet, B., Roberts, J.M., Buckley, D.L., Paulk, J., Dastjerdi, S., Yang, A., Leggett, A.L.,
1530 Erb, M.A., Lawlor, M.A., Souza, A., et al. (2018). The dTAG system for immediate and
1531 target-specific protein degradation. Nat Chem Biol *14*, 431-441. 10.1038/s41589-018-
1532 0021-8.
1533 24. Nabet, B., Ferguson, F.M., Seong, B.K.A., Kuljanin, M., Leggett, A.L., Mohardt, M.L.,
1534 Robichaud, A., Conway, A.S., Buckley, D.L., Mancias, J.D., et al. (2020). Rapid and
1535 direct control of target protein levels with VHL-recruiting dTAG molecules. Nat
1536 Commun *11*, 4687. 10.1038/s41467-020-18377-w.
1537 25. Johnson, C.N., Sojitra, K.A., Sohn, E.J., Moreno-Romero, A.K., Baudin, A., Xu, X.,
1538 Mittal, J., and Libich, D.S. (2023). Insights into Molecular Diversity within the FET

1539 Family: Unraveling Phase Separation of the N-Terminal Low Complexity Domain from
1540 RNA-Binding Protein EWS. bioRxiv. 10.1101/2023.10.27.564484.
1541 26. Katz, Y., Wang, E.T., Airoldi, E.M., and Burge, C.B. (2010). Analysis and design of
1542 RNA sequencing experiments for identifying isoform regulation. Nat Methods *7*, 1009-
1543 1015. 10.1038/nmeth.1528.
1544 27. Shen, S., Park, J.W., Lu, Z.X., Lin, L., Henry, M.D., Wu, Y.N., Zhou, Q., and Xing, Y.
1545 (2014). rMATS: robust and flexible detection of differential alternative splicing from
1546 replicate RNA-Seq data. Proc Natl Acad Sci U S A *111*, E5593-5601.
1547 10.1073/pnas.1419161111.
1548 28. Harada, N., Asada, S., Jiang, L., Nguyen, H., Moreau, L., Marina, R.J., Adelman, K.,
1549 Iyer, D.R., and D'Andrea, A.D. (2024). The splicing factor CCAR1 regulates the Fanconi
1550 anemia/BRCA pathway. Mol Cell *84*, 2618-2633 e2610. 10.1016/j.molcel.2024.06.031.
1551 29. Nicholson-Shaw, A.L., Kofman, E.R., Yeo, G.W., and Pasquinelli, A.E. (2022). Nuclear
1552 and cytoplasmic poly(A) binding proteins (PABPs) favor distinct transcripts and
1553 isoforms. Nucleic Acids Res *50*, 4685-4702. 10.1093/nar/gkac263.
1554 30. Lawrence, M.S., Stojanov, P., Polak, P., Kryukov, G.V., Cibulskis, K., Sivachenko, A.,
1555 Carter, S.L., Stewart, C., Mermel, C.H., Roberts, S.A., et al. (2013). Mutational
1556 heterogeneity in cancer and the search for new cancer-associated genes. Nature *499*, 214-
1557 218. 10.1038/nature12213.
1558 31. Thatikonda, V., Islam, S.M.A., Autry, R.J., Jones, B.C., Grobner, S.N., Warsow, G.,
1559 Hutter, B., Huebschmann, D., Frohling, S., Kool, M., et al. (2023). Comprehensive
1560 analysis of mutational signatures reveals distinct patterns and molecular processes across
1561 27 pediatric cancers. Nat Cancer *4*, 276-289. 10.1038/s43018-022-00509-4.
1562 32. Schimmel, J., Kool, H., van Schendel, R., and Tijsterman, M. (2017). Mutational
1563 signatures of non-homologous and polymerase theta-mediated end-joining in embryonic
1564 stem cells. EMBO J *36*, 3634-3649. 10.15252/embj.201796948.
1565 33. Johnson, C.N., Sojitra, K.A., Sohn, E.J., Moreno-Romero, A.K., Baudin, A., Xu, X.,
1566 Mittal, J., and Libich, D.S. (2024). Insights into Molecular Diversity within the
1567 FUS/EWS/TAF15 Protein Family: Unraveling Phase Separation of the N-Terminal Low-
1568 Complexity Domain from RNA-Binding Protein EWS. J Am Chem Soc *146*, 8071-8085.
1569 10.1021/jacs.3c12034.
1570 34. Ebersberger, S., Hipp, C., Mulorz, M.M., Buchbender, A., Hubrich, D., Kang, H.S.,
1571 Martinez-Lumbreras, S., Kristofori, P., Sutandy, F.X.R., Llacsahuanga Allcca, L., et al.
1572 (2023). FUBP1 is a general splicing factor facilitating 3' splice site recognition and
1573 splicing of long introns. Mol Cell *83*, 2653-2672 e2615. 10.1016/j.molcel.2023.07.002.
1574 35. Graham, G.T., Selvanathan, S.P., Zollner, S.K., Stahl, E., Shlien, A., Caplen, N.J., Uren,
1575 A., and Toretsky, J.A. (2022). Comprehensive profiling of mRNA splicing indicates that
1576 GC content signals altered cassette exon inclusion in Ewing sarcoma. NAR Cancer *4*,
1577 zcab052. 10.1093/narcan/zcab052.
1578 36. Selvanathan, S.P., Graham, G.T., Erkizan, H.V., Dirksen, U., Natarajan, T.G., Dakic, A.,
1579 Yu, S., Liu, X., Paulsen, M.T., Ljungman, M.E., et al. (2015). Oncogenic fusion protein
1580 EWS-FLI1 is a network hub that regulates alternative splicing. Proc Natl Acad Sci U S A
1581 *112*, E1307-1316. 10.1073/pnas.1500536112.
1582 37. Zatreanu, D., Robinson, H.M.R., Alkhatib, O., Boursier, M., Finch, H., Geo, L., Grande,
1583 D., Grinkevich, V., Heald, R.A., Langdon, S., et al. (2021). Poltheta inhibitors elicit

1584 BRCA-gene synthetic lethality and target PARP inhibitor resistance. Nat Commun *12*,
1585 3636. 10.1038/s41467-021-23463-8.
1586 38. Llorens-Agost, M., Ensminger, M., Le, H.P., Gawai, A., Liu, J., Cruz-Garcia, A.,
1587 Bhetawal, S., Wood, R.D., Heyer, W.D., and Lobrich, M. (2021). POLtheta-mediated end
1588 joining is restricted by RAD52 and BRCA2 until the onset of mitosis. Nat Cell Biol *23*,
1589 1095-1104. 10.1038/s41556-021-00764-0.
1590 39. Gelot, C., Kovacs, M.T., Miron, S., Mylne, E., Haan, A., Boeffard-Dosierre, L., Ghouil,
1591 R., Popova, T., Dingli, F., Loew, D., et al. (2023). Poltheta is phosphorylated by PLK1 to
1592 repair double-strand breaks in mitosis. Nature *621*, 415-422. 10.1038/s41586-023-06506-
1593 6.
1594 40. Feng, W., Simpson, D.A., Carvajal-Garcia, J., Price, B.A., Kumar, R.J., Mose, L.E.,
1595 Wood, R.D., Rashid, N., Purvis, J.E., Parker, J.S., et al. (2019). Genetic determinants of
1596 cellular addiction to DNA polymerase theta. Nat Commun *10*, 4286. 10.1038/s41467-
1597 019-12234-1.
1598 41. Ceccaldi, R., Liu, J.C., Amunugama, R., Hajdu, I., Primack, B., Petalcorin, M.I.,
1599 O'Connor, K.W., Konstantinopoulos, P.A., Elledge, S.J., Boulton, S.J., et al. (2015).
1600 Homologous-recombination-deficient tumours are dependent on Poltheta-mediated
1601 repair. Nature *518*, 258-262. 10.1038/nature14184.
1602 42. Rogers, C.B., Kram, R.E., Lin, K., Myers, C.L., Sobeck, A., Hendrickson, E.A., and
1603 Bielinsky, A.K. (2023). Fanconi anemia-associated chromosomal radial formation is
1604 dependent on POLtheta-mediated alternative end joining. Cell Rep *42*, 112428.
1605 10.1016/j.celrep.2023.112428.
1606 43. Ceccaldi, R., Sarangi, P., and D'Andrea, A.D. (2016). The Fanconi anaemia pathway:
1607 new players and new functions. Nat Rev Mol Cell Biol *17*, 337-349.
1608 10.1038/nrm.2016.48.
1609 44. Kohsaka, S., Yagishita, S., Shirai, Y., Matsuno, Y., Ueno, T., Kojima, S., Ikeuchi, H.,
1610 Ikegami, M., Kitada, R., Yoshioka, K.I., et al. (2024). A molecular glue RBM39-degrader
1611 induces synthetic lethality in cancer cells with homologous recombination repair
1612 deficiency. NPJ Precis Oncol *8*, 117. 10.1038/s41698-024-00610-0.
1613 45. Kumar, R.J., Chao, H.X., Simpson, D.A., Feng, W., Cho, M.G., Roberts, V.R., Sullivan,
1614 A.R., Shah, S.J., Wozny, A.S., Fagan-Solis, K., et al. (2020). Dual inhibition of DNA-PK
1615 and DNA polymerase theta overcomes radiation resistance induced by p53 deficiency.
1616 NAR Cancer *2*, zcaa038. 10.1093/narcan/zcaa038.
1617 46. Patterson-Fortin, J., Bose, A., Tsai, W.C., Grochala, C., Nguyen, H., Zhou, J., Parmar,
1618 K., Lazaro, J.B., Liu, J., McQueen, K., et al. (2022). Targeting DNA Repair with
1619 Combined Inhibition of NHEJ and MMEJ Induces Synthetic Lethality in TP53-Mutant
1620 Cancers. Cancer Res *82*, 3815-3829. 10.1158/0008-5472.CAN-22-1124.
1621 47. Collins, V.J., Ludwig, K.R., Nelson, A.E., Sundara Rajan, S., Yeung, C., Vulikh, K.,
1622 Isanogle, K.A., Mendoza, A., Difilippantonio, S., Karim, B.O., et al. (2024). Enhancing
1623 standard of care chemotherapy efficacy using DNA-dependent protein kinase (DNA-PK)
1624 inhibition in preclinical models of Ewing sarcoma. Mol Cancer Ther. 10.1158/1535-
1625 7163.MCT-23-0641.
1626 48. Dubbury, S.J., Boutz, P.L., and Sharp, P.A. (2018). CDK12 regulates DNA repair genes
1627 by suppressing intronic polyadenylation. Nature *564*, 141-145. 10.1038/s41586-018-
1628 0758-y.

1629 49. Iniguez, A.B., Stolte, B., Wang, E.J., Conway, A.S., Alexe, G., Dharia, N.V.,
1630 Kwiatkowski, N., Zhang, T., Abraham, B.J., Mora, J., et al. (2018). EWS/FLI Confers
1631 Tumor Cell Synthetic Lethality to CDK12 Inhibition in Ewing Sarcoma. Cancer Cell *33*,
1632 202-216 e206. 10.1016/j.ccell.2017.12.009.
1633 50. Gounder, M.M., Agaram, N.P., Trabucco, S.E., Robinson, V., Ferraro, R.A., Millis, S.Z.,
1634 Krishnan, A., Lee, J., Attia, S., Abida, W., et al. (2022). Clinical genomic profiling in the
1635 management of patients with soft tissue and bone sarcoma. Nat Commun *13*, 3406.
1636 10.1038/s41467-022-30496-0.
1637 51. Tirode, F., Surdez, D., Ma, X., Parker, M., Le Deley, M.C., Bahrami, A., Zhang, Z.,
1638 Lapouble, E., Grossetete-Lalami, S., Rusch, M., et al. (2014). Genomic landscape of
1639 Ewing sarcoma defines an aggressive subtype with co-association of STAG2 and TP53
1640 mutations. Cancer Discov *4*, 1342-1353. 10.1158/2159-8290.CD-14-0622.
1641 52. Dutertre, M., Sanchez, G., De Cian, M.C., Barbier, J., Dardenne, E., Gratadou, L.,
1642 Dujardin, G., Le Jossic-Corcos, C., Corcos, L., and Auboeuf, D. (2010).
1643 Cotranscriptional exon skipping in the genotoxic stress response. Nat Struct Mol Biol *17*,
1644 1358-1366. 10.1038/nsmb.1912.
1645 53. Paronetto, M.P., Minana, B., and Valcarcel, J. (2011). The Ewing sarcoma protein
1646 regulates DNA damage-induced alternative splicing. Mol Cell *43*, 353-368.
1647 10.1016/j.molcel.2011.05.035.
1648 54. Verdile, V., Svetoni, F., La Rosa, P., Ferrante, G., Cesari, E., Sette, C., and Paronetto,
1649 M.P. (2022). EWS splicing regulation contributes to balancing Foxp1 isoforms required
1650 for neuronal differentiation. Nucleic Acids Res *50*, 3362-3378. 10.1093/nar/gkac154.
1651 55. Maurer, L.M., Daley, J.D., Mukherjee, E., Venier, R.E., Julian, C.M., Bailey, N.G.,
1652 Jacobs, M.F., Kumar-Sinha, C., Raphael, H., Periyapatna, N., et al. (2022). BRCA1-
1653 associated RING domain-1 (BARD1) loss and GBP1 expression enhance sensitivity to
1654 DNA damage in Ewing sarcoma. Cancer Res Commun *2*, 220-232. 10.1158/2767-
1655 9764.crc-21-0047.
1656 56. Menon, S., Breese, M.R., Lin, Y.P., Allegakoen, H., Perati, S., Heslin, A., Horlbeck,
1657 M.A., Weissman, J., Sweet-Cordero, E.A., Bivona, T.G., and Tulpule, A. (2023). FET
1658 fusion oncoproteins disrupt physiologic DNA repair networks and induce ATR synthetic
1659 lethality in cancer. Res Sq. 10.21203/rs.3.rs-2869150/v1.
1660 57. Mateos-Gomez, P.A., Gong, F., Nair, N., Miller, K.M., Lazzerini-Denchi, E., and Sfeir,
1661 A. (2015). Mammalian polymerase theta promotes alternative NHEJ and suppresses
1662 recombination. Nature *518*, 254-257. 10.1038/nature14157.
1663 58. Bhat, P., Chow, A., Emert, B., Ettlin, O., Quinodoz, S.A., Strehle, M., Takei, Y., Burr,
1664 A., Goronzy, I.N., Chen, A.W., et al. (2024). Genome organization around nuclear
1665 speckles drives mRNA splicing efficiency. Nature *629*, 1165-1173. 10.1038/s41586-024-
1666 07429-6.
1667 59. Wang, J., Schultz, P.G., and Johnson, K.A. (2018). Mechanistic studies of a small-
1668 molecule modulator of SMN2 splicing. Proc Natl Acad Sci U S A *115*, E4604-E4612.
1669 10.1073/pnas.1800260115.
1670 60. Duncan, R., Collins, I., Tomonaga, T., Zhang, T., and Levens, D. (1996). A unique
1671 transactivation sequence motif is found in the carboxyl-terminal domain of the single-
1672 strand-binding protein FBP. Mol Cell Biol *16*, 2274-2282. 10.1128/MCB.16.5.2274.
1673 61. Farag, M., Cohen, S.R., Borcherds, W.M., Bremer, A., Mittag, T., and Pappu, R.V.
1674 (2022). Condensates formed by prion-like low-complexity domains have small-world

1675 network structures and interfaces defined by expanded conformations. Nat Commun *13*,
1676 7722. 10.1038/s41467-022-35370-7.
1677 62. Wang, J., Choi, J.M., Holehouse, A.S., Lee, H.O., Zhang, X., Jahnel, M., Maharana, S.,
1678 Lemaitre, R., Pozniakovsky, A., Drechsel, D., et al. (2018). A Molecular Grammar
1679 Governing the Driving Forces for Phase Separation of Prion-like RNA Binding Proteins.
1680 Cell *174*, 688-699 e616. 10.1016/j.cell.2018.06.006.
1681 63. Seong, B.K.A., Dharia, N.V., Lin, S., Donovan, K.A., Chong, S., Robichaud, A.,
1682 Conway, A., Hamze, A., Ross, L., Alexe, G., et al. (2021). TRIM8 modulates the
1683 EWS/FLI oncoprotein to promote survival in Ewing sarcoma. Cancer Cell *39*, 1262-1278
1684 e1267. 10.1016/j.ccell.2021.07.003.
1685 64. Abeykoon, J., Asada, S., Zhu, G., Hirohashi, Y., Moreau, L., Iyer, D.R., Mukkavalli, S.,
1686 Parmar, K., Zambrano, G., Jiang, L., et al. (2025). Cyclin D1 overexpression induces
1687 replication stress and microhomology-mediated end-joining dependence in mantle cell
1688 lymphoma. J Clin Invest. 10.1172/JCI193006.
1689 65. Chaudhary, U.B., and Haldas, J.R. (2003). Long-term complications of chemotherapy for
1690 germ cell tumours. Drugs *63*, 1565-1577. 10.2165/00003495-200363150-00004.
1691 66. Lim, K.S., Li, H., Roberts, E.A., Gaudiano, E.F., Clairmont, C., Sambel, L.A.,
1692 Ponnienselvan, K., Liu, J.C., Yang, C., Kozono, D., et al. (2018). USP1 Is Required for
1693 Replication Fork Protection in BRCA1-Deficient Tumors. Mol Cell *72*, 925-941 e924.
1694 10.1016/j.molcel.2018.10.045.
1695 67. Hayer, A., Shao, L., Chung, M., Joubert, L.M., Yang, H.W., Tsai, F.C., Bisaria, A.,
1696 Betzig, E., and Meyer, T. (2016). Engulfed cadherin fingers are polarized junctional
1697 structures between collectively migrating endothelial cells. Nat Cell Biol *18*, 1311-1323.
1698 10.1038/ncb3438.
1699 68. Sanjana, N.E., Shalem, O., and Zhang, F. (2014). Improved vectors and genome-wide
1700 libraries for CRISPR screening. Nat Methods *11*, 783-784. 10.1038/nmeth.3047.
1701 69. Tyanova, S., Temu, T., Sinitcyn, P., Carlson, A., Hein, M.Y., Geiger, T., Mann, M., and
1702 Cox, J. (2016). The Perseus computational platform for comprehensive analysis of
1703 (prote)omics data. Nat Methods *13*, 731-740. 10.1038/nmeth.3901.
1704 70. Ritchie, M.E., Phipson, B., Wu, D., Hu, Y., Law, C.W., Shi, W., and Smyth, G.K. (2015).
1705 limma powers differential expression analyses for RNA-sequencing and microarray
1706 studies. Nucleic Acids Res *43*, e47. 10.1093/nar/gkv007.
1707 71. Bray, N.L., Pimentel, H., Melsted, P., and Pachter, L. (2016). Near-optimal probabilistic
1708 RNA-seq quantification. Nat Biotechnol *34*, 525-527. 10.1038/nbt.3519.
1709 72. Frankish, A., Diekhans, M., Jungreis, I., Lagarde, J., Loveland, J.E., Mudge, J.M., Sisu,
1710 C., Wright, J.C., Armstrong, J., Barnes, I., et al. (2021). Gencode 2021. Nucleic Acids
1711 Res *49*, D916-D923. 10.1093/nar/gkaa1087.
1712 73. Soneson, C., Love, M.I., and Robinson, M.D. (2015). Differential analyses for RNA-seq:
1713 transcript-level estimates improve gene-level inferences. F1000Res *4*, 1521.
1714 10.12688/f1000research.7563.2.
1715 74. Robinson, M.D., McCarthy, D.J., and Smyth, G.K. (2010). edgeR: a Bioconductor
1716 package for differential expression analysis of digital gene expression data.
1717 Bioinformatics *26*, 139-140. 10.1093/bioinformatics/btp616.
1718 75. Love, M.I., Huber, W., and Anders, S. (2014). Moderated estimation of fold change and
1719 dispersion for RNA-seq data with DESeq2. Genome Biol *15*, 550. 10.1186/s13059-014-
1720 0550-8.

1721 76. Dobin, A., Davis, C.A., Schlesinger, F., Drenkow, J., Zaleski, C., Jha, S., Batut, P.,
1722 Chaisson, M., and Gingeras, T.R. (2013). STAR: ultrafast universal RNA-seq aligner.
1723 Bioinformatics *29*, 15-21. 10.1093/bioinformatics/bts635.
1724 77. Anders, S., Reyes, A., and Huber, W. (2012). Detecting differential usage of exons from
1725 RNA-seq data. Genome Res *22*, 2008-2017. 10.1101/gr.133744.111.
1726 78. Abramson, J., Adler, J., Dunger, J., Evans, R., Green, T., Pritzel, A., Ronneberger, O.,
1727 Willmore, L., Ballard, A.J., Bambrick, J., et al. (2024). Accurate structure prediction of
1728 biomolecular interactions with AlphaFold 3. Nature *630*, 493-500. 10.1038/s41586-024-
1729 07487-w.
1730 79. Chandramouly, G., Zhao, J., McDevitt, S., Rusanov, T., Hoang, T., Borisonnik, N.,
1731 Treddinick, T., Lopezcolorado, F.W., Kent, T., Siddique, L.A., et al. (2021). Poltheta
1732 reverse transcribes RNA and promotes RNA-templated DNA repair. Sci Adv *7*.
1733 10.1126/sciadv.abf1771.
1734 80. McLeod, C., Gout, A.M., Zhou, X., Thrasher, A., Rahbarinia, D., Brady, S.W., Macias,
1735 M., Birch, K., Finkelstein, D., Sunny, J., et al. (2021). St. Jude Cloud: A Pediatric Cancer
1736 Genomic Data-Sharing Ecosystem. Cancer Discov *11*, 1082-1099. 10.1158/2159-
1737 8290.CD-20-1230.
1738 81. Wang, Y., Xie, Z., Kutschera, E., Adams, J.I., Kadash-Edmondson, K.E., and Xing, Y.
1739 (2024). rMATS-turbo: an efficient and flexible computational tool for alternative splicing
1740 analysis of large-scale RNA-seq data. Nat Protoc *19*, 1083-1104. 10.1038/s41596-023-
1741 00944-2.
1742 82. Tobalina, L., Armenia, J., Irving, E., O'Connor, M.J., and Forment, J.V. (2021). A meta-
1743 analysis of reversion mutations in BRCA genes identifies signatures of DNA end-joining
1744 repair mechanisms driving therapy resistance. Ann Oncol *32*, 103-112.
1745 10.1016/j.annonc.2020.10.470.
1746 83. Taheri-Ghahfarokhi, A., Taylor, B.J.M., Nitsch, R., Lundin, A., Cavallo, A.L., Madeyski-
1747 Bengtson, K., Karlsson, F., Clausen, M., Hicks, R., Mayr, L.M., et al. (2018). Decoding
1748 non-random mutational signatures at Cas9 targeted sites. Nucleic Acids Res *46*, 8417-
1749 8434. 10.1093/nar/gky653.
1750 84. van Schendel, R., Roerink, S.F., Portegijs, V., van den Heuvel, S., and Tijsterman, M.
1751 (2015). Polymerase Theta is a key driver of genome evolution and of CRISPR/Cas9-
1752 mediated mutagenesis. Nat Commun *6*, 7394. 10.1038/ncomms8394.
1753 85. Yu, A.M., and McVey, M. (2010). Synthesis-dependent microhomology-mediated end
1754 joining accounts for multiple types of repair junctions. Nucleic Acids Res *38*, 5706-5717.
1755 10.1093/nar/gkq379.
1756 86. Smith, T.F., and Waterman, M.S. (1981). Identification of common molecular
1757 subsequences. J Mol Biol *147*, 195-197. 10.1016/0022-2836(81)90087-5.
1758

Figure 1

A

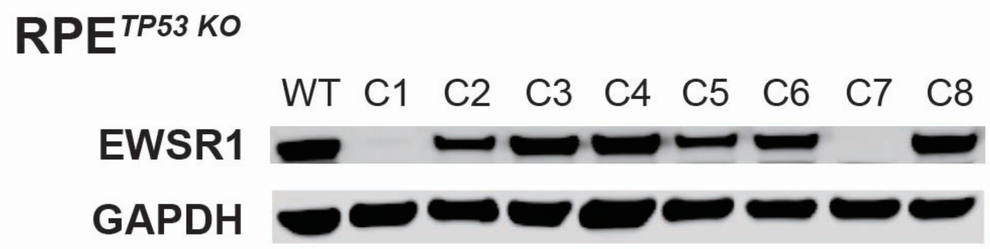

B

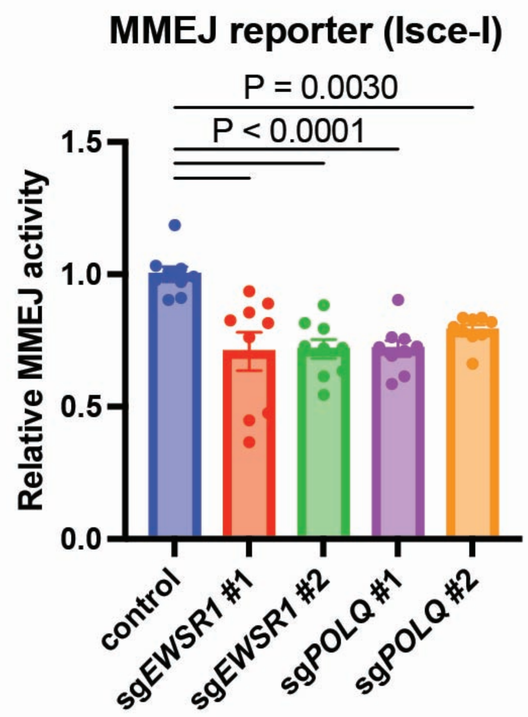

C

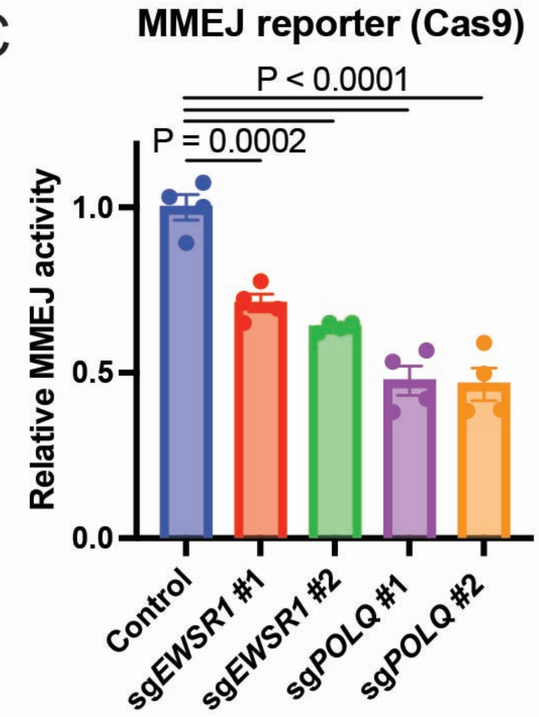

D

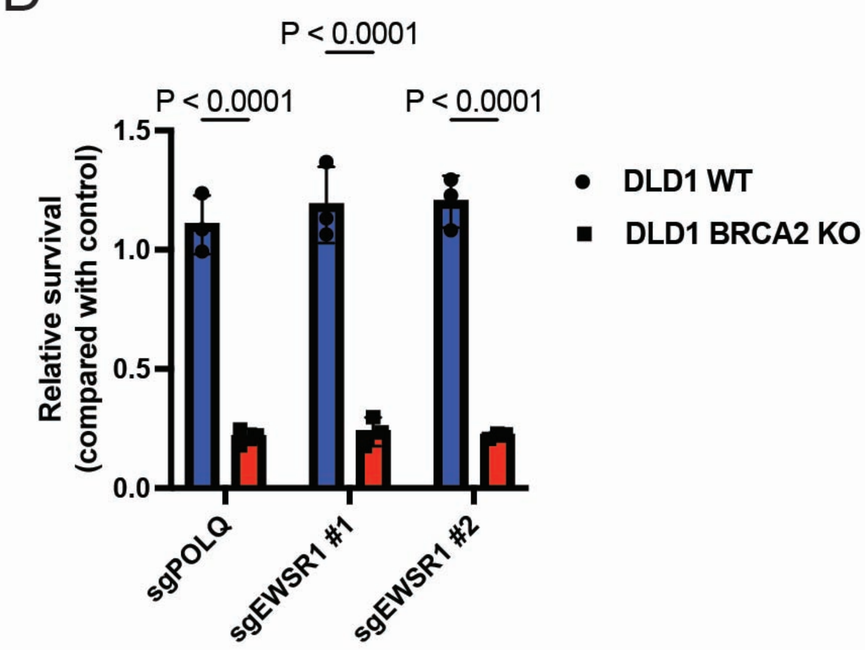

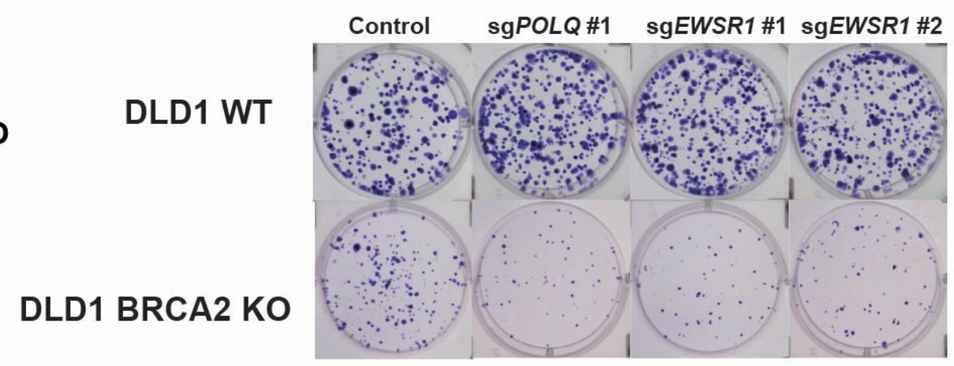

E

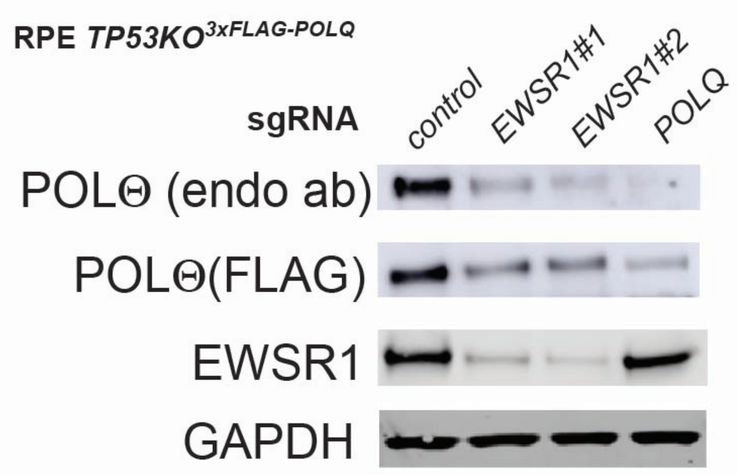

F

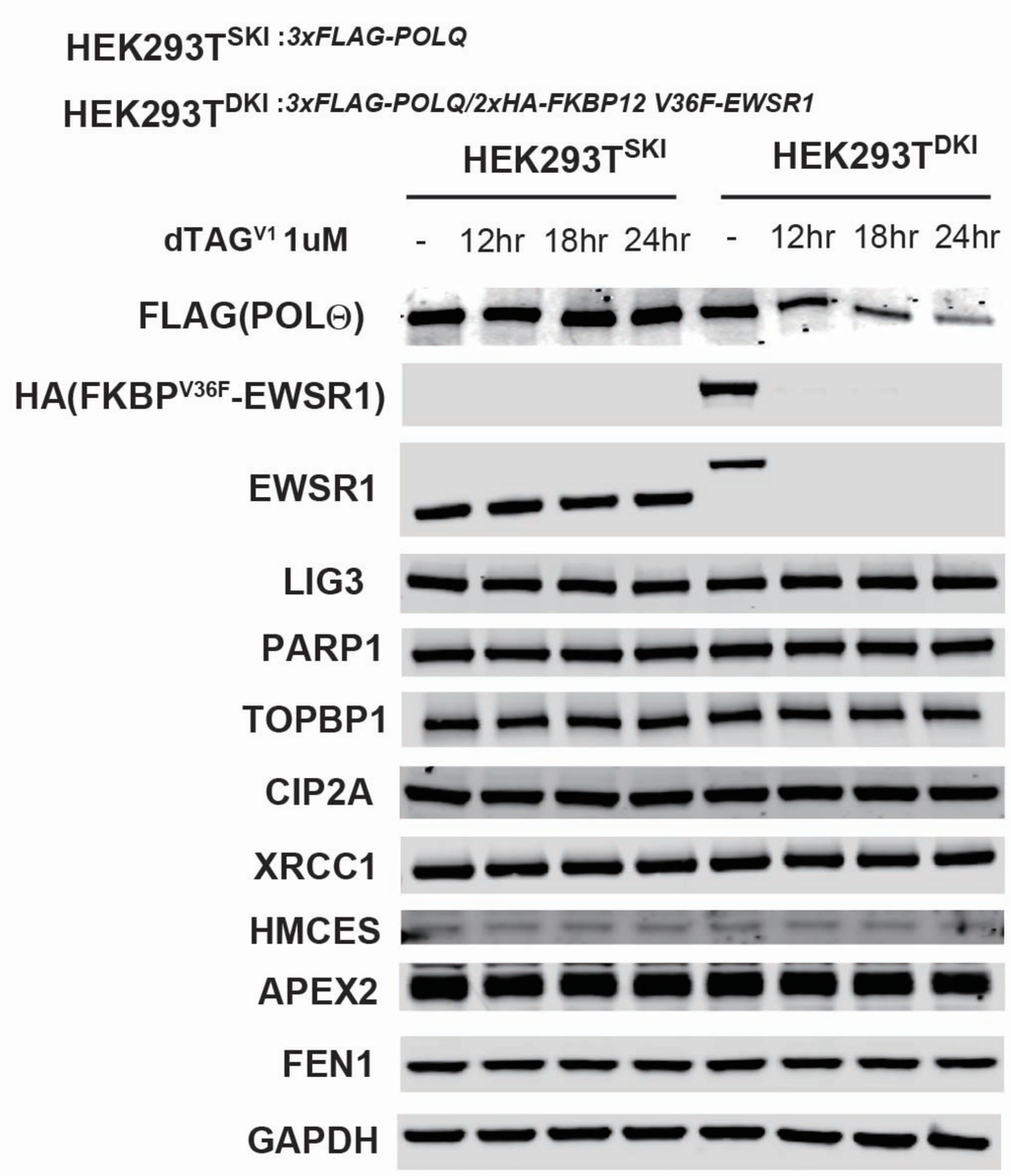

G

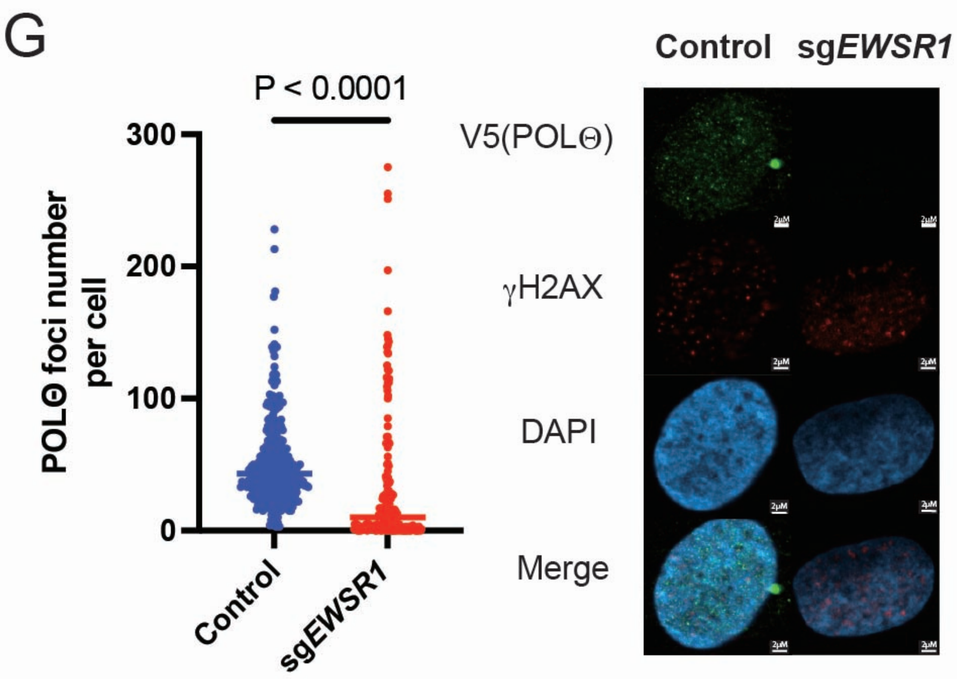

H

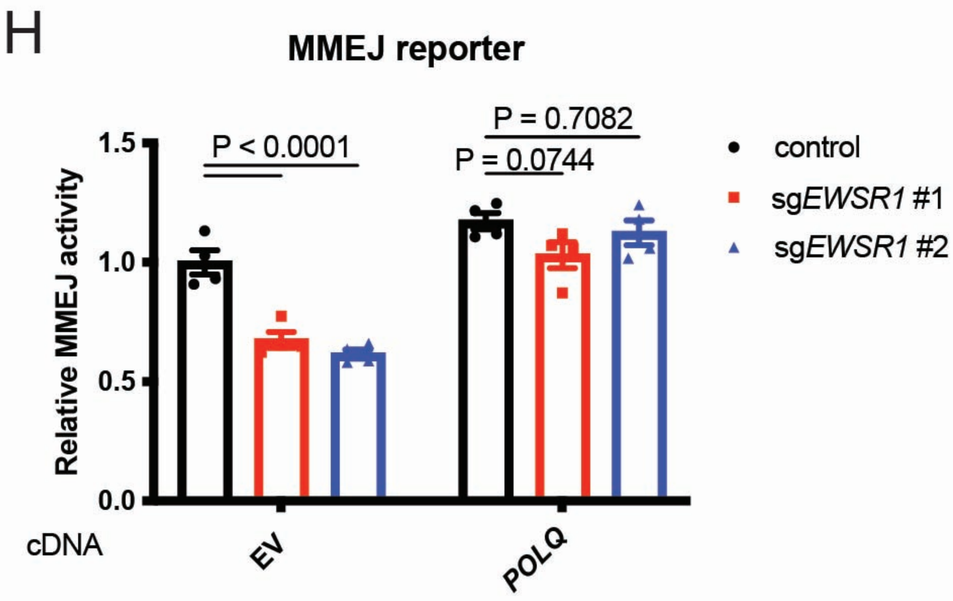

I

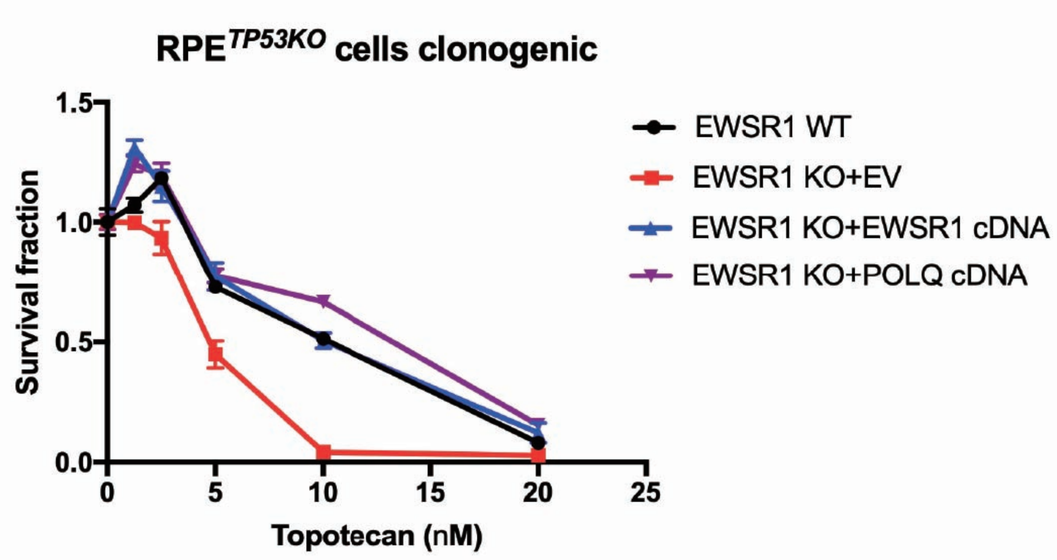

Figure 2

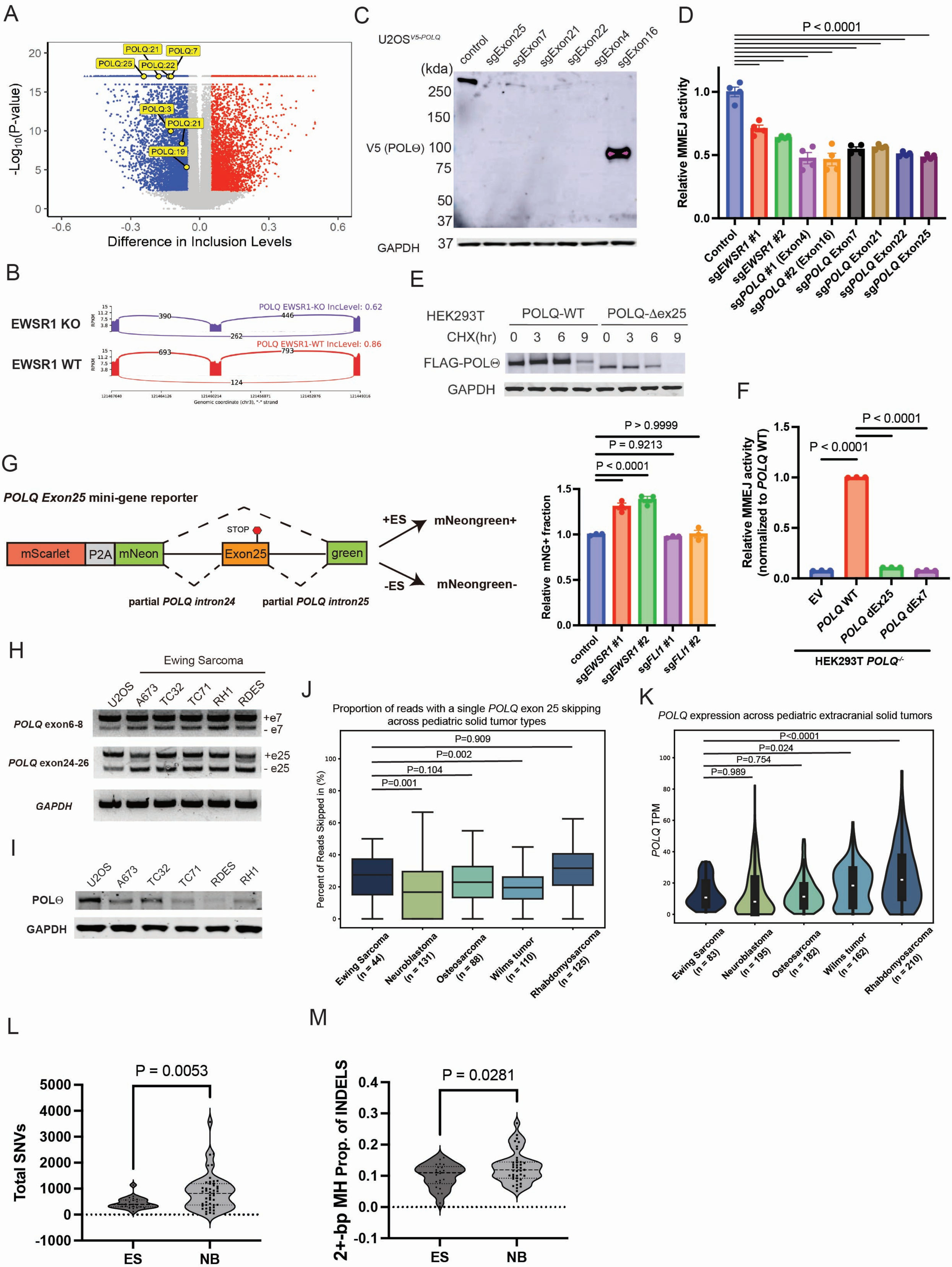
A
POLQ:21
POLQ:7
POLQ:25
POLQ:22
POLQ:3
POLQ:21
POLQ:19
-Log10(P-value)
Difference in Inclusion Levels
B
EWSR1 KO
EWSR1 WT
POLQ EWSR1-KO IncLevel: 0.62
POLQ EWSR1-WT IncLevel: 0.86
Genomic coordinate (chr3), "-" strand
C
U2OS V5-POLQ
control
sgExon25
sgExon7
sgExon21
sgExon22
sgExon4
sgExon16
(kda)
V5 (POLΘ)
GAPDH
D
P < 0.0001
Relative MMEJ activity
Control
sgEWSR1 #1
sgEWSR1 #2
sgPOLQ #1 (Exon4)
sgPOLQ #2 (Exon16)
sgPOLQ Exon7
sgPOLQ Exon21
sgPOLQ Exon22
sgPOLQ Exon25
E
HEK293T
POLQ-WT
POLQ-Δex25
CHX(hr)
FLAG-POLΘ
GAPDH
F
P < 0.0001
Relative MMEJ activity (normalized to POLQ WT)
EV
POLQ WT
POLQ dEx25
POLQ dEx7
HEK293T POLQ-/-
G
POLQ Exon25 mini-gene reporter
mScarlet
P2A
mNeon
STOP
Exon25
green
+ES
mNeongreen+
-ES
mNeongreen-
partial POLQ intron24
partial POLQ intron25
P > 0.9999
P = 0.9213
P < 0.0001
Relative mNG+ fraction
control
sgEWSR1 #1
sgEWSR1 #2
sgFLI1 #1
sgFLI1 #2
H
Ewing Sarcoma
U2OS
A673
TC32
TC71
RH1
RDES
POLQ exon6-8
+e7
- e7
POLQ exon24-26
+e25
- e25
GAPDH
I
U2OS
A673
TC32
TC71
RDES
RH1
POLΘ
GAPDH
J
Proportion of reads with a single POLQ exon 25 skipping across pediatric solid tumor types
P=0.909
P=0.002
P=0.104
P=0.001
Percent of Reads Skipped in (%)
Ewing Sarcoma (n = 44)
Neuroblastoma (n = 131)
Osteosarcoma (n = 88)
Wilms tumor (n = 110)
Rhabdomyosarcoma (n = 125)
K
POLQ expression across pediatric extracranial solid tumors
P<0.0001
P=0.024
P=0.754
P=0.989
POLQ TPM
Ewing Sarcoma (n = 83)
Neuroblastoma (n = 195)
Osteosarcoma (n = 182)
Wilms tumor (n = 162)
Rhabdomyosarcoma (n = 210)
L
P = 0.0053
Total SNVs
ES
NB
M
P = 0.0281
2+-bp MH Prop. of INDELS
ES
NB

Figure 3

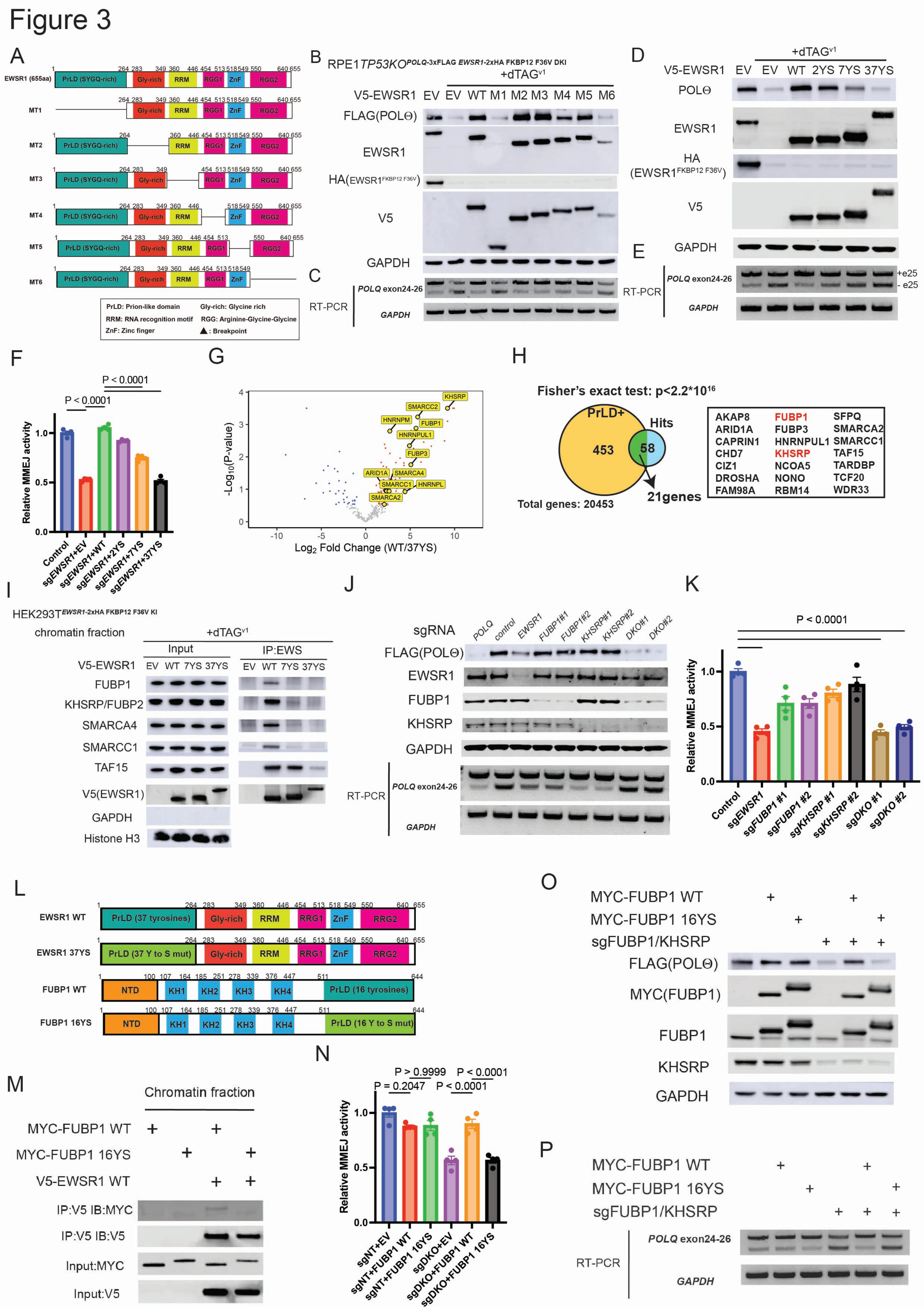
A
EWSR1 (655aa)
MT1
MT2
MT3
MT4
MT5
MT6
PrLD (SYGQ-rich)
Gly-rich
RRM
RGG1
ZnF
RGG2
PrLD: Prion-like domain
Gly-rich: Glycine rich
RRM: RNA recognition motif
RGG: Arginine-Glycine-Glycine
ZnF: Zinc finger
▲: Breakpoint
B
RPE1 TP53KO POLQ-3xFLAG EWSR1-2xHA FKBP12 F36V DKI
+dTAGv1
V5-EWSR1 EV EV WT M1 M2 M3 M4 M5 M6
FLAG(POLΘ)
EWSR1
HA(EWSR1FKBP12 F36V)
V5
GAPDH
C
RT-PCR
POLQ exon24-26
GAPDH
D
+dTAGv1
V5-EWSR1 EV EV WT 2YS 7YS 37YS
POLΘ
EWSR1
HA (EWSR1FKBP12 F36V)
V5
GAPDH
E
RT-PCR
POLQ exon24-26
+e25
- e25
GAPDH
F
P < 0.0001
P < 0.0001
Relative MMEJ activity
Control
sgEWSR1+EV
sgEWSR1+WT
sgEWSR1+2YS
sgEWSR1+7YS
sgEWSR1+37YS
G
-Log10(P-value)
Log2 Fold Change (WT/37YS)
KHSRP
SMARCC2
HNRNPM
FUBP1
HNRNPUL1
FUBP3
ARID1A
SMARCA4
SMARCC1
HNRNPL
SMARCA2
H
Fisher's exact test: p<2.2*10^16
PrLD+
453
Hits
58
21genes
Total genes: 20453
AKAP8 FUBP1 SFPQ
ARID1A FUBP3 SMARCA2
CAPRIN1 HNRNPUL1 SMARCC1
CHD7 KHSRP TAF15
CIZ1 NCOA5 TARDBP
DROSHA NONO TCF20
FAM98A RBM14 WDR33
I
HEK293T EWSR1-2xHA FKBP12 F36V KI
chromatin fraction
+dTAGv1
Input
IP:EWS
V5-EWSR1 EV WT 7YS 37YS EV WT 7YS 37YS
FUBP1
KHSRP/FUBP2
SMARCA4
SMARCC1
TAF15
V5(EWSR1)
GAPDH
Histone H3
J
sgRNA POLQ control EWSR1 FUBP1#1 FUBP1#2 KHSRP#1 KHSRP#2 DKO#1 DKO#2
FLAG(POLΘ)
EWSR1
FUBP1
KHSRP
GAPDH
RT-PCR
POLQ exon24-26
GAPDH
K
P < 0.0001
Relative MMEJ activity
Control
sgEWSR1
sgFUBP1 #1
sgFUBP1 #2
sgKHSRP #1
sgKHSRP #2
sgDKO #1
sgDKO #2
L
EWSR1 WT
EWSR1 37YS
PrLD (37 tyrosines)
PrLD (37 Y to S mut)
Gly-rich
RRM
RRG1
ZnF
RRG2
FUBP1 WT
FUBP1 16YS
NTD
KH1
KH2
KH3
KH4
PrLD (16 tyrosines)
PrLD (16 Y to S mut)
M
Chromatin fraction
MYC-FUBP1 WT
MYC-FUBP1 16YS
V5-EWSR1 WT
IP:V5 IB:MYC
IP:V5 IB:V5
Input:MYC
Input:V5
N
P > 0.9999
P < 0.0001
P = 0.2047
P < 0.0001
Relative MMEJ activity
sgNT+EV
sgNT+FUBP1 WT
sgNT+FUBP1 16YS
sgDKO+EV
sgDKO+FUBP1 WT
sgDKO+FUBP1 16YS
O
MYC-FUBP1 WT
MYC-FUBP1 16YS
sgFUBP1/KHSRP
FLAG(POLΘ)
MYC(FUBP1)
FUBP1
KHSRP
GAPDH
P
MYC-FUBP1 WT
MYC-FUBP1 16YS
sgFUBP1/KHSRP
RT-PCR
POLQ exon24-26
GAPDH

Figure 4

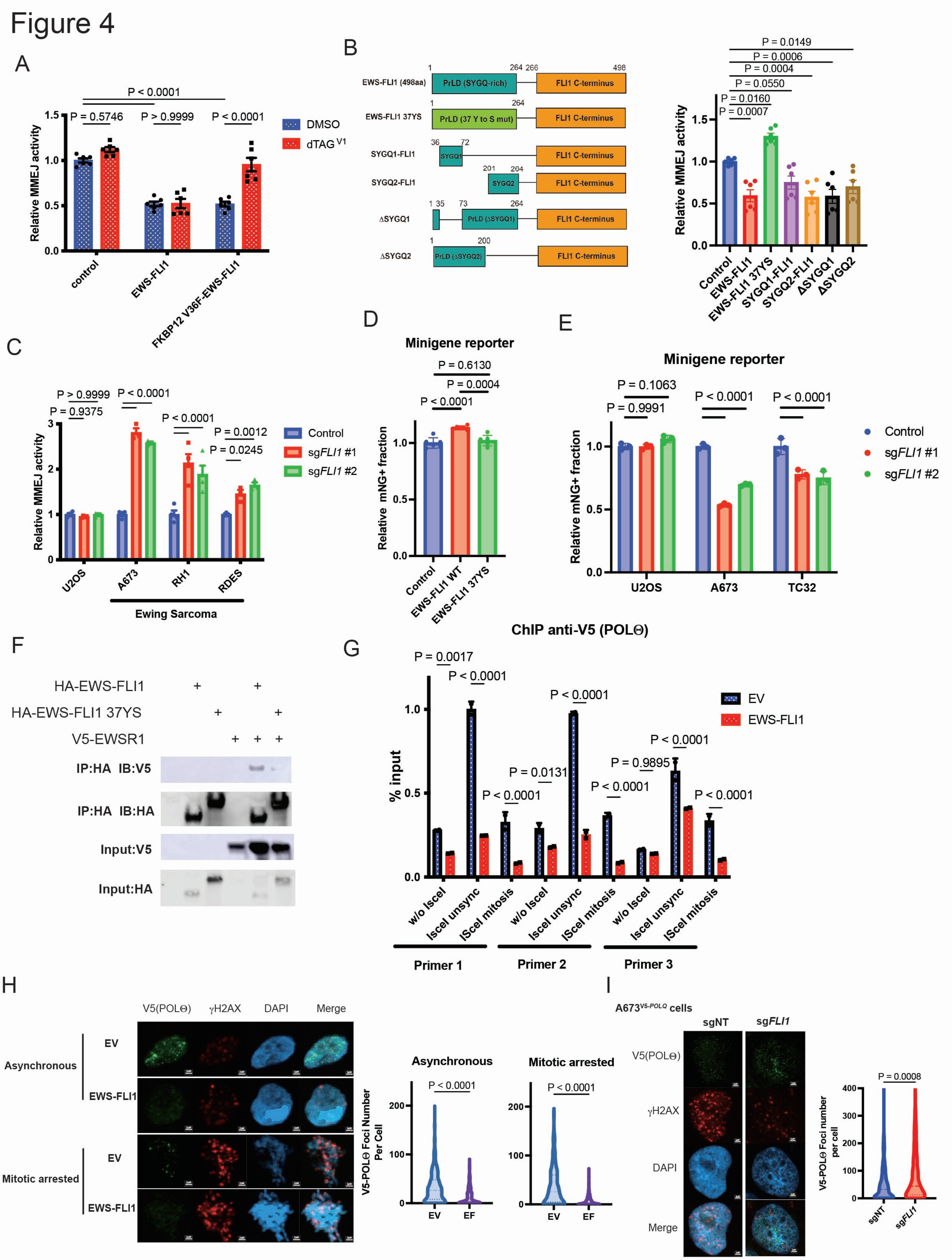
A
P < 0.0001
P = 0.5746
P > 0.9999
P < 0.0001
Relative MMEJ activity
DMSO
dTAG V1
control
EWS-FLI1
FKBP12 V36F-EWS-FLI1
B
EWS-FLI1 (498aa)
PrLD (SYGQ-rich)
FLI1 C-terminus
EWS-FLI1 37YS
PrLD (37 Y to S mut)
SYGQ1-FLI1
SYGQ1
SYGQ2-FLI1
SYGQ2
ΔSYGQ1
PrLD (ΔSYGQ1)
ΔSYGQ2
PrLD (ΔSYGQ2)
P = 0.0149
P = 0.0006
P = 0.0004
P = 0.0550
P = 0.0160
P = 0.0007
Control
EWS-FLI1
EWS-FLI1 37YS
SYGQ1-FLI1
SYGQ2-FLI1
ΔSYGQ1
ΔSYGQ2
C
P > 0.9999
P = 0.9375
P < 0.0001
P < 0.0001
P = 0.0012
P = 0.0245
Control
sgFLI1 #1
sgFLI1 #2
U2OS
A673
RH1
RDES
Ewing Sarcoma
D
Minigene reporter
P = 0.6130
P = 0.0004
P < 0.0001
Relative mNG+ fraction
Control
EWS-FLI1 WT
EWS-FLI1 37YS
E
Minigene reporter
P = 0.1063
P = 0.9991
P < 0.0001
P < 0.0001
U2OS
A673
TC32
F
HA-EWS-FLI1
HA-EWS-FLI1 37YS
V5-EWSR1
IP:HA IB:V5
IP:HA IB:HA
Input:V5
Input:HA
G
ChIP anti-V5 (POLΘ)
P = 0.0017
P < 0.0001
P < 0.0001
P = 0.0131
P < 0.0001
P < 0.0001
P = 0.9895
P < 0.0001
P < 0.0001
% input
EV
EWS-FLI1
w/o IScel
IScel unsync
IScel mitosis
Primer 1
Primer 2
Primer 3
H
V5(POLΘ)
γH2AX
DAPI
Merge
Asynchronous
Mitotic arrested
EV
EWS-FLI1
V5-POLΘ Foci Number Per Cell
P < 0.0001
P < 0.0001
EV
EF
I
A673V5-POLQ cells
sgNT
sgFLI1
V5(POLΘ)
γH2AX
DAPI
Merge
P = 0.0008
V5-POLΘ Foci number per cell
sgNT
sgFLI1

Figure 5

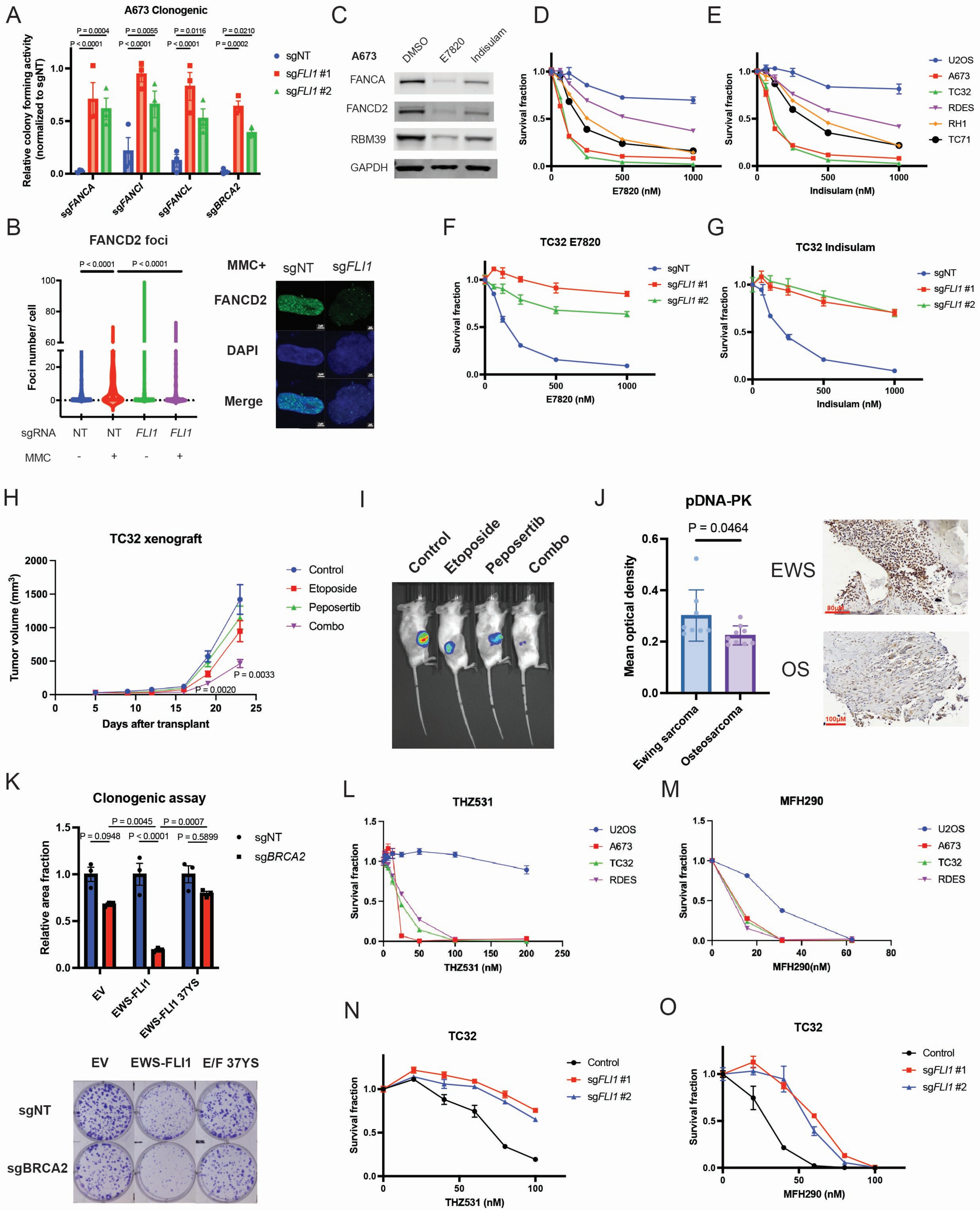
A
A673 Clonogenic
Relative colony forming activity (normalized to sgNT)
P = 0.0004
P < 0.0001
P = 0.0055
P < 0.0001
P = 0.0116
P < 0.0001
P = 0.0210
P = 0.0002
sgNT
sgFLI1 #1
sgFLI1 #2
sgFANCA
sgFANCI
sgFANCL
sgBRCA2
C
A673
DMSO
E7820
Indisulam
FANCA
FANCD2
RBM39
GAPDH
D
Survival fraction
E7820 (nM)
E
Indisulam (nM)
U2OS
A673
TC32
RDES
RH1
TC71
B
FANCD2 foci
Foci number/ cell
P < 0.0001
P < 0.0001
sgRNA
NT
NT
FLI1
FLI1
MMC
-
+
-
+
MMC+
sgNT
sgFLI1
FANCD2
DAPI
Merge
F
TC32 E7820
G
TC32 Indisulam
H
TC32 xenograft
Tumor volume (mm3)
Days after transplant
Control
Etoposide
Peposertib
Combo
P = 0.0033
P = 0.0020
I
Control
Etoposide
Peposertib
Combo
J
pDNA-PK
P = 0.0464
Mean optical density
Ewing sarcoma
Osteosarcoma
EWS
OS
K
Clonogenic assay
Relative area fraction
P = 0.0045
P = 0.0007
P = 0.0948
P < 0.0001
P = 0.5899
sgNT
sgBRCA2
EV
EWS-FLI1
EWS-FLI1 37YS
EV
EWS-FLI1
E/F 37YS
sgNT
sgBRCA2
L
THZ531
THZ531 (nM)
M
MFH290
MFH290(nM)
N
TC32
THZ531 (nM)
O
TC32
MFH290 (nM)

Figure S1

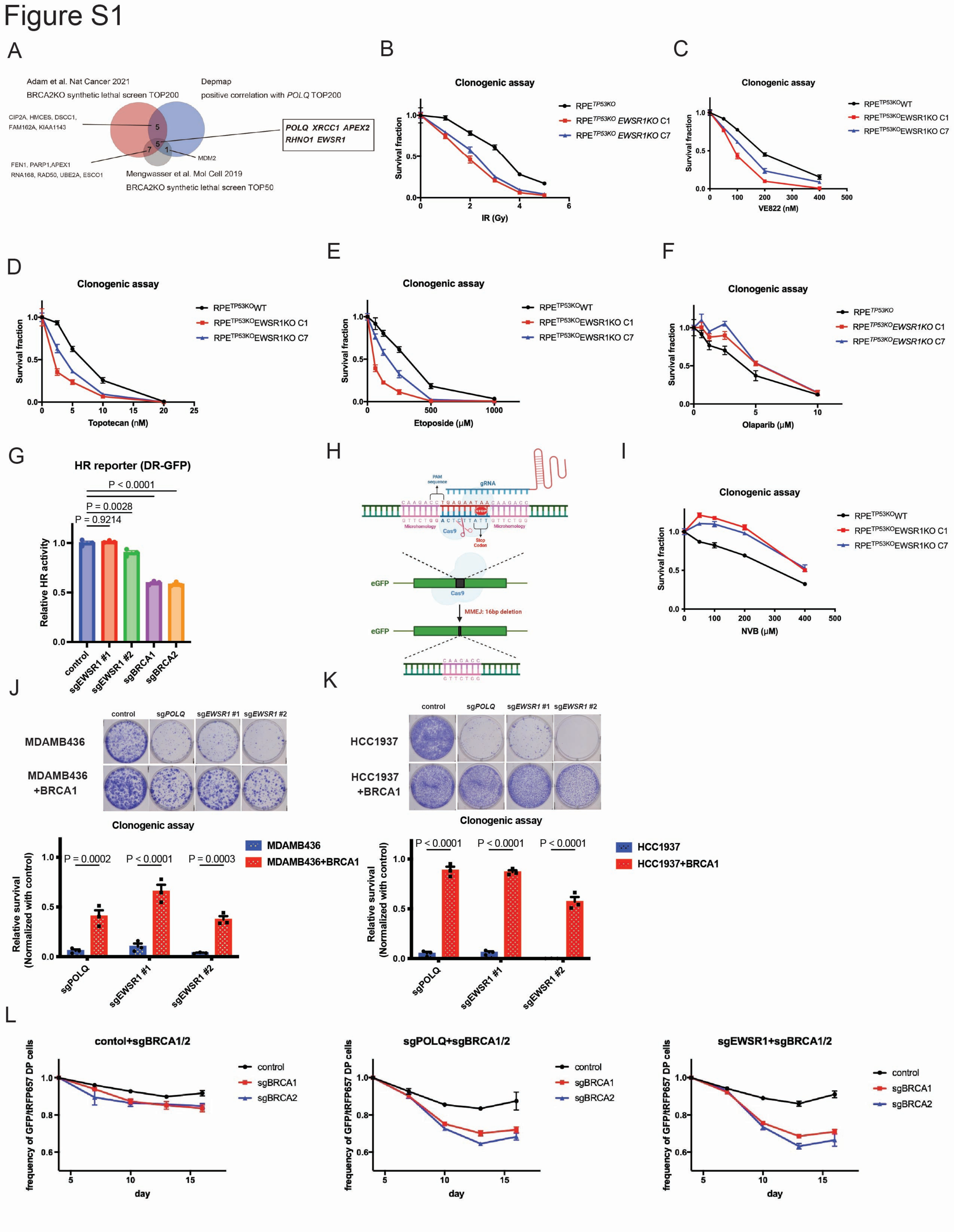
A
Adam et al. Nat Cancer 2021
BRCA2KO synthetic lethal screen TOP200
Depmap
positive correlation with POLQ TOP200
CIP2A, HMCES, DSCC1, FAM162A, KIAA1143
5
5
7
1
MDM2
POLQ XRCC1 APEX2 RHNO1 EWSR1
FEN1, PARP1,APEX1 RNA168, RAD50, UBE2A, ESCO1
Mengwasser et al. Mol Cell 2019
BRCA2KO synthetic lethal screen TOP50
B
Clonogenic assay
Survival fraction
IR (Gy)
RPE TP53KO
RPE TP53KO EWSR1KO C1
RPE TP53KO EWSR1KO C7
C
Clonogenic assay
Survival fraction
VE822 (nM)
RPE TP53KO WT
RPE TP53KO EWSR1KO C1
RPE TP53KO EWSR1KO C7
D
Clonogenic assay
Survival fraction
Topotecan (nM)
RPE TP53KO WT
RPE TP53KO EWSR1KO C1
RPE TP53KO EWSR1KO C7
E
Clonogenic assay
Survival fraction
Etoposide (μM)
RPE TP53KO WT
RPE TP53KO EWSR1KO C1
RPE TP53KO EWSR1KO C7
F
Clonogenic assay
Survival fraction
Olaparib (μM)
RPE TP53KO
RPE TP53KO EWSR1KO C1
RPE TP53KO EWSR1KO C7
G
HR reporter (DR-GFP)
P < 0.0001
P = 0.0028
P = 0.9214
Relative HR activity
control
sgEWSR1 #1
sgEWSR1 #2
sgBRCA1
sgBRCA2
H
PAM sequence
gRNA
STOP
Microhomology
Cas9
Stop Codon
eGFP
MMEJ: 16bp deletion
I
Clonogenic assay
Survival fraction
NVB (μM)
RPE TP53KO WT
RPE TP53KO EWSR1KO C1
RPE TP53KO EWSR1KO C7
J
control
sgPOLQ
sgEWSR1 #1
sgEWSR1 #2
MDAMB436
MDAMB436 +BRCA1
Clonogenic assay
Relative survival (Normalized with control)
P = 0.0002
P < 0.0001
P = 0.0003
MDAMB436
MDAMB436+BRCA1
sgPOLQ
sgEWSR1 #1
sgEWSR1 #2
K
control
sgPOLQ
sgEWSR1 #1
sgEWSR1 #2
HCC1937
HCC1937 +BRCA1
Clonogenic assay
Relative survival (Normalized with control)
P < 0.0001
P < 0.0001
P < 0.0001
HCC1937
HCC1937+BRCA1
sgPOLQ
sgEWSR1 #1
sgEWSR1 #2
L
contol+sgBRCA1/2
frequency of GFP/tRFP657 DP cells
day
control
sgBRCA1
sgBRCA2
sgPOLQ+sgBRCA1/2
frequency of GFP/tRFP657 DP cells
day
control
sgBRCA1
sgBRCA2
sgEWSR1+sgBRCA1/2
frequency of GFP/tRFP657 DP cells
day
control
sgBRCA1
sgBRCA2

Figure S2

A

RPE *TP53*KO$^{3xFLAG\text{-}POLQ}$

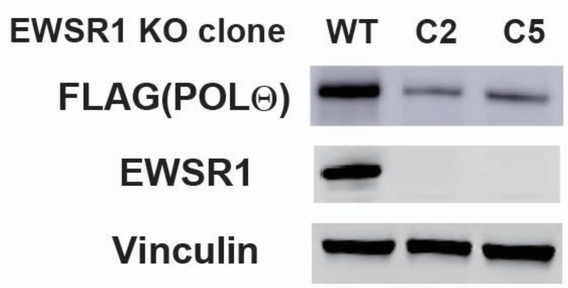

B

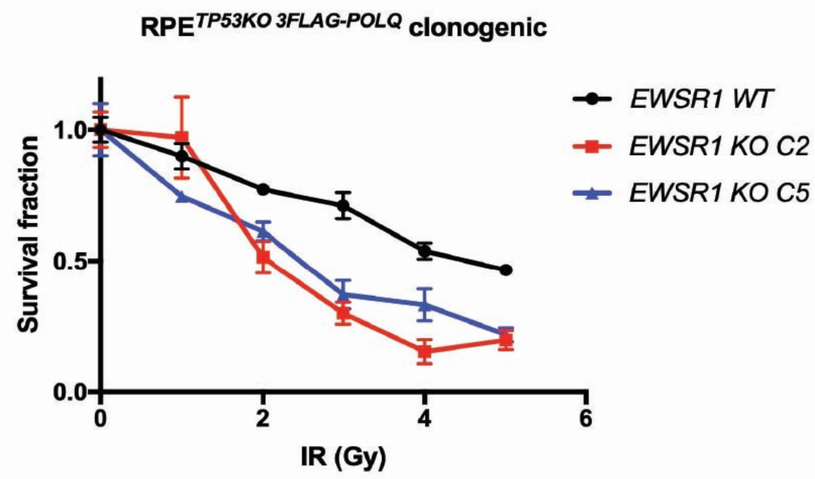

C

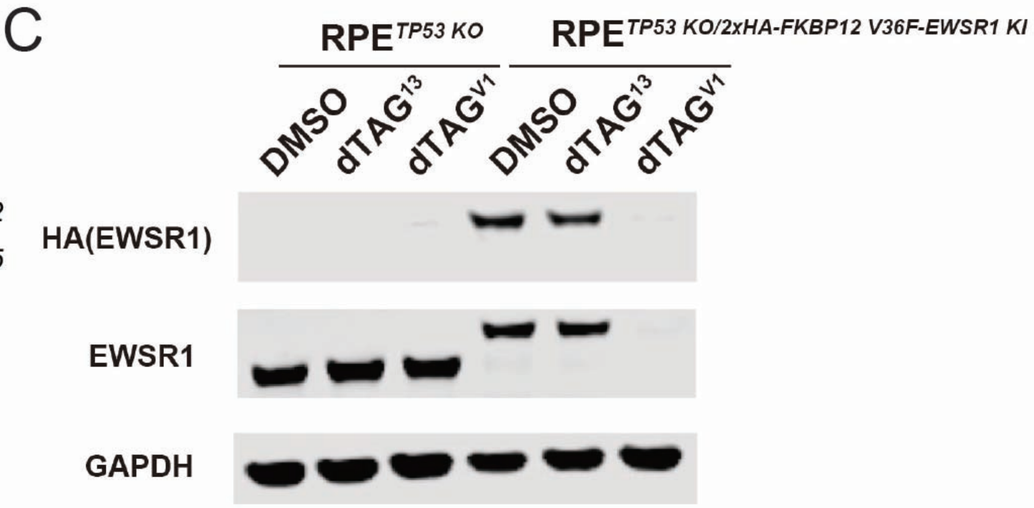

D

RPE$^{TP53\ KO/2xHA\text{-}FKBP12\ V36F\text{-}EWSR1\ KI}$

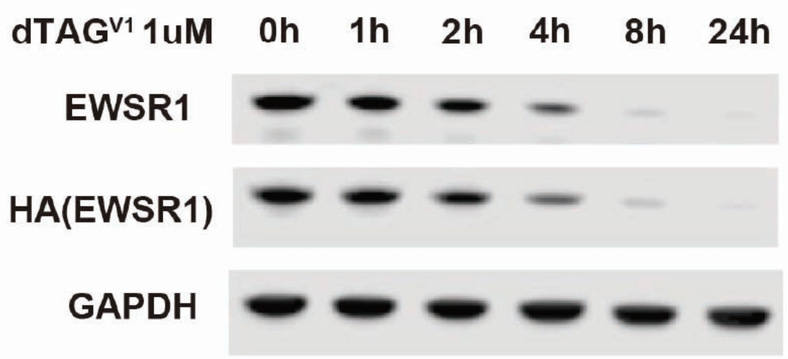

F

RPE *TP53KO*^{SKI} :*3xFLAG-POLQ*

RPE *TP53KO*^{DKI} :*3xFLAG-POLQ/2xHA-FKBP12 V36F-EWSR1*

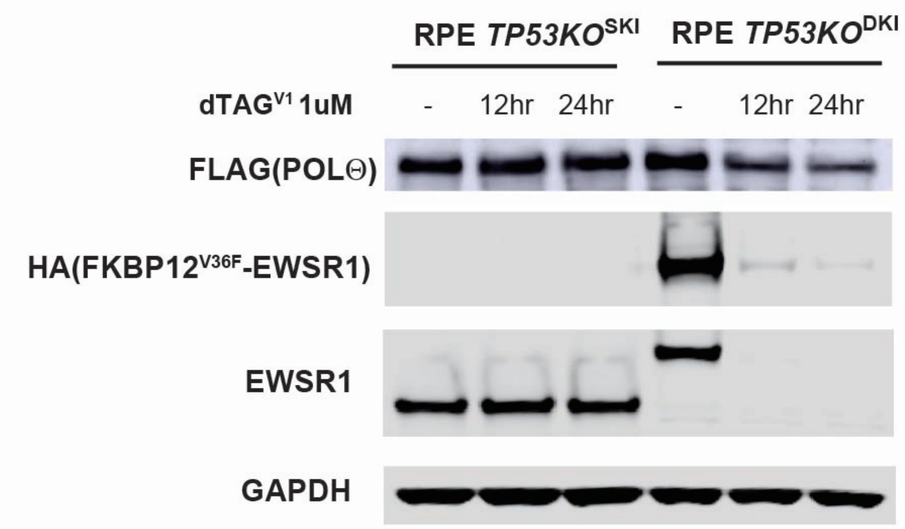

E

RPE$^{TP53\ KO/2xHA\text{-}FKBP12\ V36F\text{-}EWSR1\ KI}$

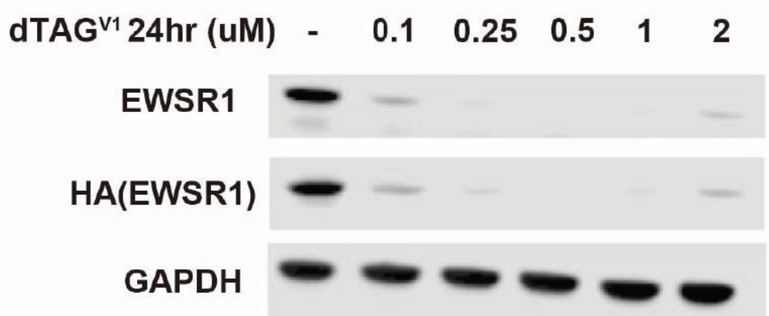

H

RPE1*TP53KO*$^{POLQ\text{-}3xFLAG\ KI}$

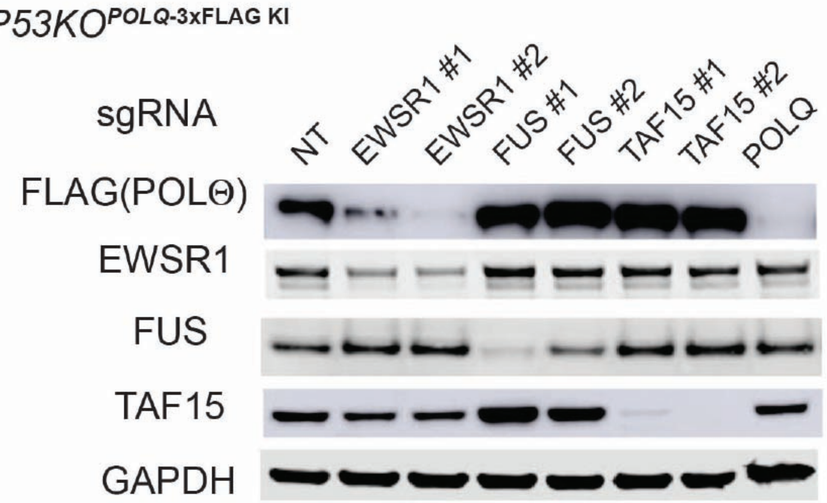

G

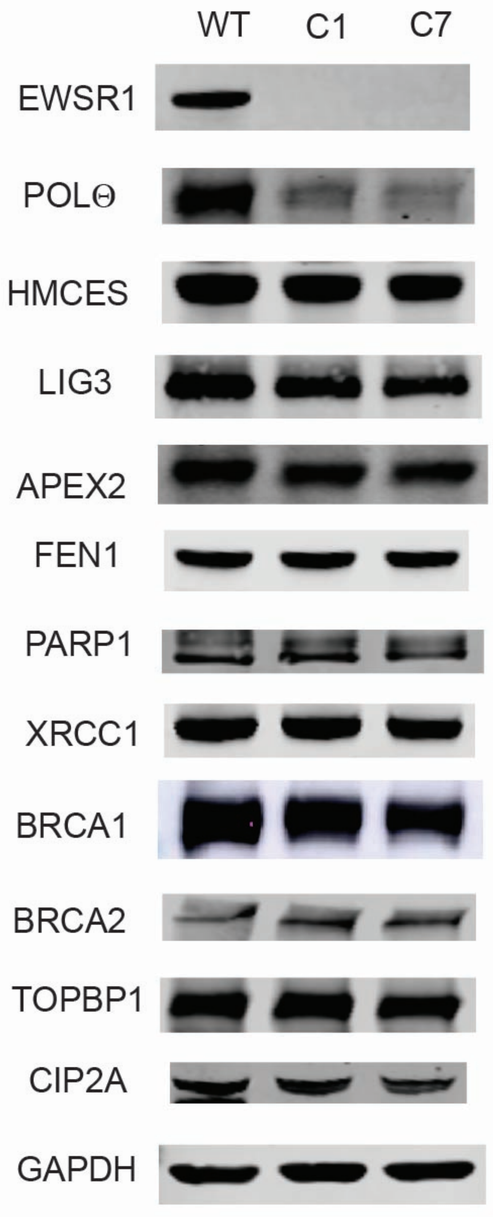

I

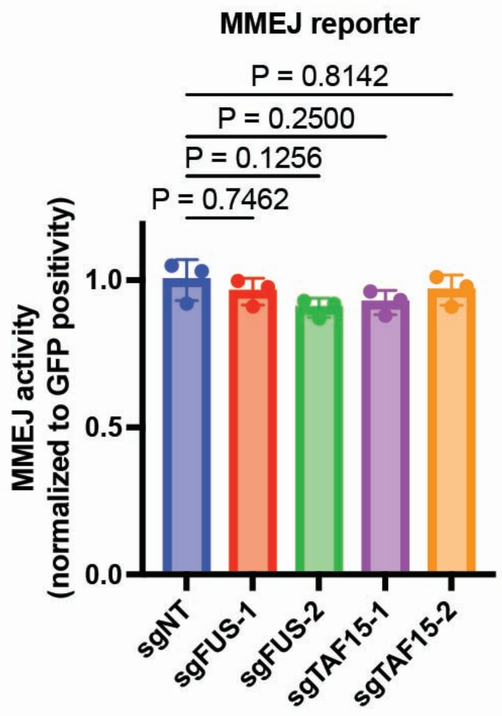

J

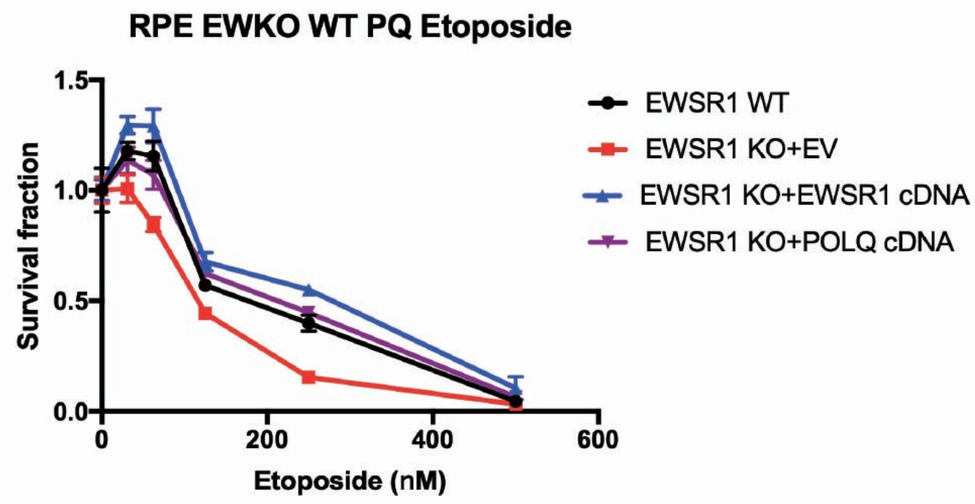

K

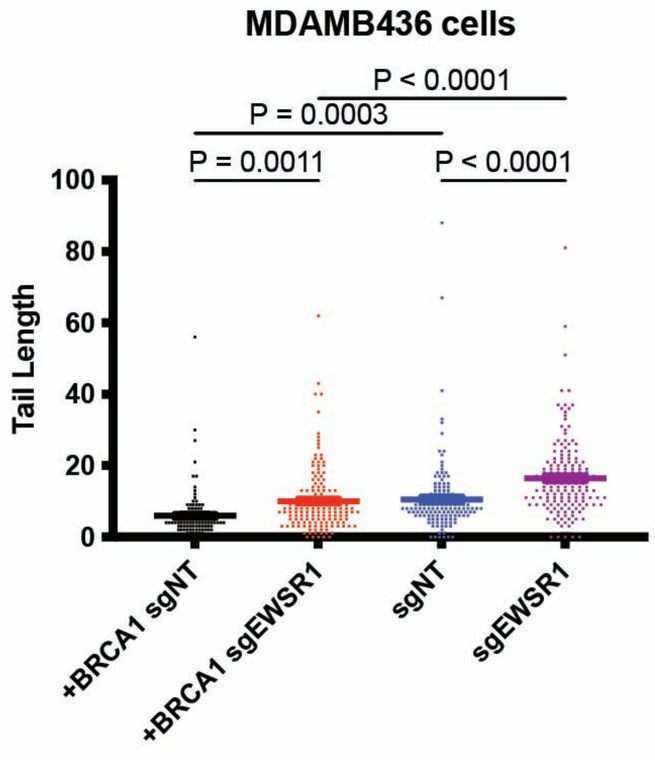

L

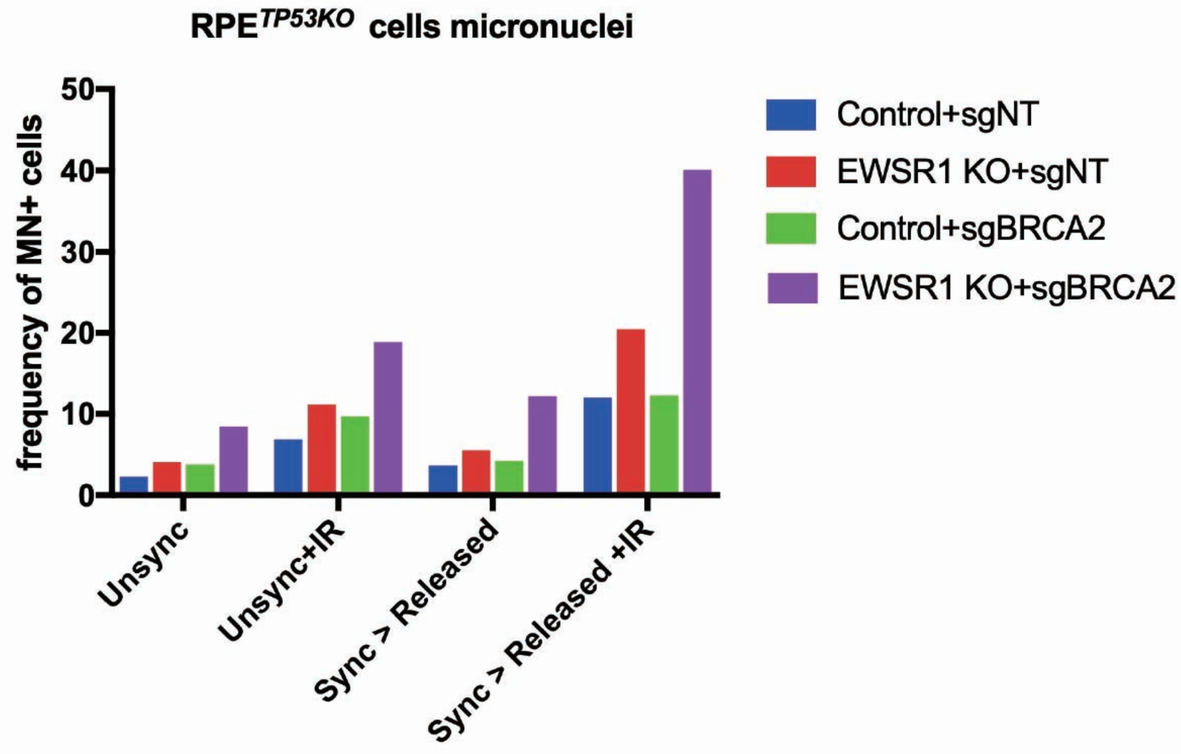

Figure S3

A

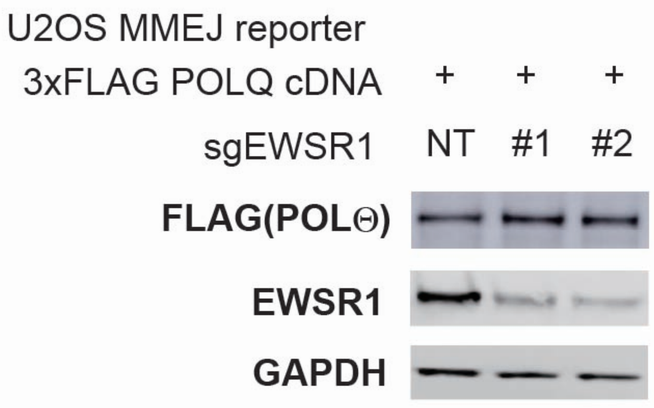

B

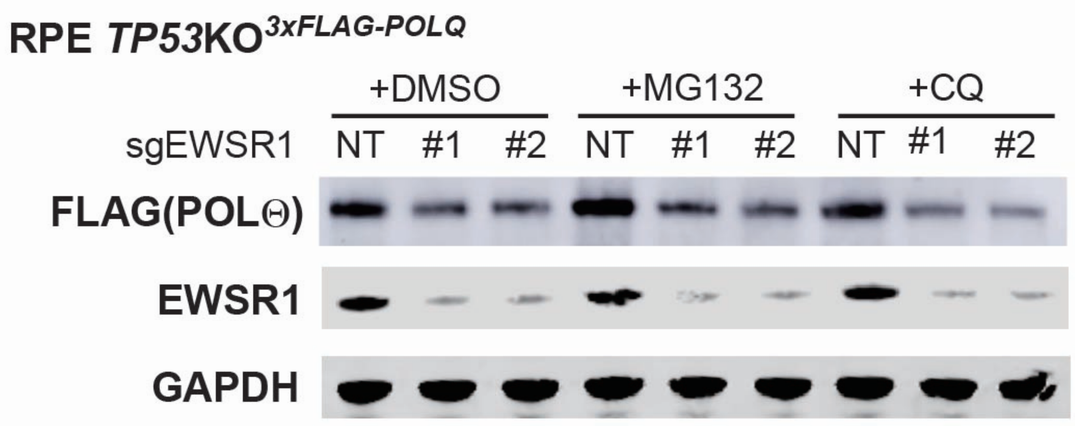

C

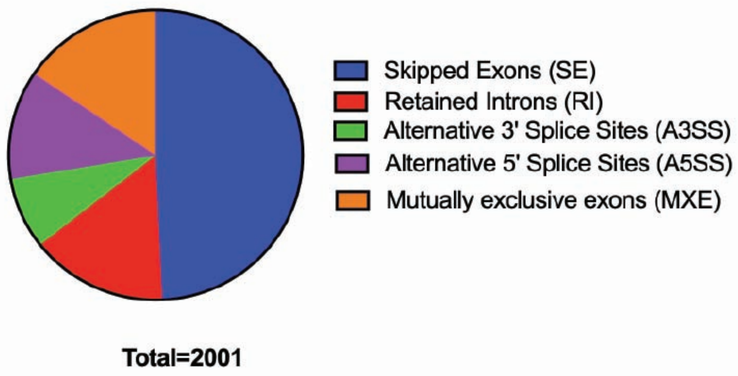

D

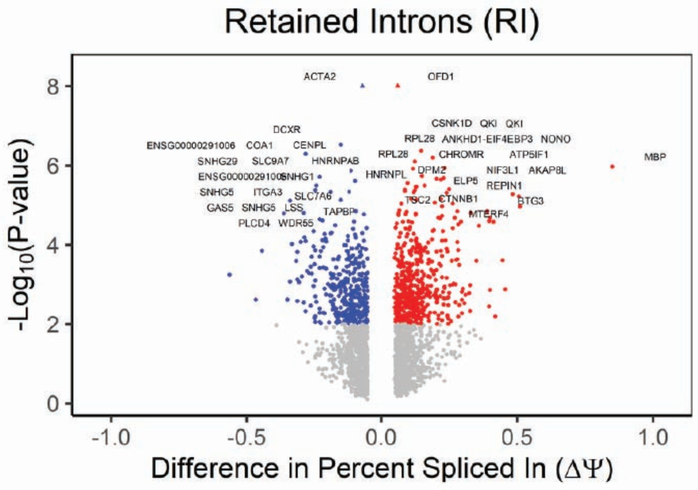

E

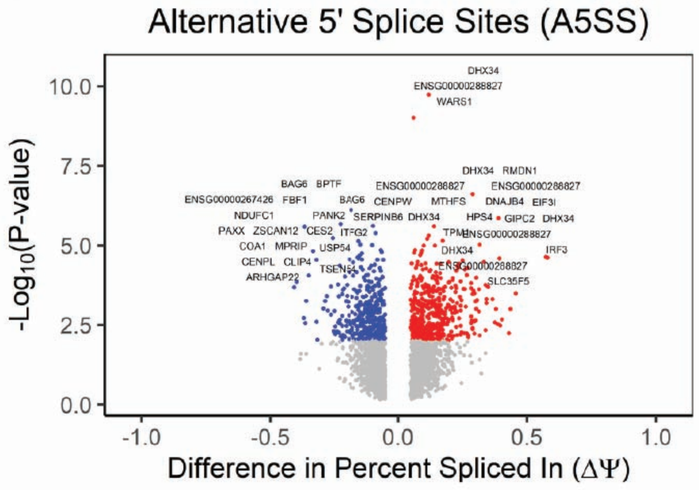

H

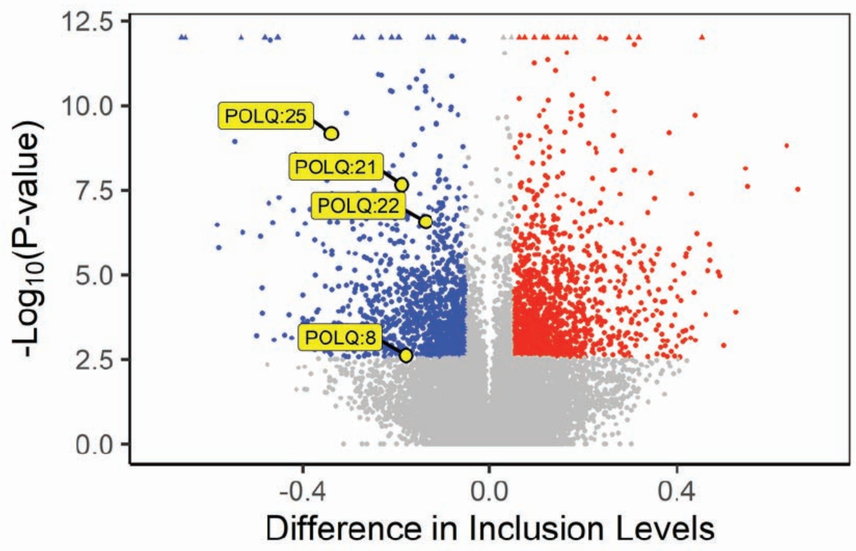

F

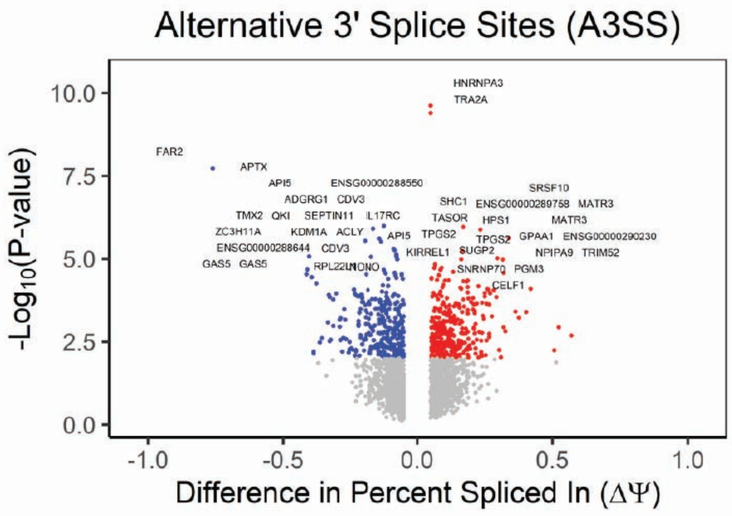

G

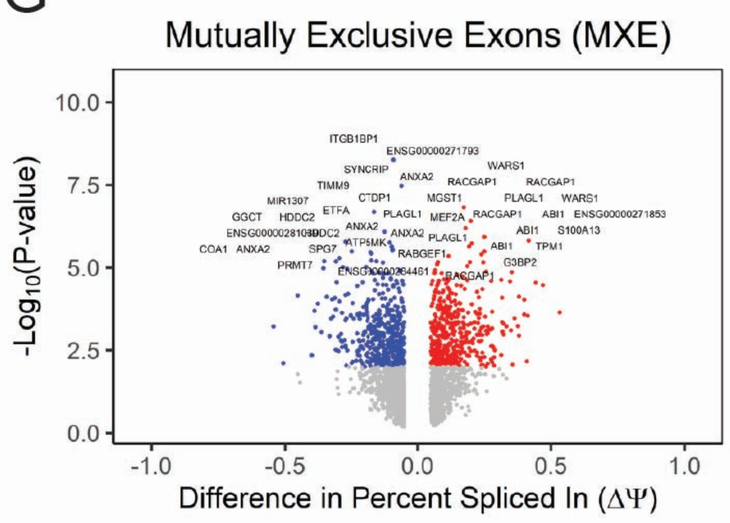

I

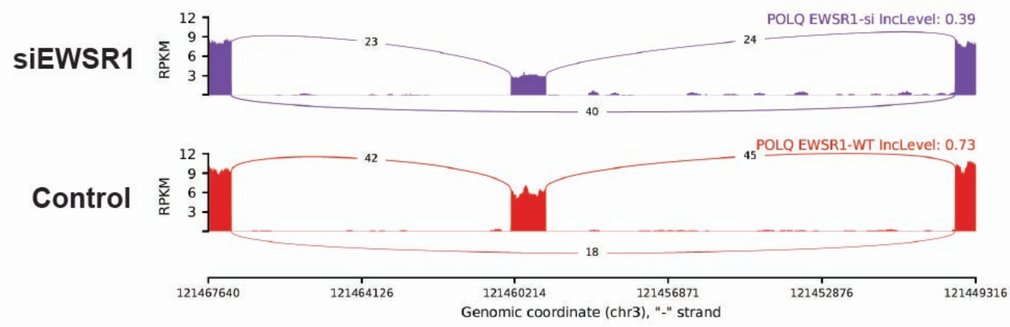

J

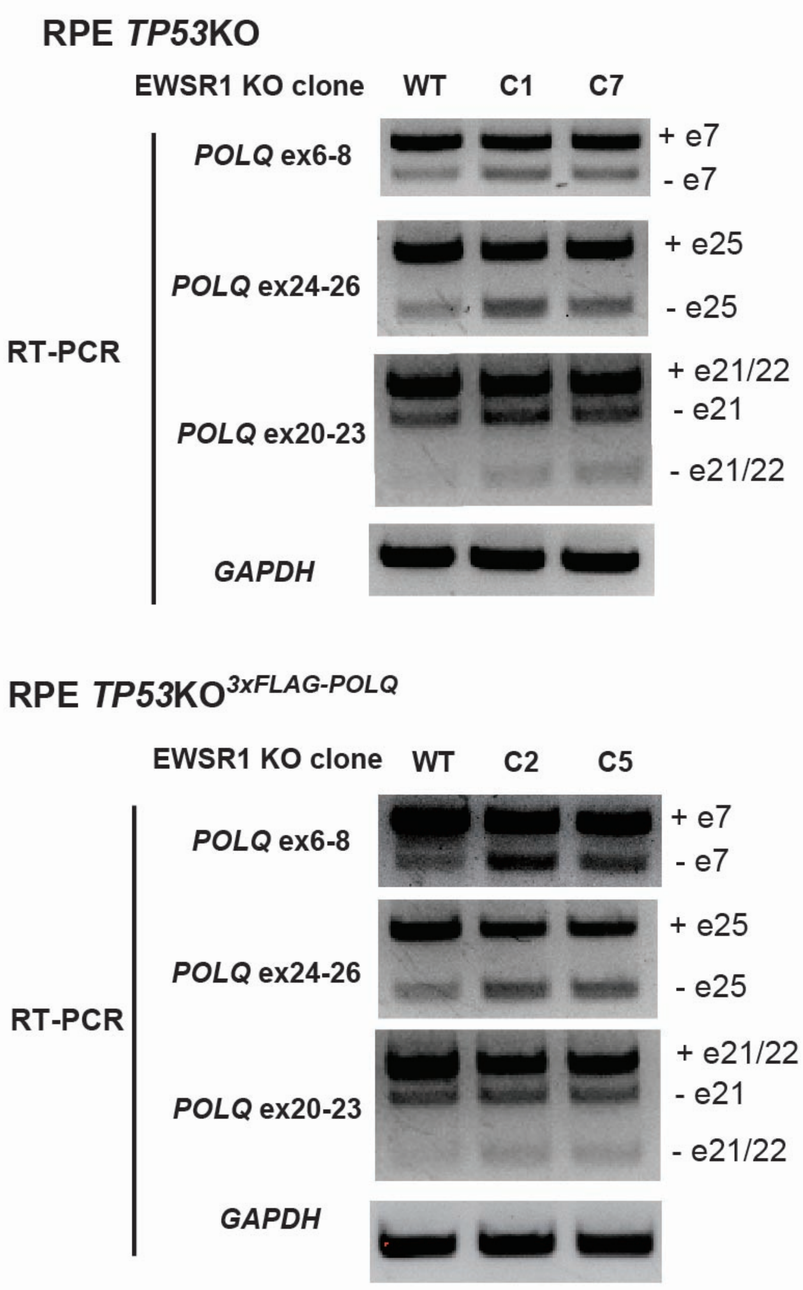

K

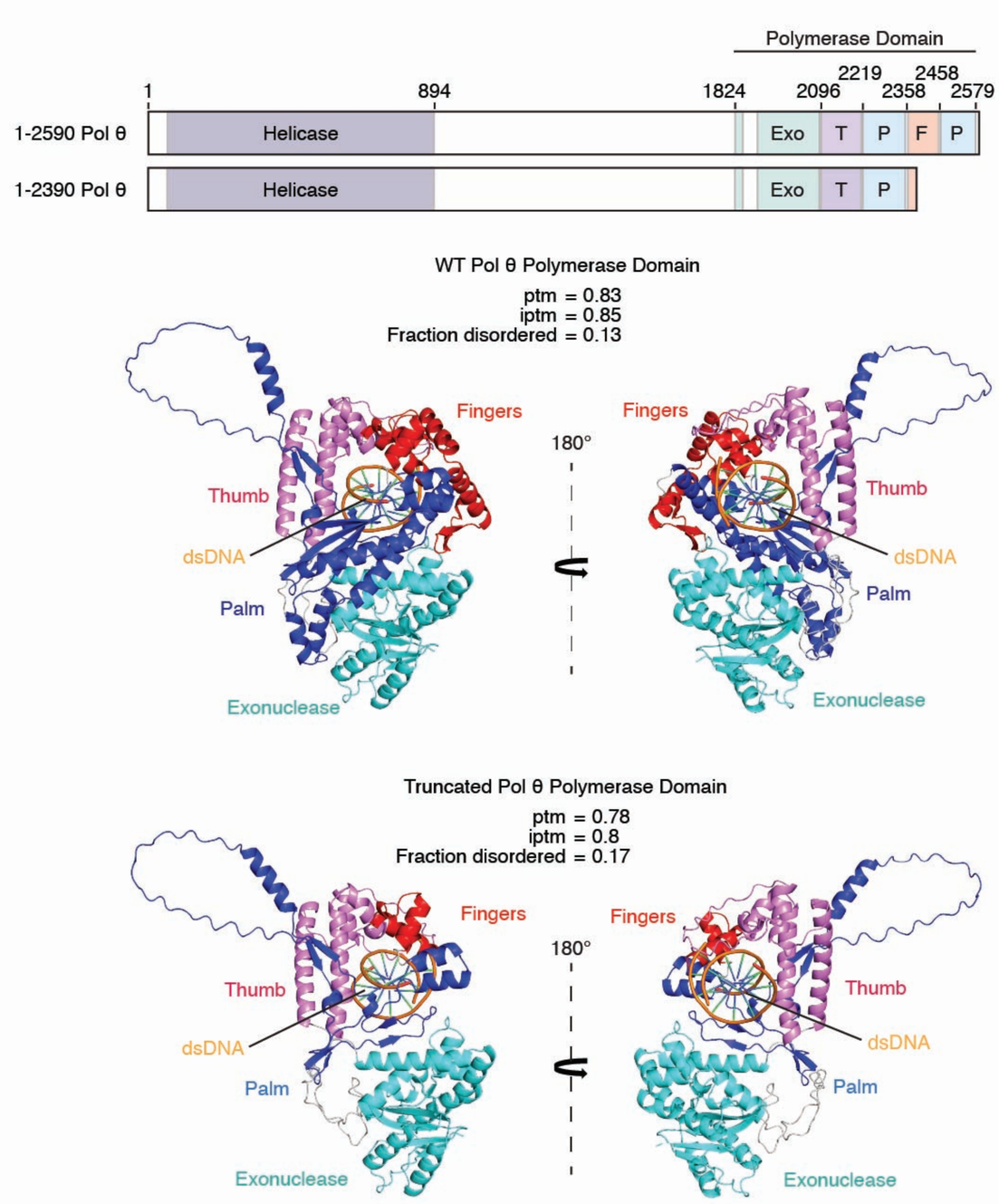

Figure S4

A

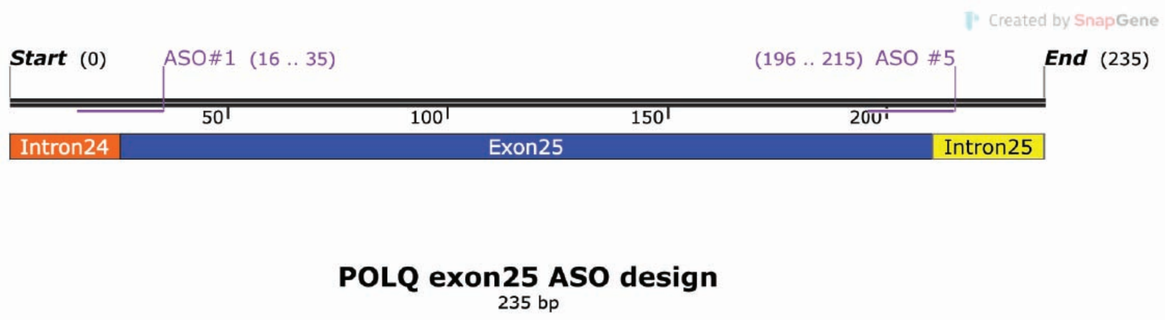

B

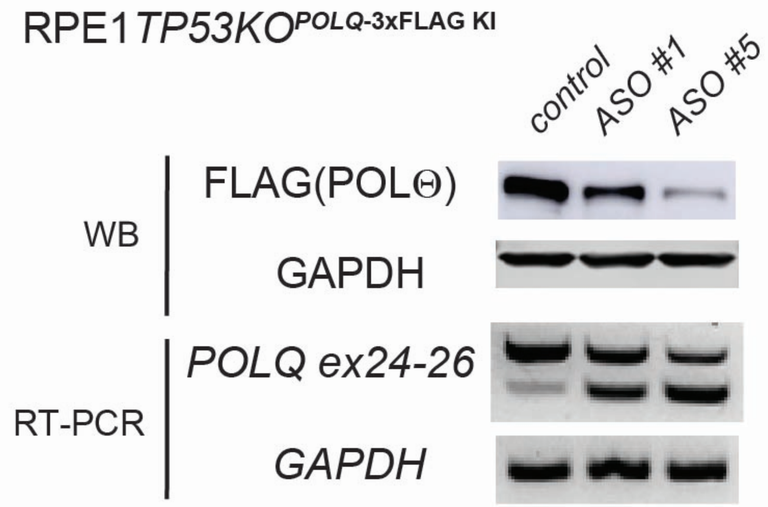

C

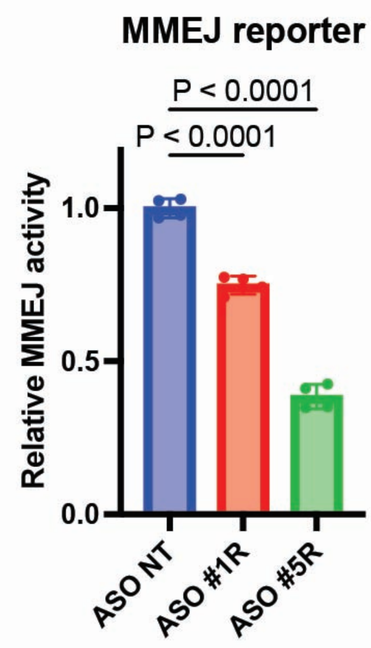

D

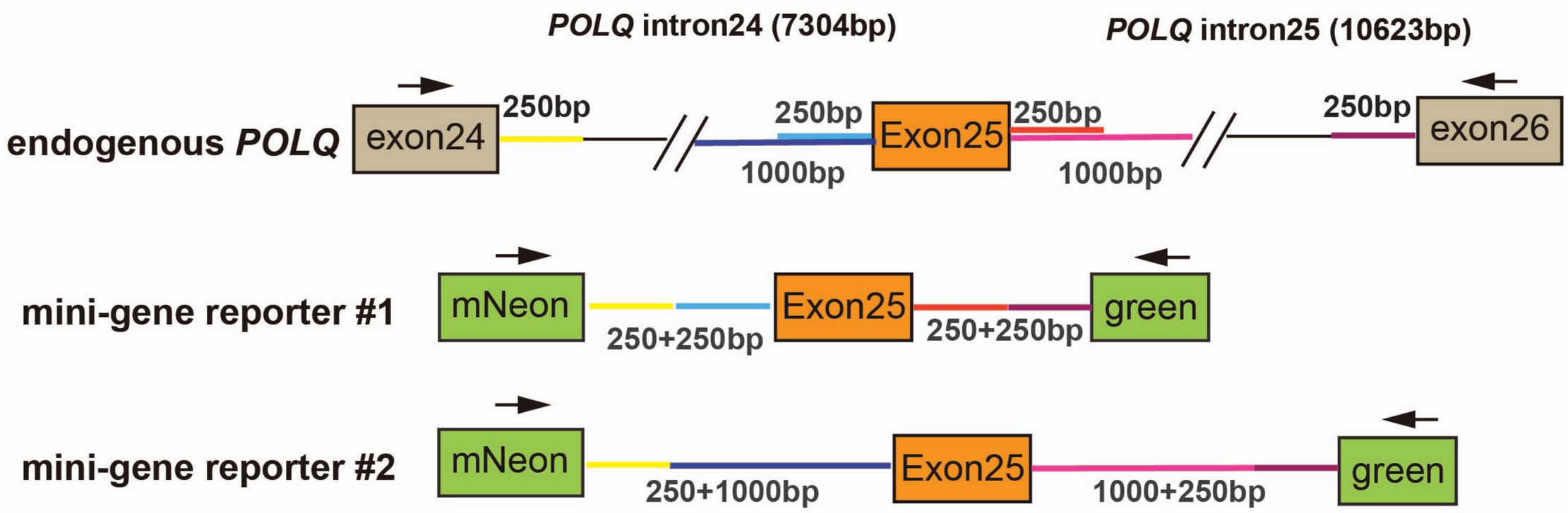

E

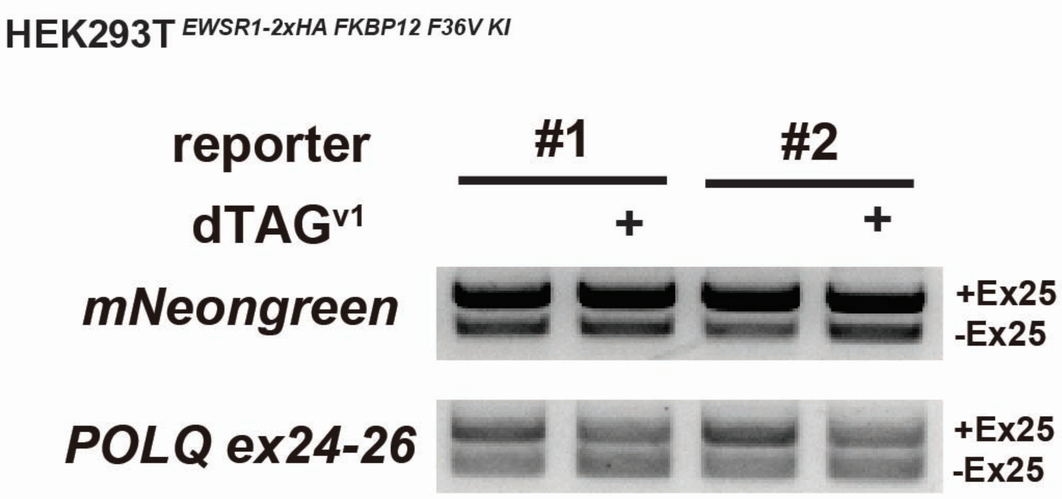

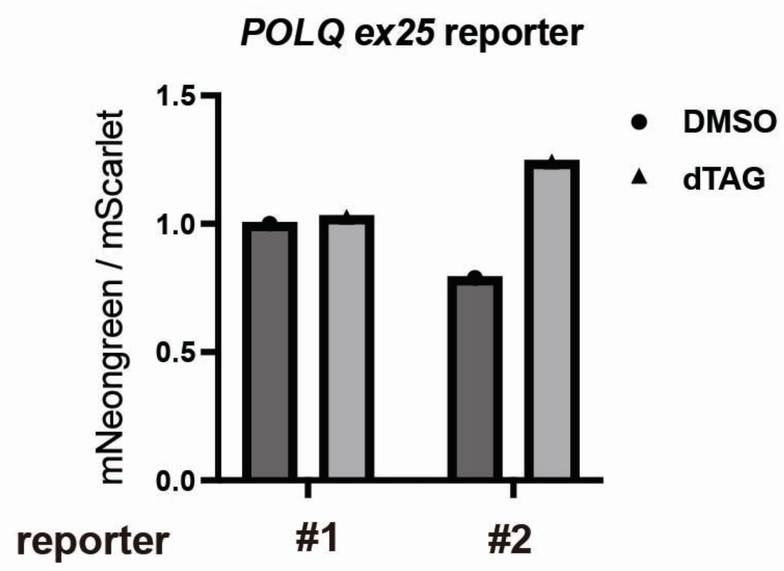

F

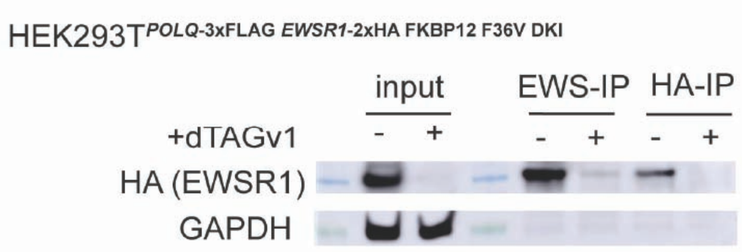

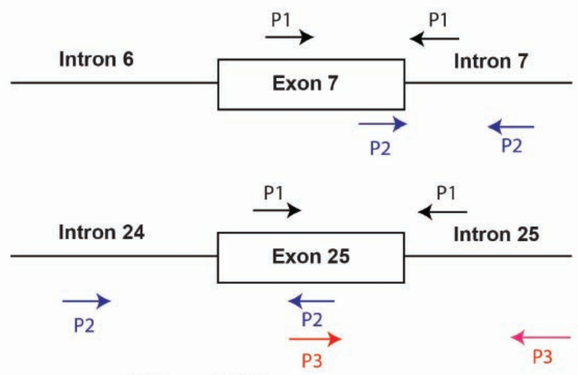

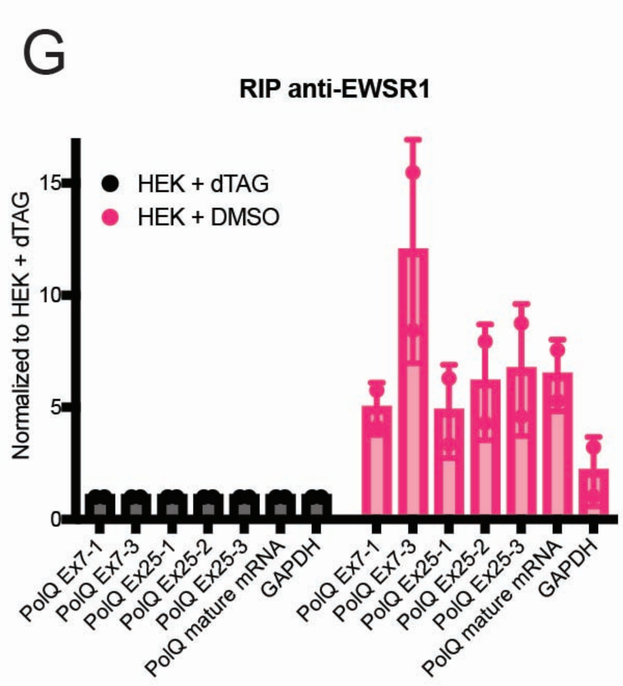

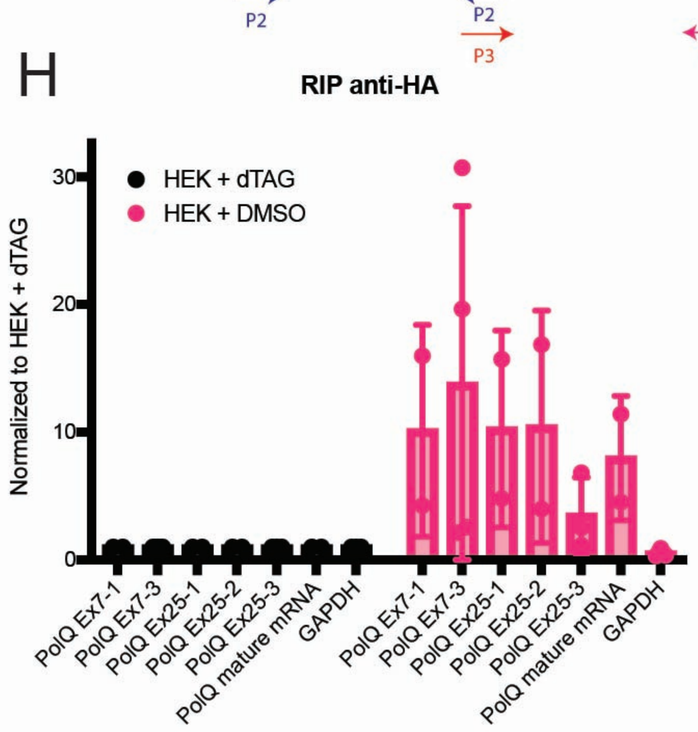

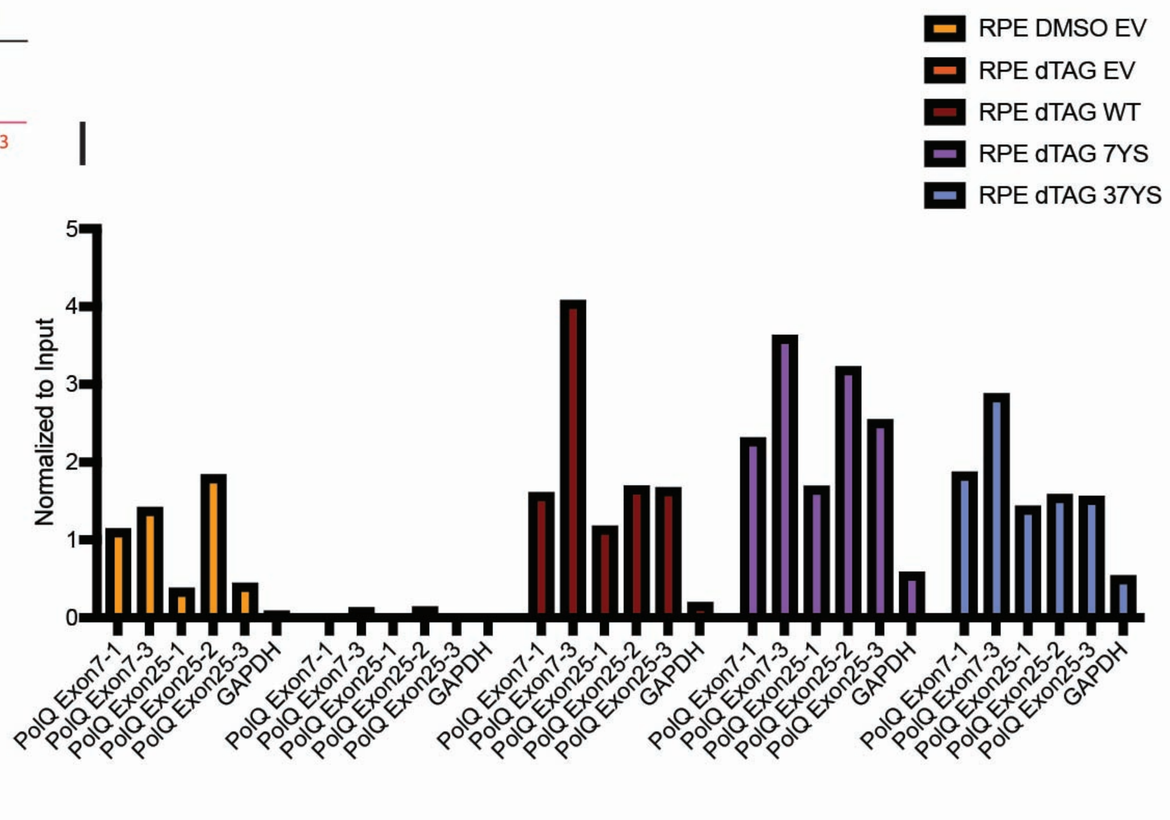

Figure S5

A

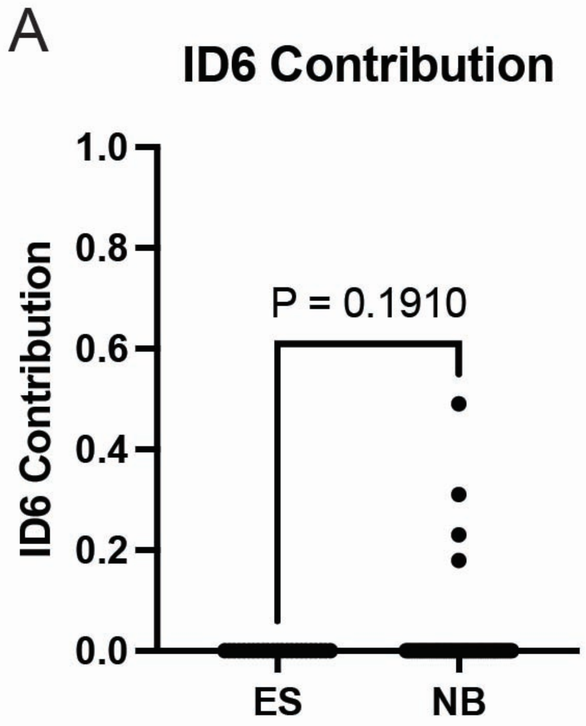

B

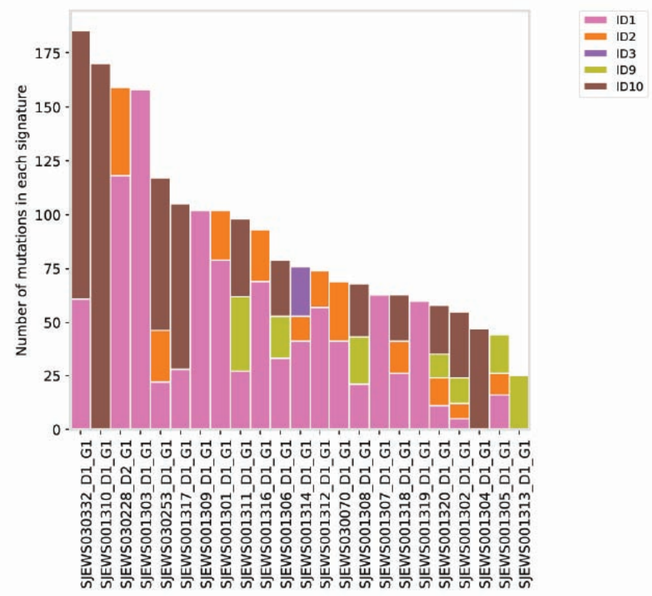

C

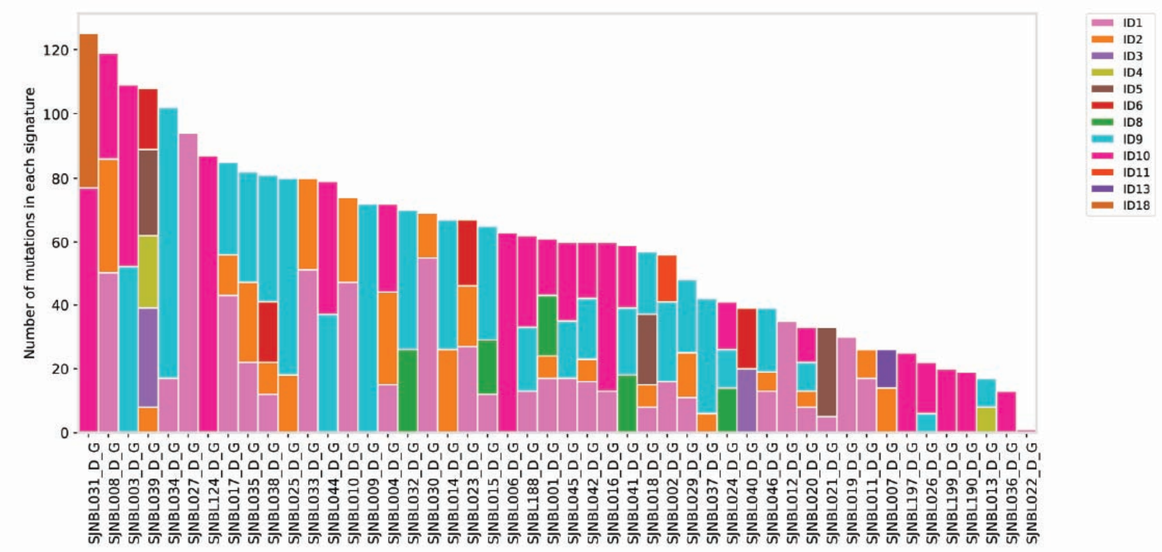

D

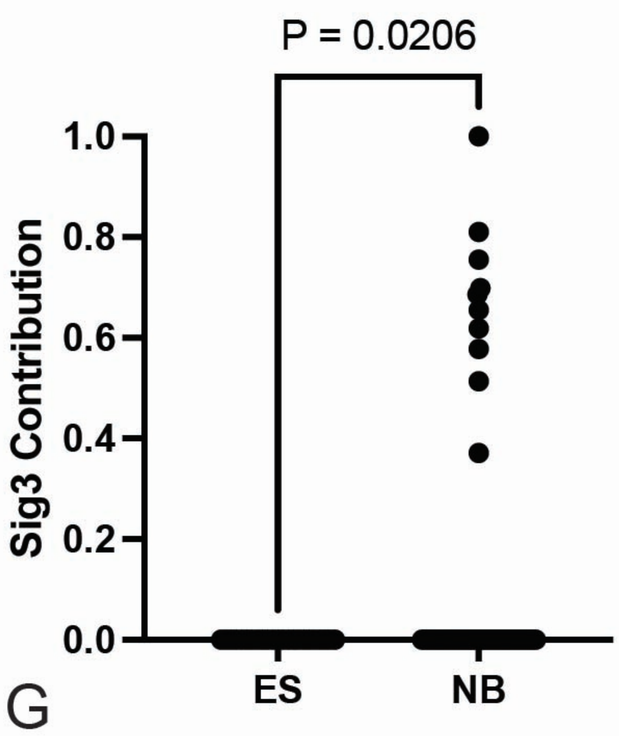

E

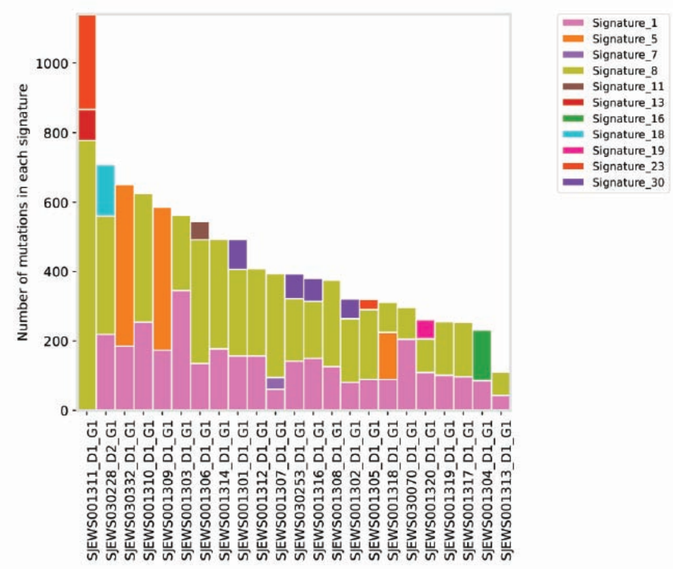

F

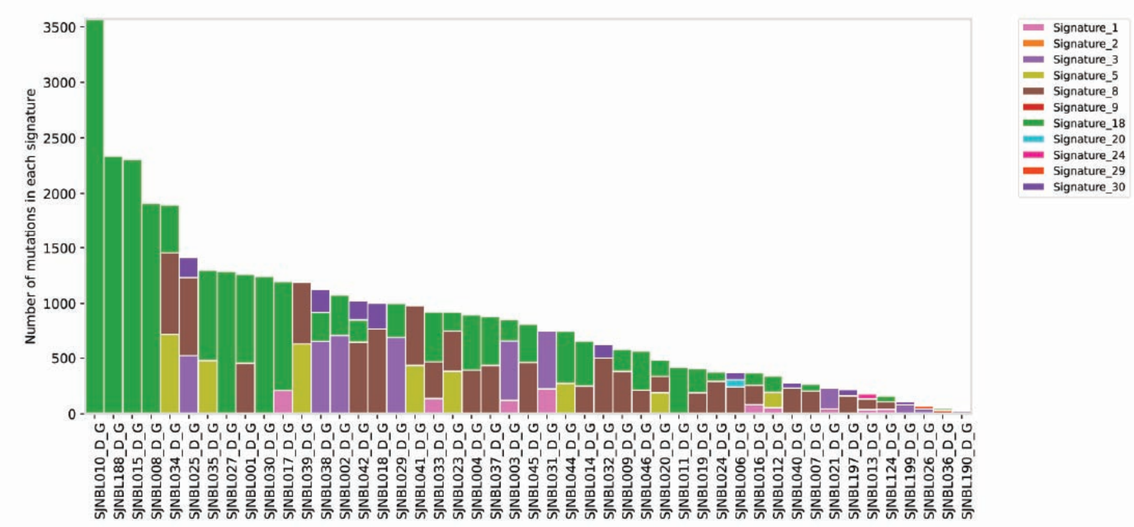

G

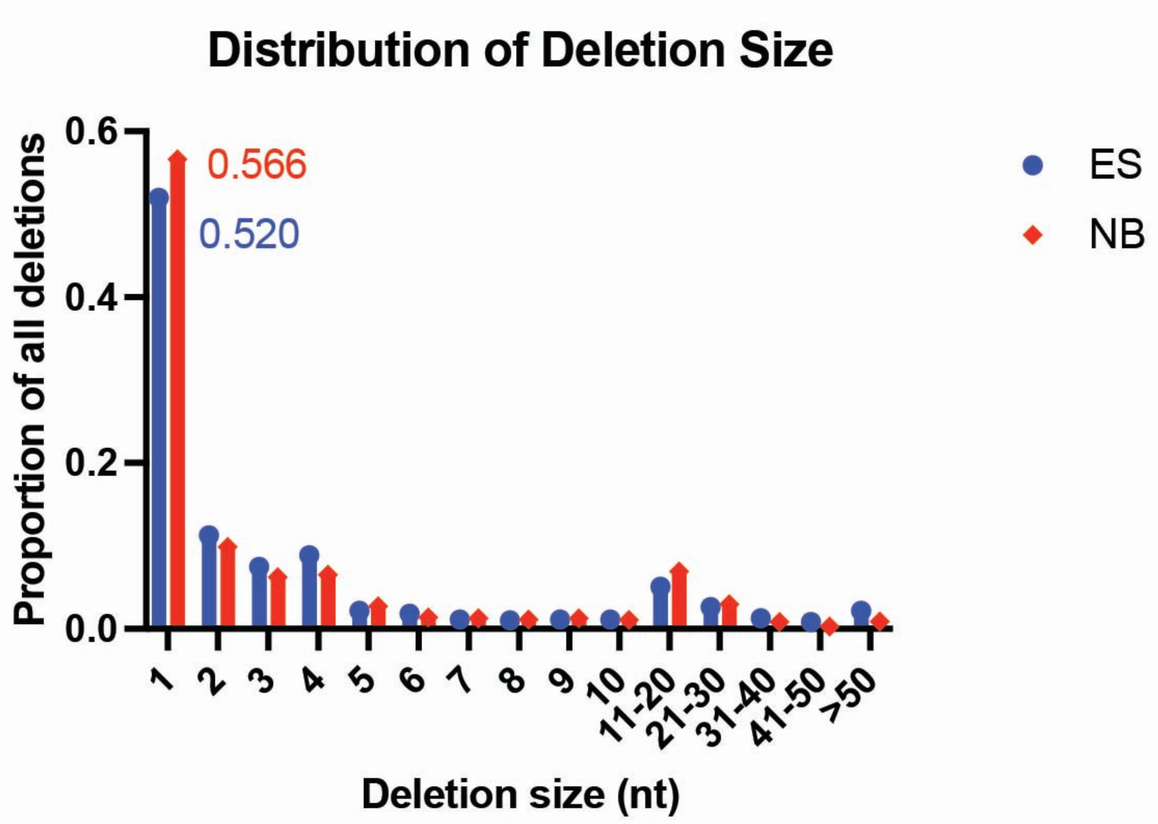

H

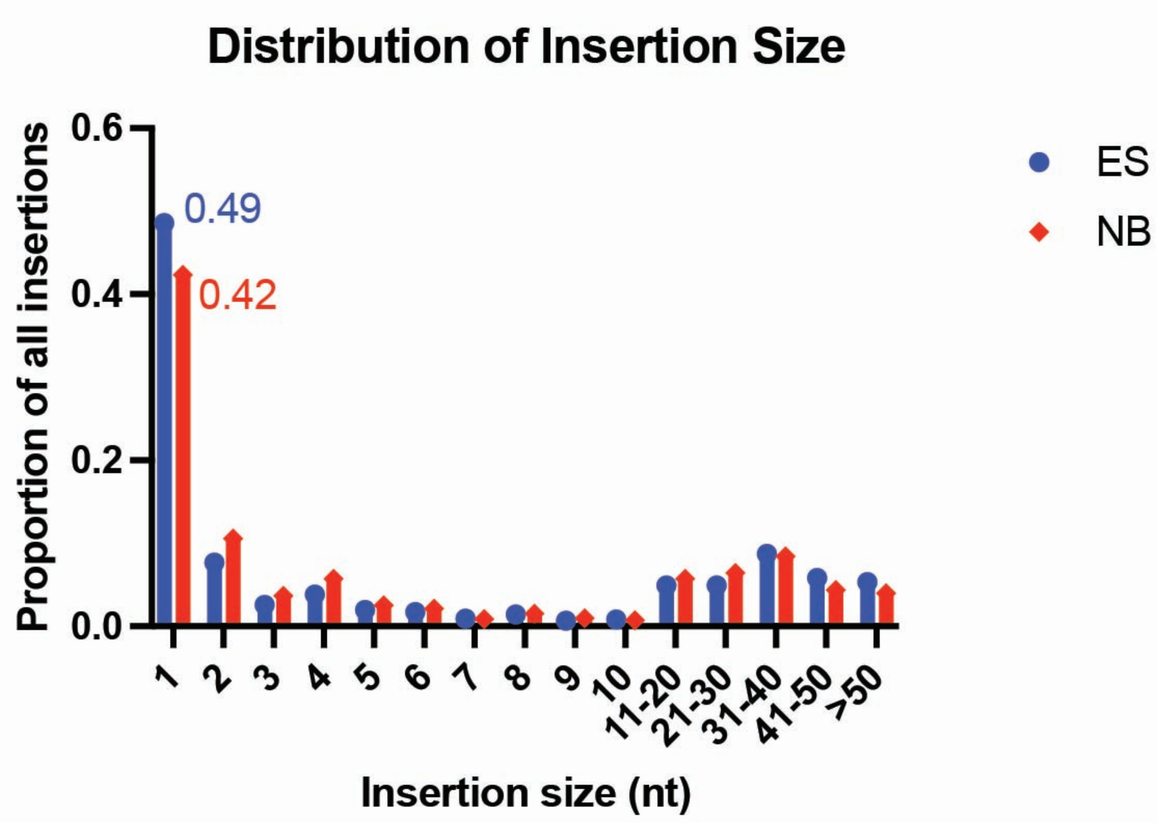

I

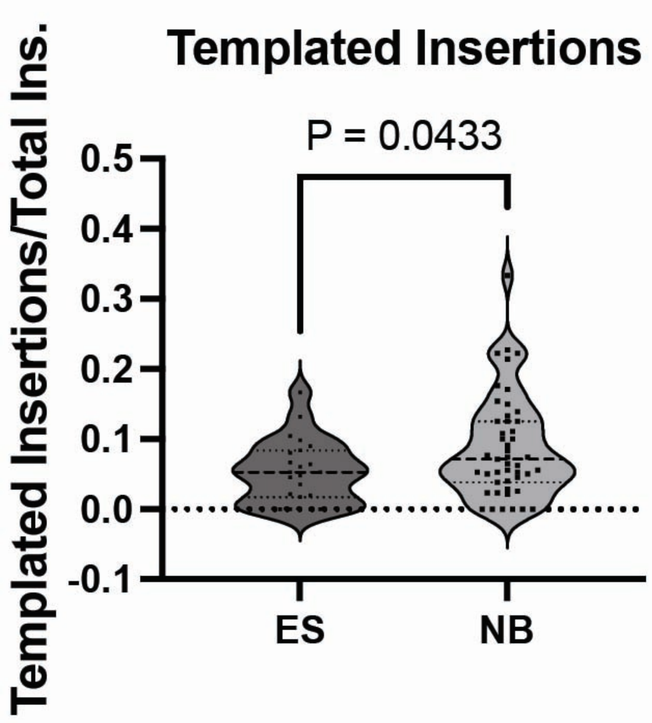

J

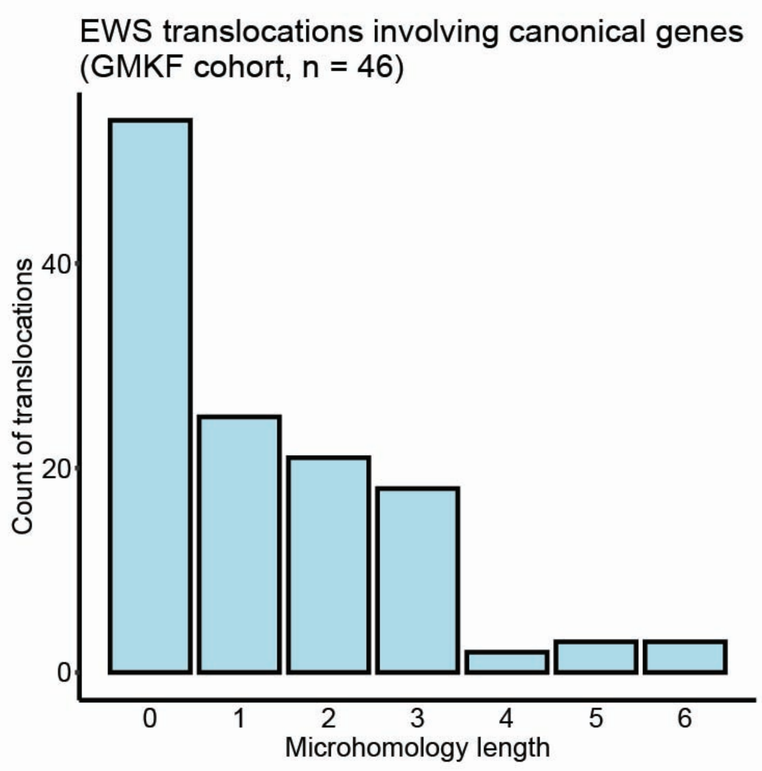

K

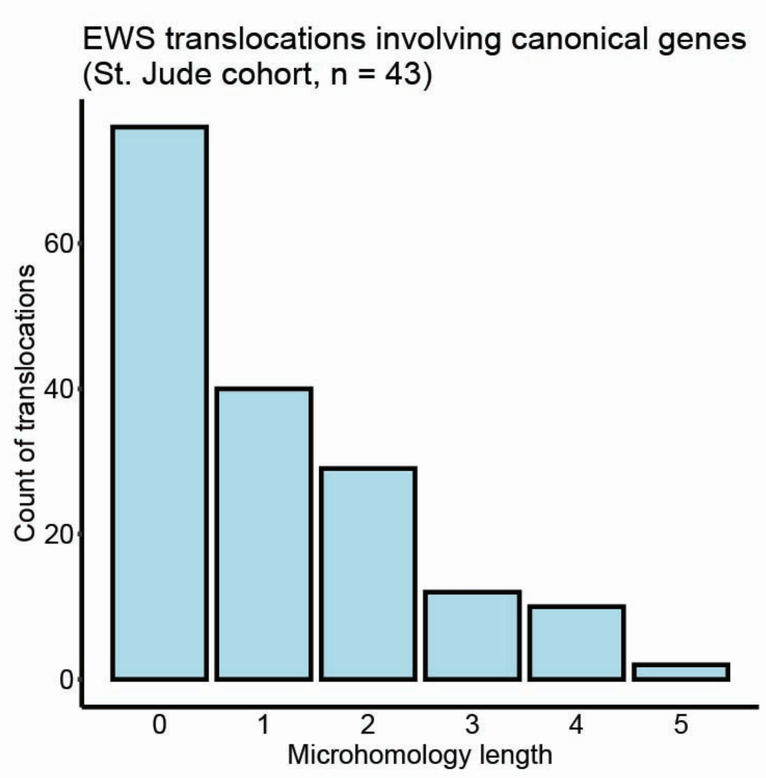

Figure S6

A

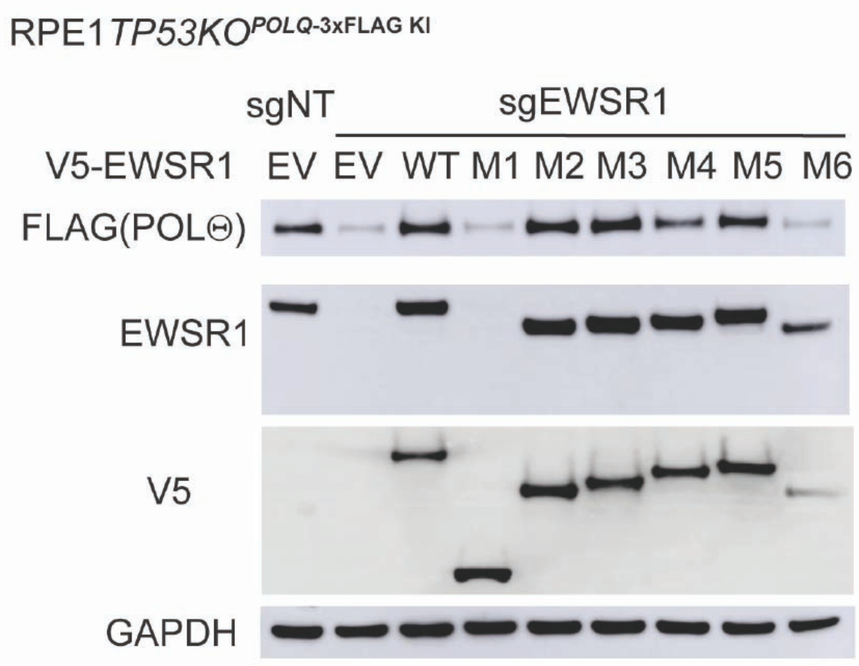

B

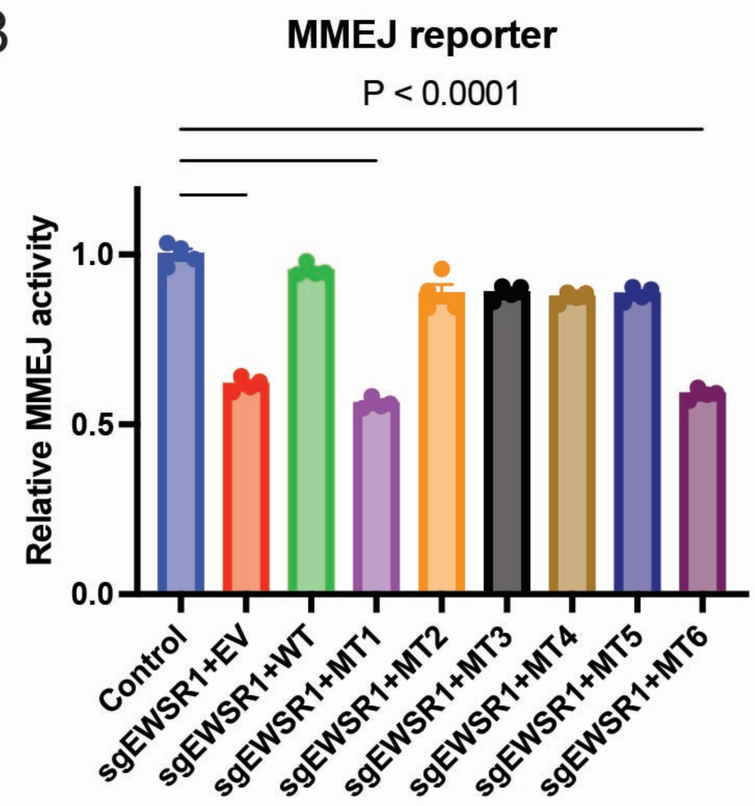

C

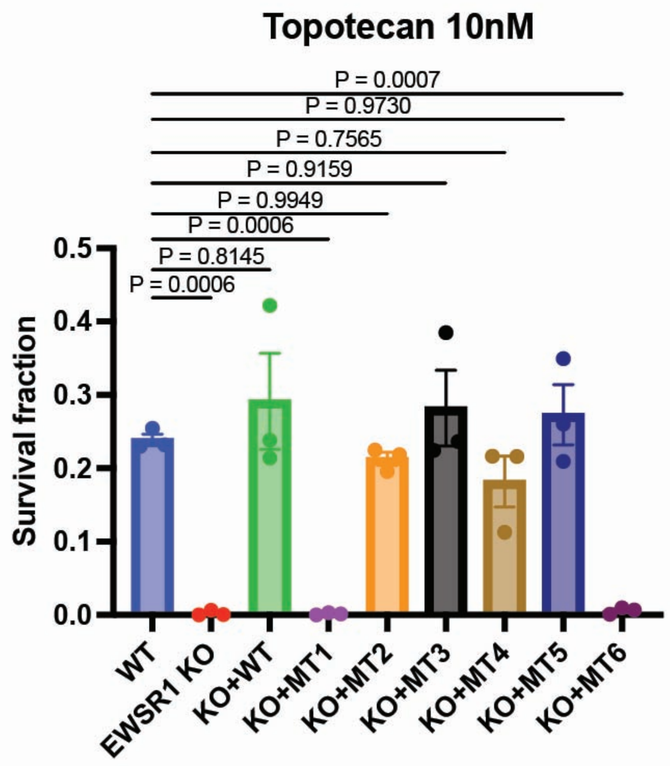

D

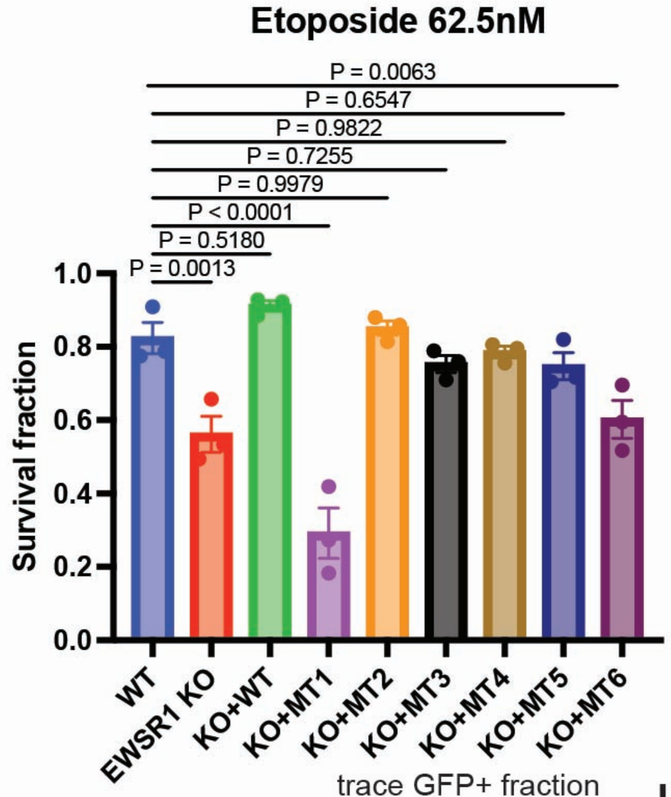

E

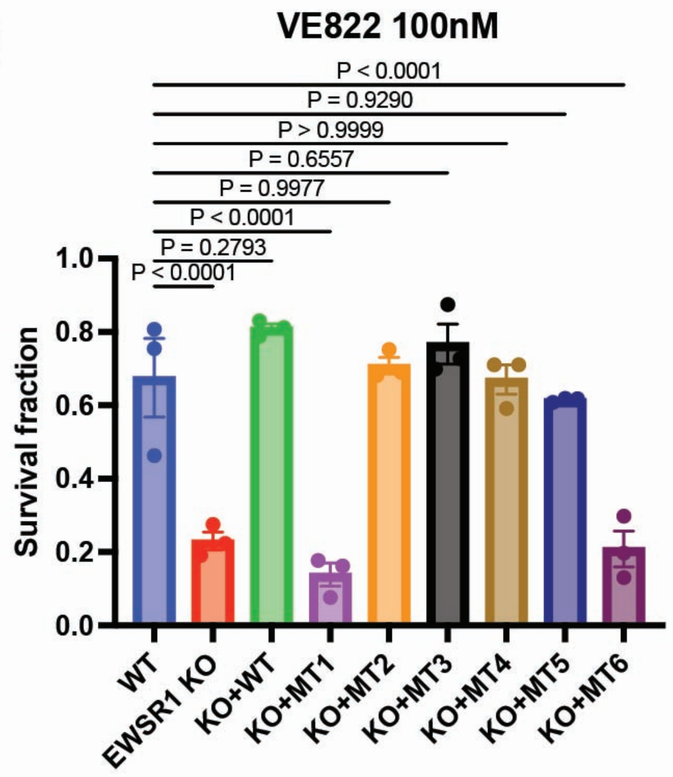

F

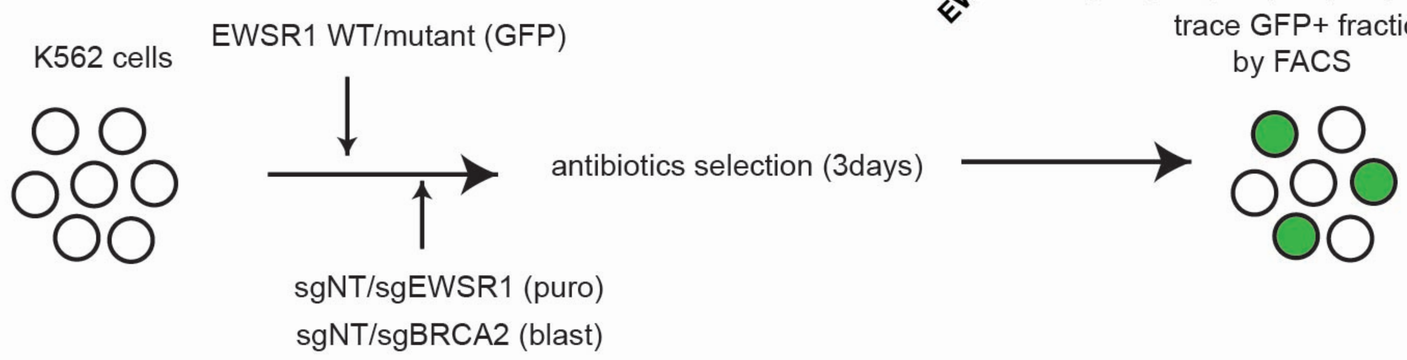

H

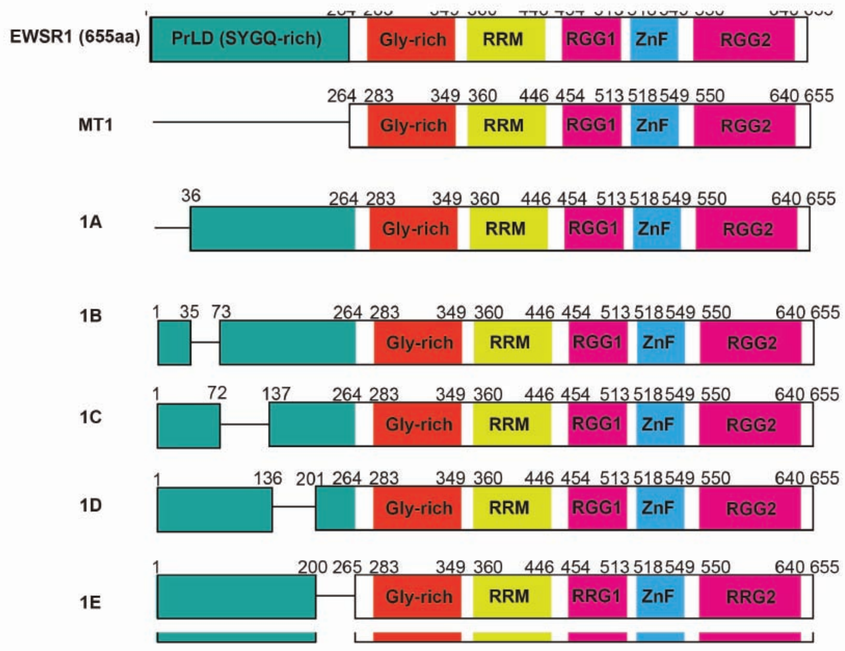

G

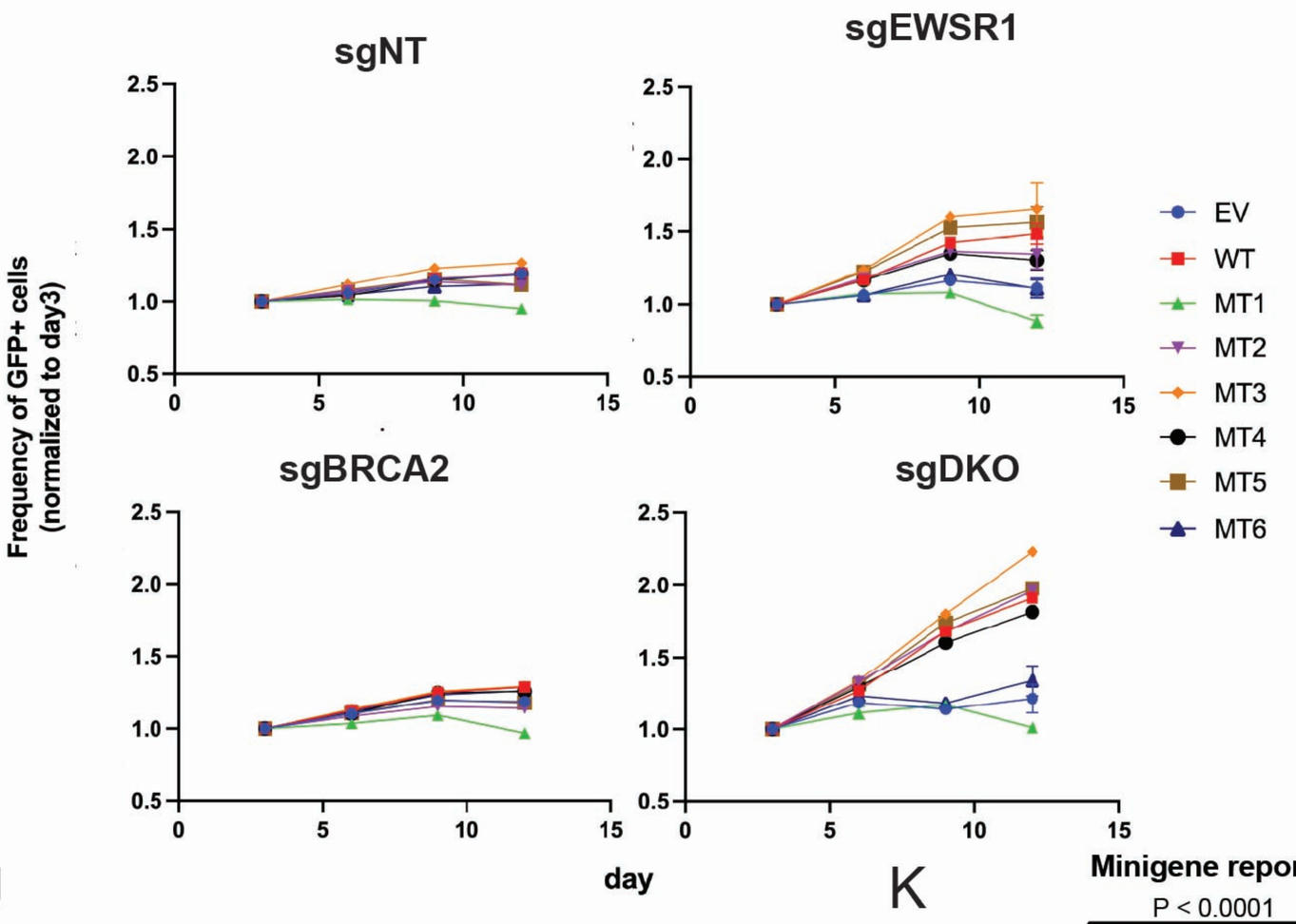

I

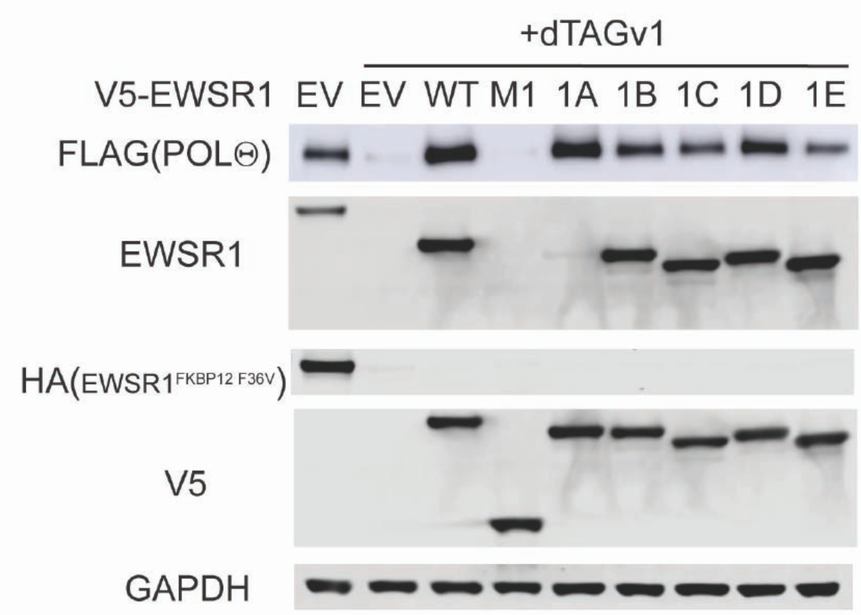

J

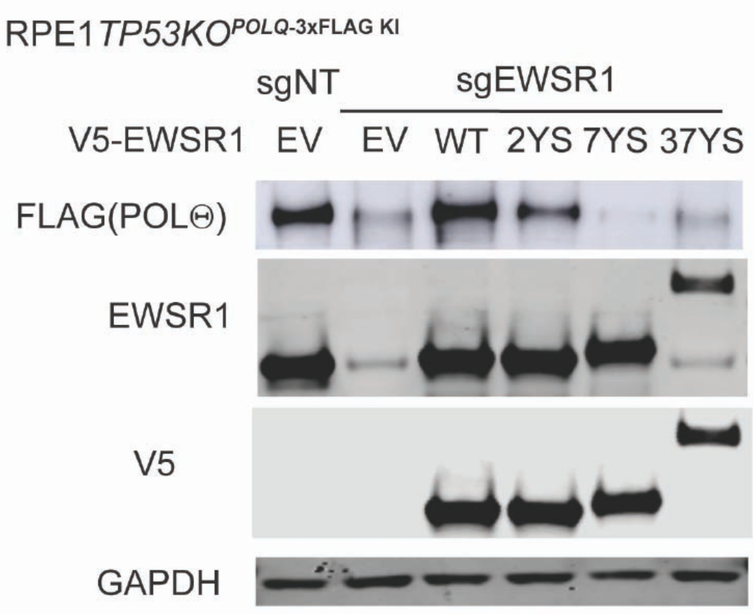

K

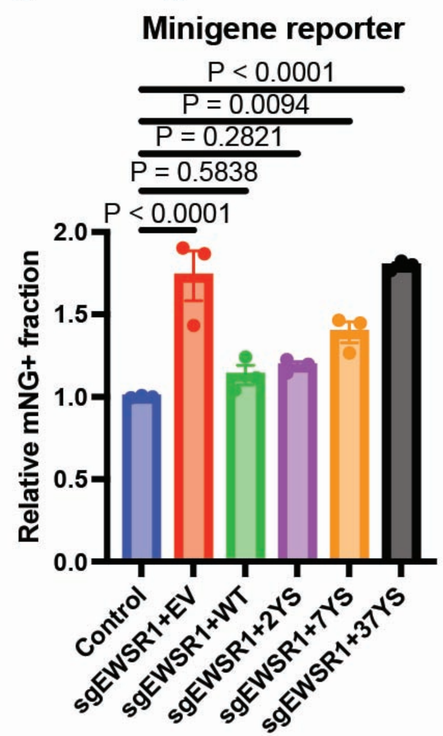

Figure S7

A

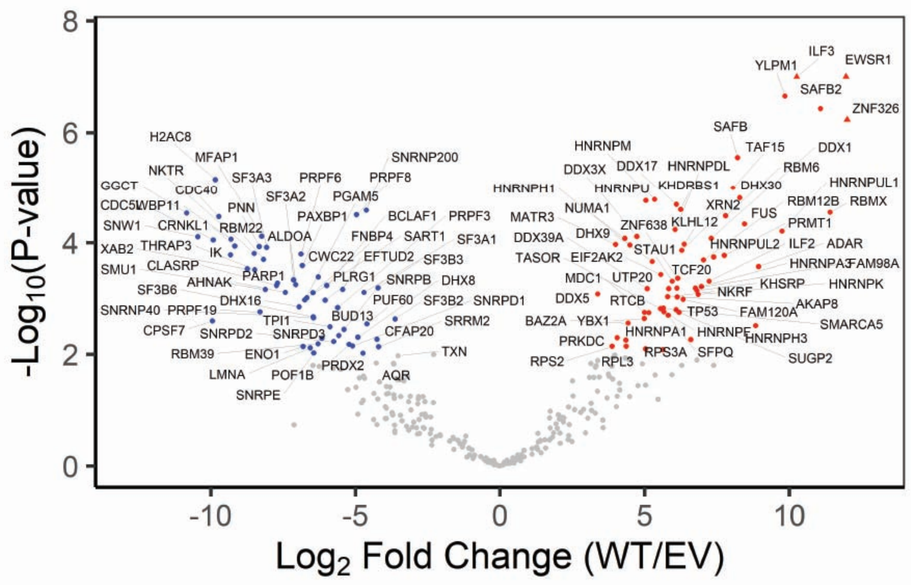

B

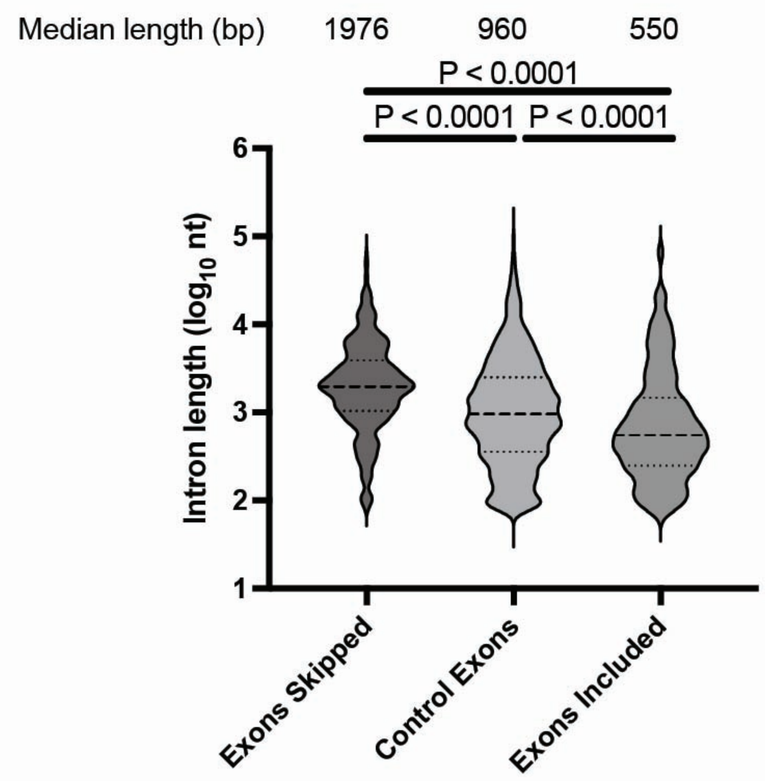

C

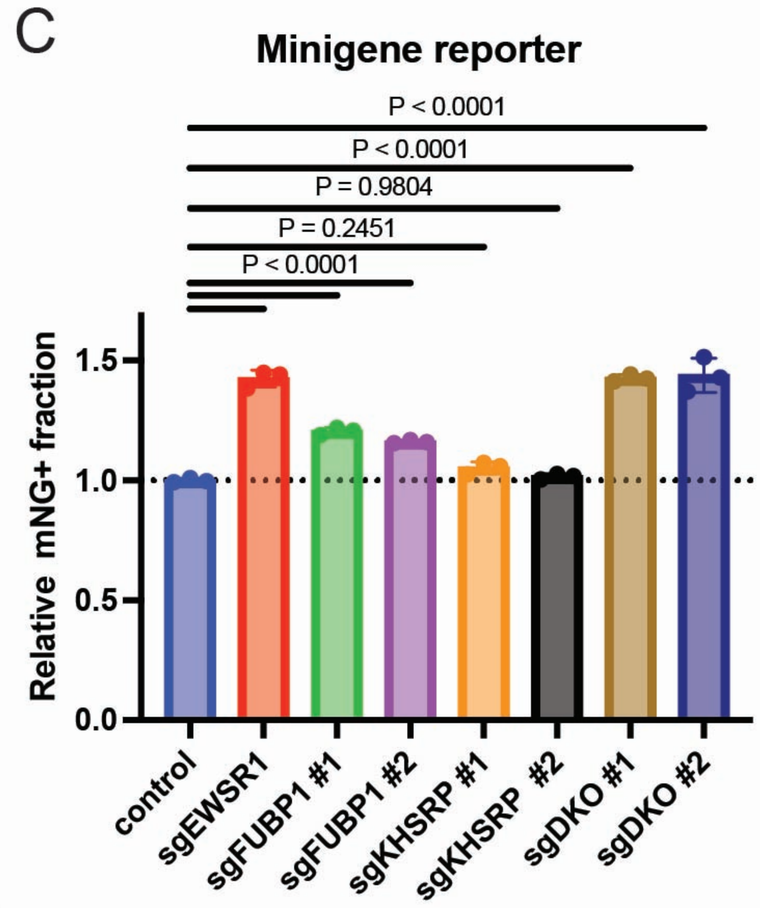

D

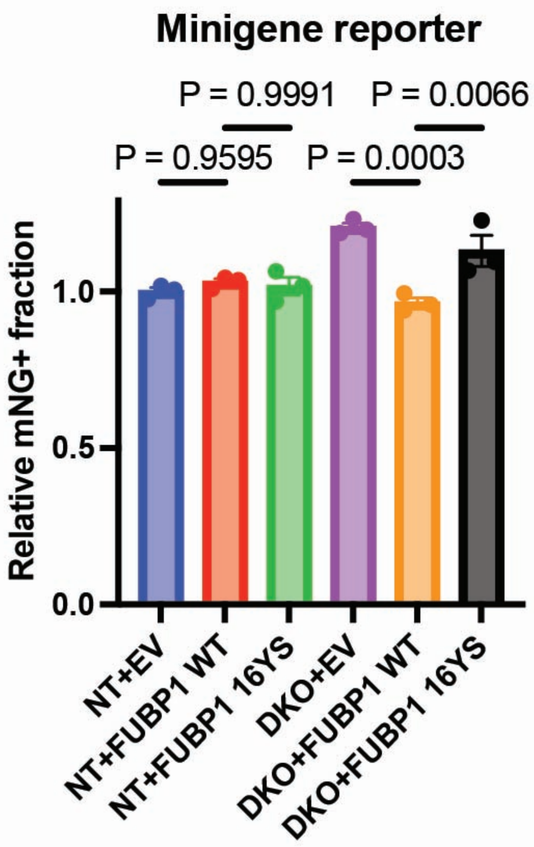

E

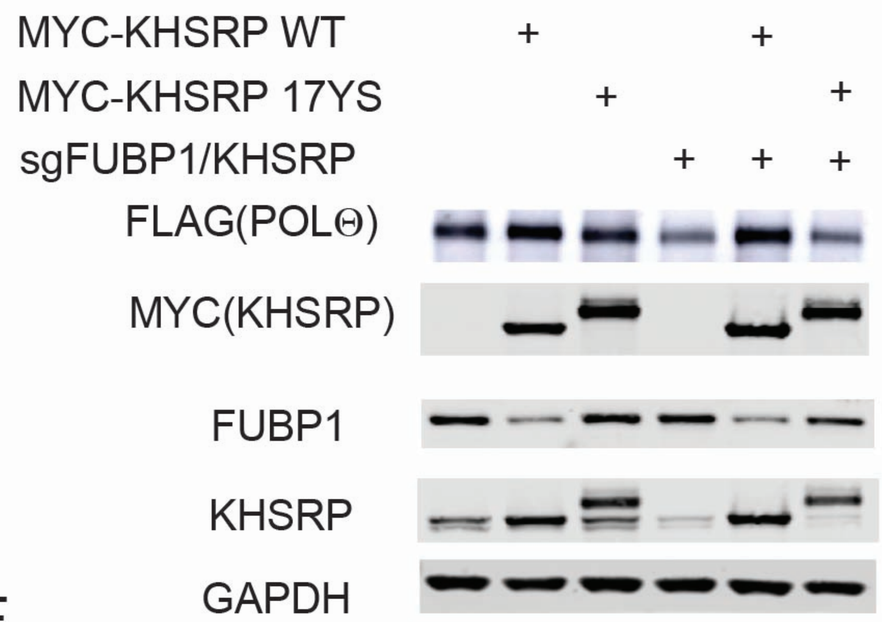

F

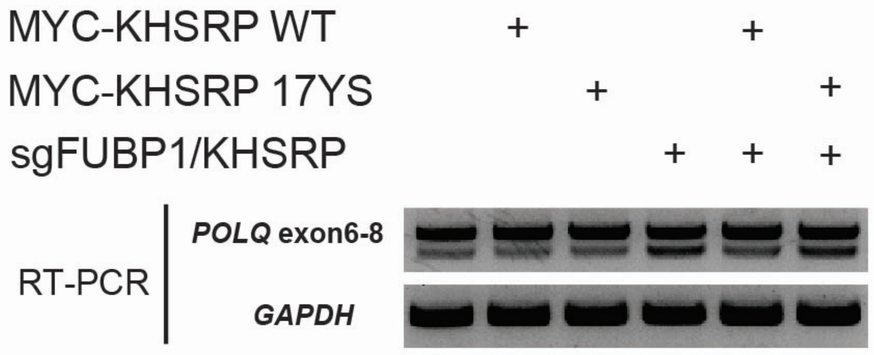

G

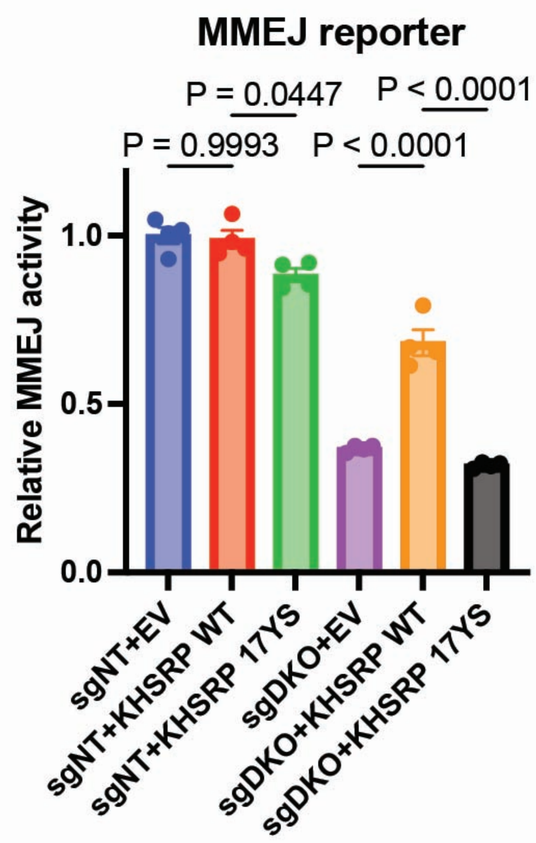

H

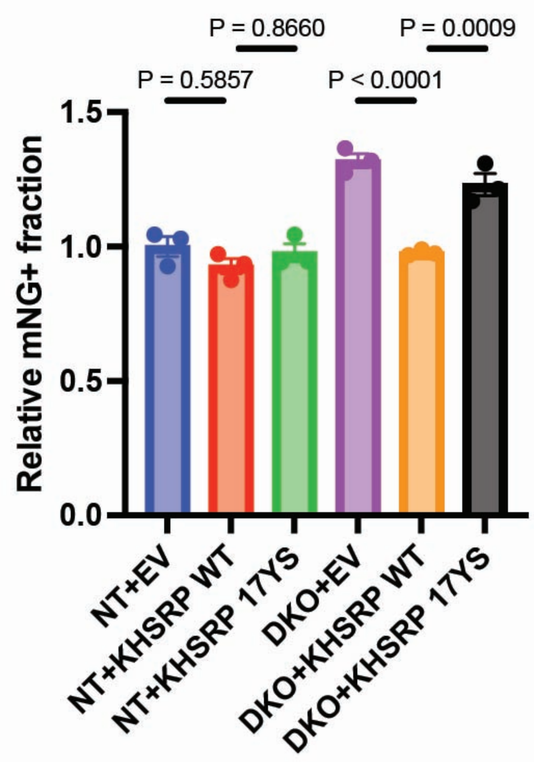

Figure S8

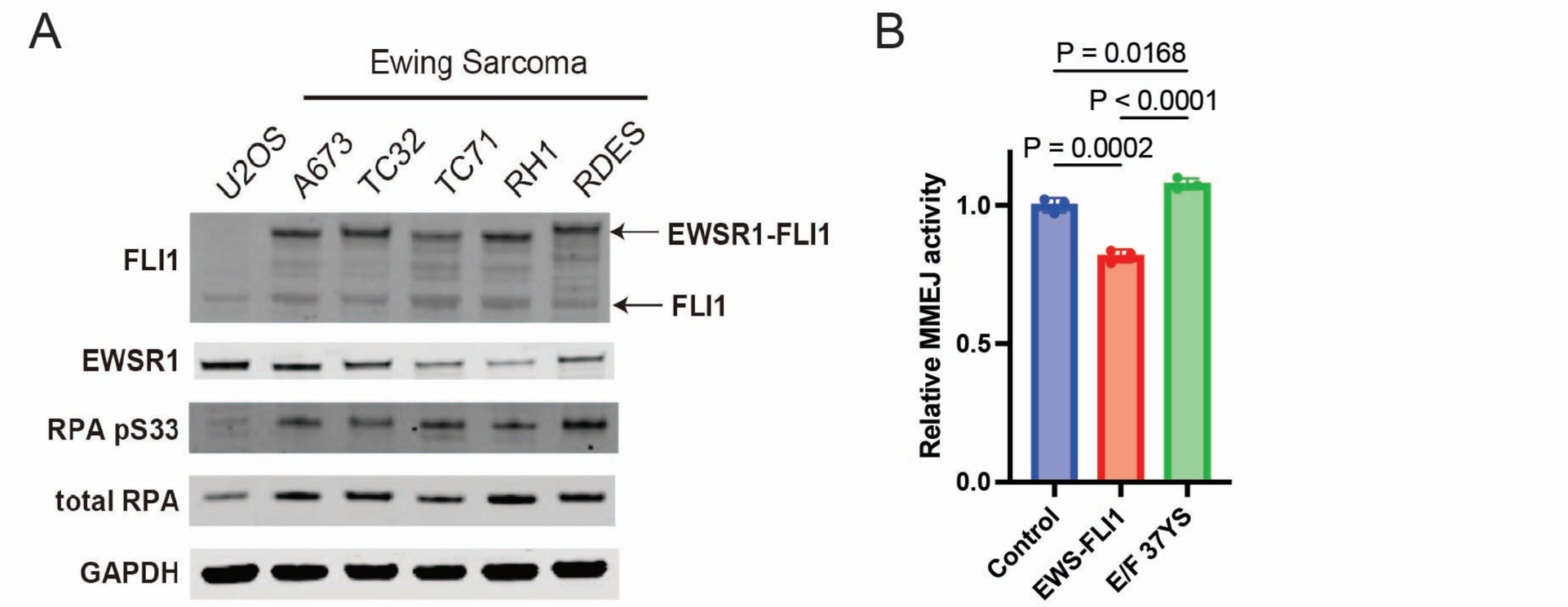
A
Ewing Sarcoma
U2OS
A673
TC32
TC71
RH1
RDES
FLI1
EWSR1-FLI1
FLI1
EWSR1
RPA pS33
total RPA
GAPDH
B
P = 0.0168
P < 0.0001
P = 0.0002
Relative MMEJ activity
Control
EWS-FLI1
E/F 37YS

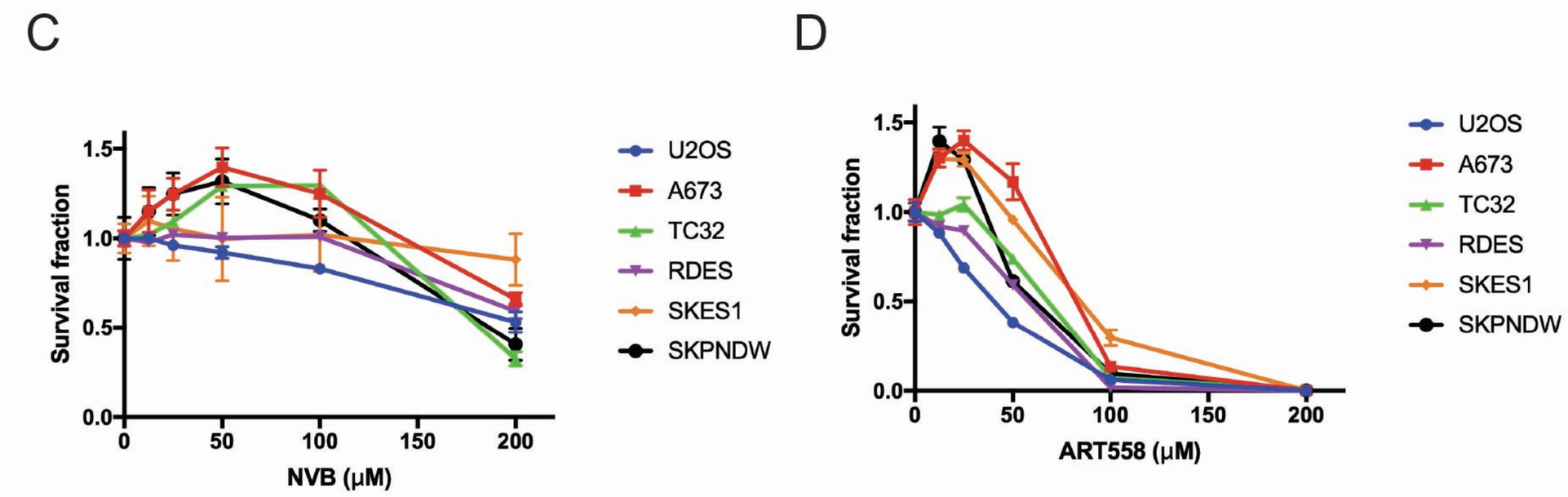
C
Survival fraction
NVB (μM)
U2OS
A673
TC32
RDES
SKES1
SKPNDW
D
Survival fraction
ART558 (μM)
U2OS
A673
TC32
RDES
SKES1
SKPNDW

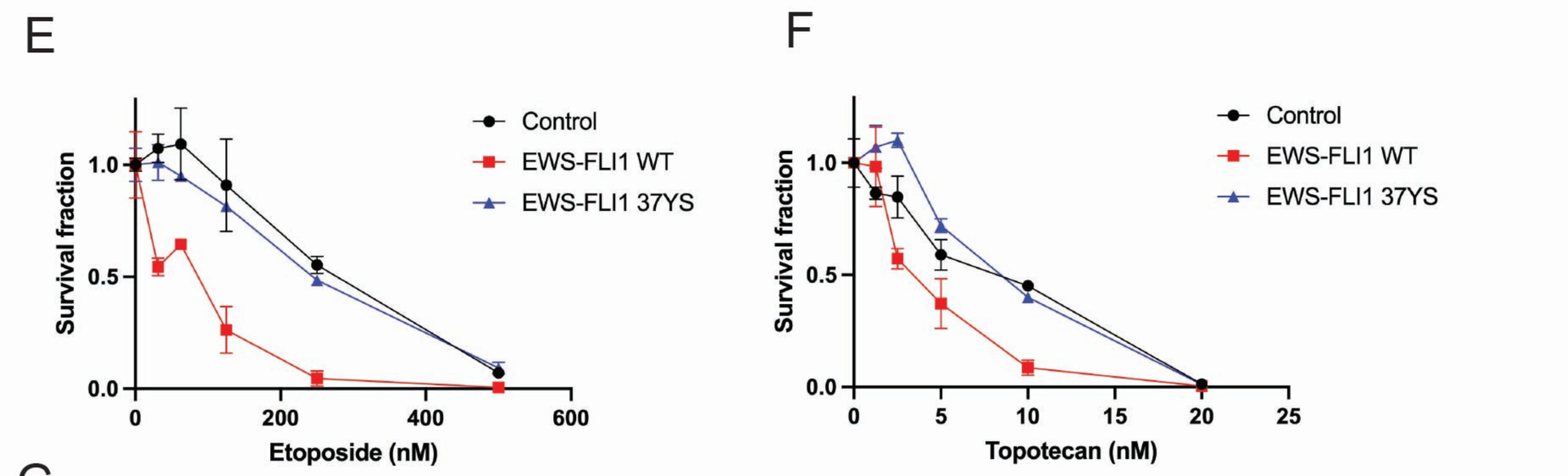
E
Survival fraction
Etoposide (nM)
Control
EWS-FLI1 WT
EWS-FLI1 37YS
F
Survival fraction
Topotecan (nM)
Control
EWS-FLI1 WT
EWS-FLI1 37YS

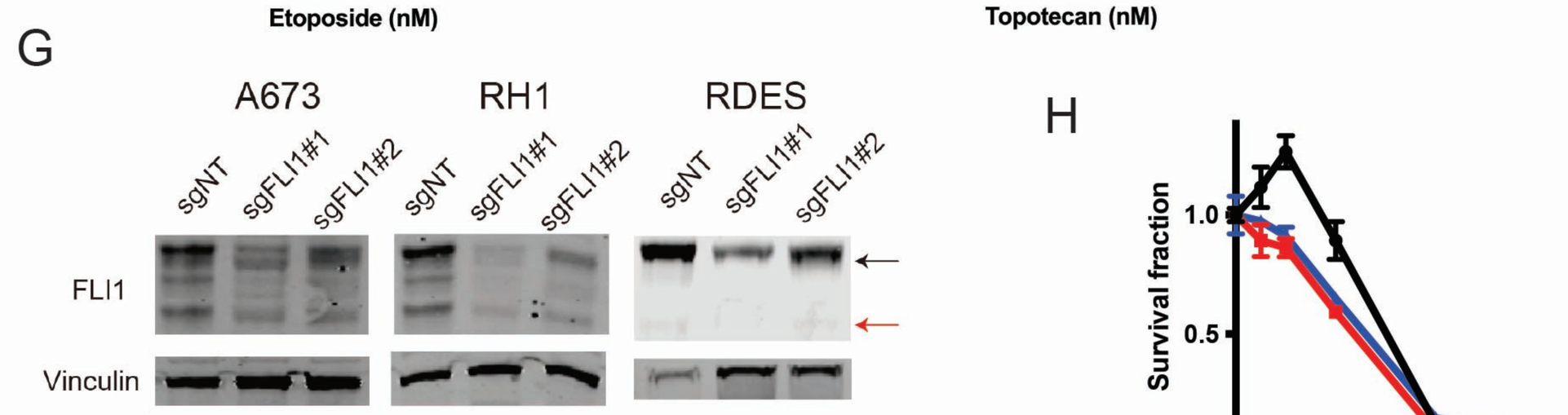
G
A673
RH1
RDES
sgNT
sgFLI1#1
sgFLI1#2
FLI1
Vinculin
H
Survival fraction
ART558 (μM)
A673 WT
A673 FLI1 KO #1
A673 FLI1 KO #2

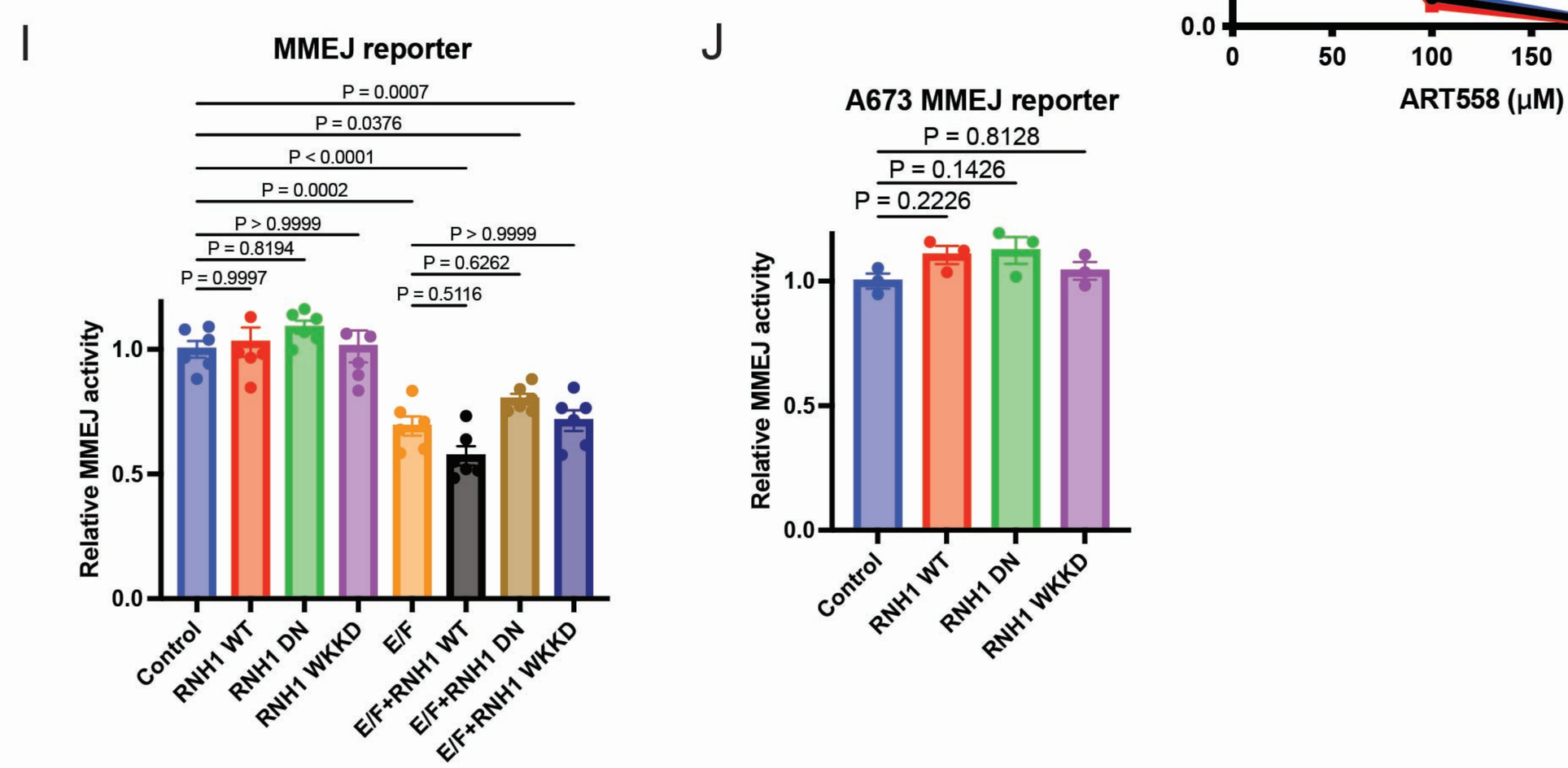
I
MMEJ reporter
P = 0.0007
P = 0.0376
P < 0.0001
P = 0.0002
P > 0.9999
P = 0.8194
P = 0.9997
P > 0.9999
P = 0.6262
P = 0.5116
Relative MMEJ activity
Control
RNH1 WT
RNH1 DN
RNH1 WKKD
E/F
E/F+RNH1 WT
E/F+RNH1 DN
E/F+RNH1 WKKD
J
A673 MMEJ reporter
P = 0.8128
P = 0.1426
P = 0.2226
Relative MMEJ activity
Control
RNH1 WT
RNH1 DN
RNH1 WKKD

Figure S9

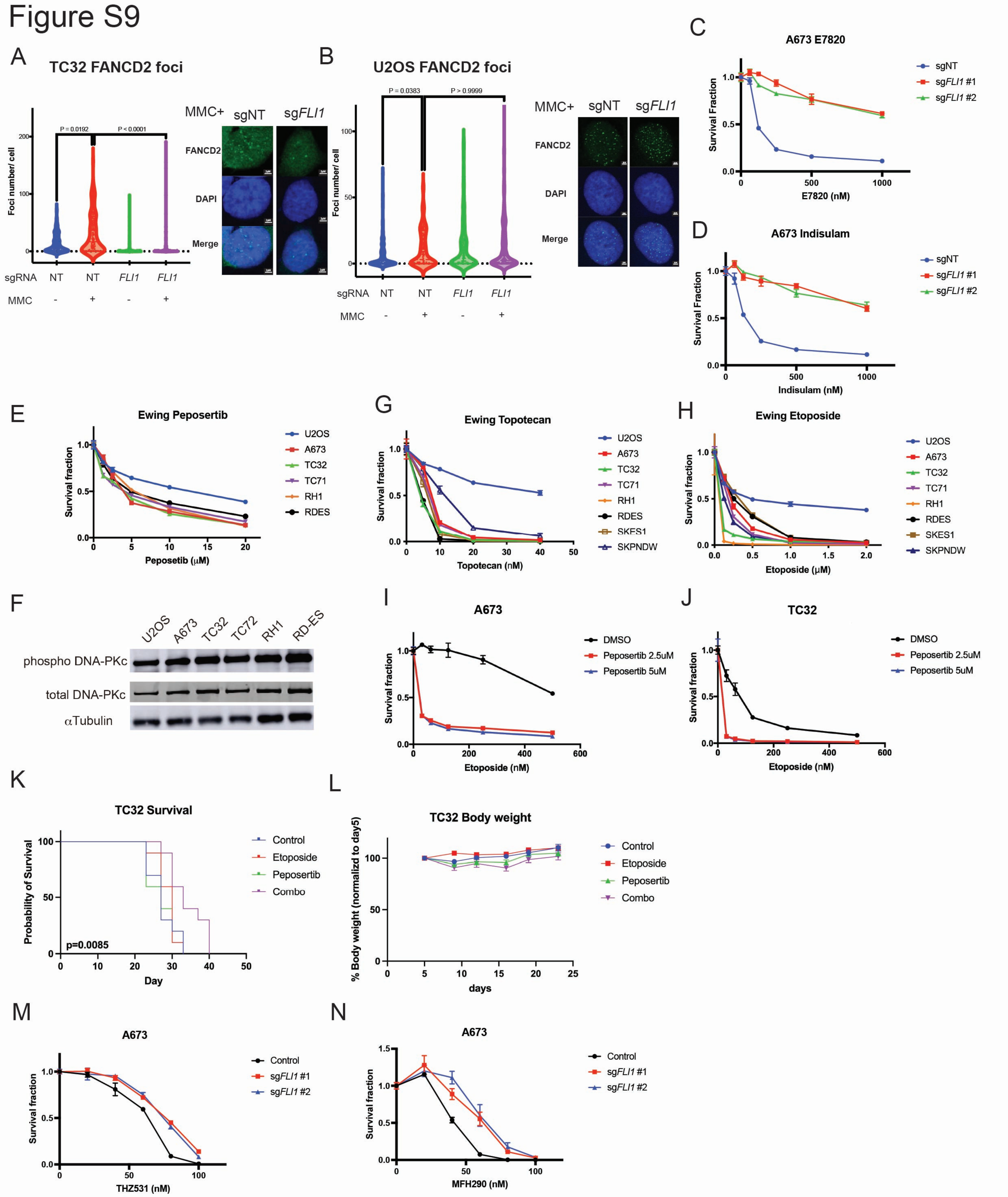
A
TC32 FANCD2 foci
Foci number/ cell
P = 0.0192
P < 0.0001
sgRNA NT NT FLI1 FLI1
MMC - + - +
MMC+ sgNT sgFLI1
FANCD2
DAPI
Merge
B
U2OS FANCD2 foci
P = 0.0383
P > 0.9999
C
A673 E7820
Survival Fraction
E7820 (nM)
sgNT
sgFLI1 #1
sgFLI1 #2
D
A673 Indisulam
Indisulam (nM)
E
Ewing Peposertib
Survival fraction
Peposetib (μM)
U2OS
A673
TC32
TC71
RH1
RDES
G
Ewing Topotecan
Topotecan (nM)
SKES1
SKPNDW
H
Ewing Etoposide
Etoposide (μM)
F
U2OS A673 TC32 TC72 RH1 RD-ES
phospho DNA-PKc
total DNA-PKc
αTubulin
I
A673
DMSO
Peposertib 2.5uM
Peposertib 5uM
Etoposide (nM)
J
TC32
K
TC32 Survival
Probability of Survival
p=0.0085
Day
Control
Etoposide
Peposertib
Combo
L
TC32 Body weight
% Body weight (normalizd to day5)
days
M
A673
THZ531 (nM)
N
A673
MFH290 (nM)

Figure S10

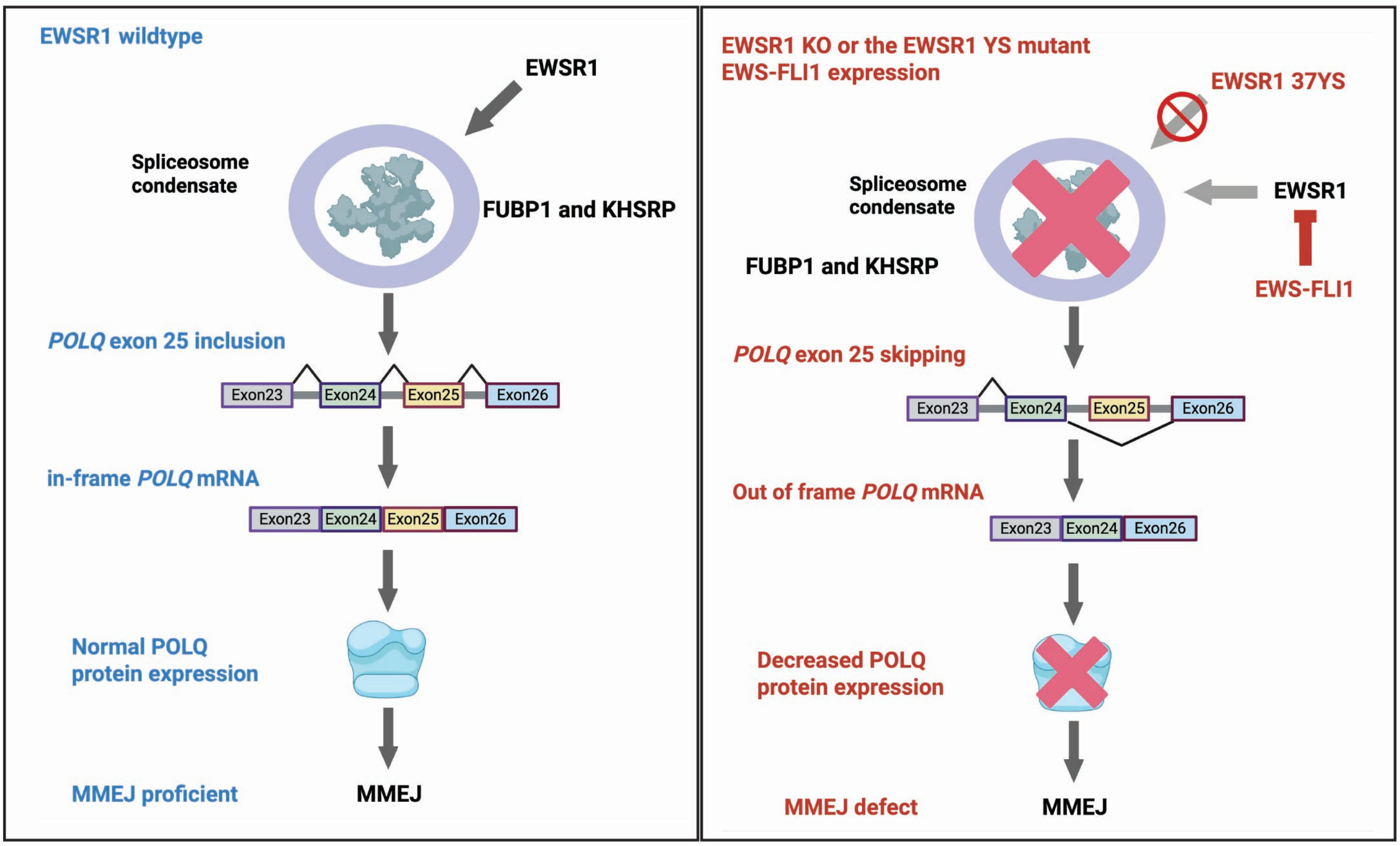
EWSR1 wildtype
EWSR1
Spliceosome condensate
FUBP1 and KHSRP
POLQ exon 25 inclusion
Exon23
Exon24
Exon25
Exon26
in-frame POLQ mRNA
Exon23
Exon24
Exon25
Exon26
Normal POLQ protein expression
MMEJ proficient
MMEJ
EWSR1 KO or the EWSR1 YS mutant EWS-FLI1 expression
EWSR1 37YS
Spliceosome condensate
EWSR1
FUBP1 and KHSRP
EWS-FLI1
POLQ exon 25 skipping
Exon23
Exon24
Exon25
Exon26
Out of frame POLQ mRNA
Exon23
Exon24
Exon26
Decreased POLQ protein expression
MMEJ defect
MMEJ